

A mathematical model for a bumper was developed and used to simulate road vehicle impact. A passive friction element was introduced into the bumper system to improve its impact attenuation and kinetic energy absorption capacity. The mathematical model of the bumper-damper system was used to simulate impact phenomena for a 1900 kg mass moving at a speed of 70 km/h (19.4 m/s), 17.5 times the speed of a typical design specification. The simulation revealed that the energy absorption capacity of the bumper was improved with the addition of a friction element. Simple experiments performed confirmed that higher energy absorption could be achieved with the addition of a friction element to traditional bumpers. It was observed that the addition of the friction element to a traditional bumper of a vehicle could increase the critical design speed from 4 km/h (1.11 m/s) to 14.9 km/h (4.1 m/s). That is, a passive friction damper system could be used to attenuate road vehicle impact energy in collisions (of vehicles of mass similar to that of a typical saloon car) at speeds 3 times higher than the speed for which current conventional bumpers are designed to attenuate (i.e. 4 km/h).

Road Vehicle Impact Attenuation



KNUST

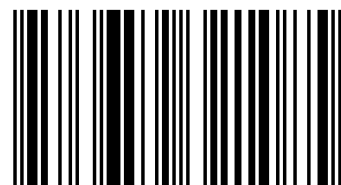
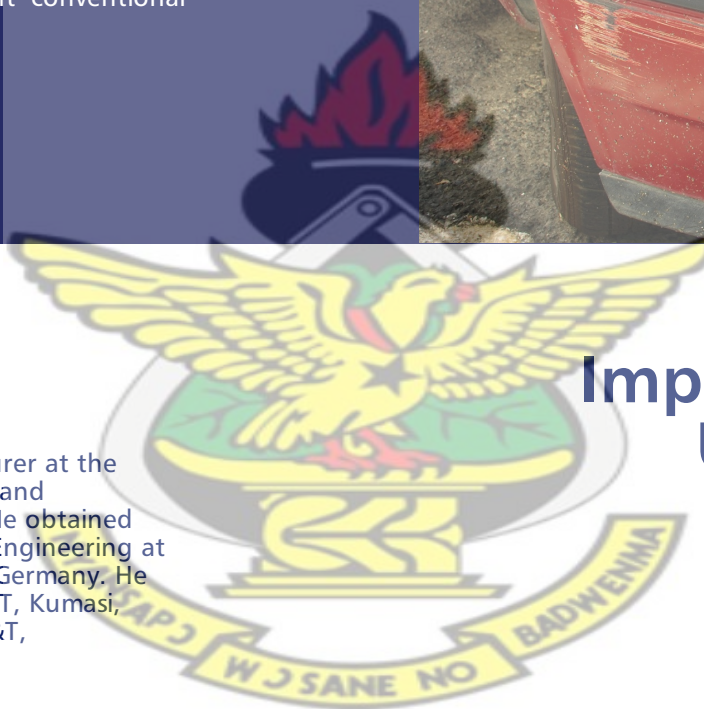
Anthony Agyei-Agyemang



Anthony Agyei-Agyemang

Dr. Anthony Agyei-Agyemang is a lecturer at the Kwame Nkrumah University of Science and Technology (KNUST), Kumasi, Ghana. He obtained BSc. and MSc. (Diplom) in Mechanical Engineering at the University of Karlsruhe, Karlsruhe, Germany. He obtained his Ph.D. degree at the KNUST, Kumasi, Ghana, in 2010 after research at NC A&T, Greensboro, NC, USA.

Impact Attenuation System Using a Passive Damper



978-3-659-32108-5

Agyei-Agyemang

LAP
LAMBERT
Academic Publishing

ABSTRACT

The goal of this work is to mitigate the degree of damage to passengers caused by automobile collisions. Crash phenomena involving road vehicles were investigated for the purpose of developing an impact attenuation design that can withstand speeds higher than the current specified range of up to 4 km/h (for a bumper). Different impact attenuation systems in the vehicle were studied with emphasis on the bumper modeling, analysis and design.

A mathematical model for a bumper was developed. Simulation of impact of the bumper against a fixed barrier was performed. A passive friction element was introduced into the bumper system to improve on the attenuation of the impact and kinetic energy absorption capacity. A mathematical model of the bumper-damper system was formulated and used to simulate impact phenomena for a 1900 kg mass moving at a speed of 70 km/h (19.4 m/s), 17.5 times the speed of a typical design specification.

The simulation revealed that the energy absorption capacity of the bumper was improved with the addition of a friction element. Design parameters for the friction damper were extracted from the results of the simulation. The extracted design parameters include stiffness, k , and coefficient of the damping, c , of the bumper. The use of the results from

the simulation in the design of the bumper was pursued with success. Friction damper designs were proposed. Two of these designs were built and used in experiments to verify their effectiveness and to validate the simulation results. The experiments revealed that higher energy absorption could be achieved with the addition of a friction element to traditional bumpers.

KNUST

From simulation, it was observed that a combination of material stiffness and damping factors could influence energy absorption ability of the damper. It was observed that the addition of a friction element to an ordinary bumper-damper system with the new design parameters can improve its energy absorption capacity by 103.6 kJ, that is about 146 %. Additionally, it was also observed that the addition of the friction element to a traditional vehicle could increase the critical design speed from 4 km/h (1.11 m/s) to 14.9 km/h (4.1 m/s).

It was concluded that a passive friction damper system could be used to attenuate road vehicle impact energy in collisions (of vehicles of mass similar to that of a typical sedan car) at speeds 3 times higher than the speed for which current conventional bumpers are designed to attenuate (i.e. 4 km/h).

LIST OF FIGURES

1.1	Global Road Traffic fatalities by sex and age.	7
2.1	Automobile production by United States, Japan and Germany	15
2.2	Light Vehicle Defects in 1999 Roadworthiness tests . . .	18
2.3	Deployment of an airbag a. and b.	31
2.4	Picture of a crushed car showing the crumple zone . . .	36
2.5	An assembly of the frontal structure showing the cable and brake system	38
2.6	Frontal structure with cable system to involve the not directly loaded beam in an offset crash	39
2.7	A concept for energy absorption by axial friction through an applied normal force F_2	39
2.8	Longitudinal member of the Telescopic Structure . . .	41
2.9	Interior view of the longitudinal member of the Telescopic Structure	41

2.10	Principle sketch of a cable-supported longitudinal structure	42
2.11	Top view of the cable-supported longitudinal structure	42
2.12	Cross-section of the cable and the cable guide disk inside the bar	43
2.13	A bumper reinforcement bar, shown without the plastic Bumper cover	45
2.14	An IIHS test barrier with a steel barrier and a plastic absorber and flexible cover	48
2.15	Slotted Bolted Connection Assemblage	54
2.16	Sumitomo Friction Damper	56
2.17	Piezoelectric Friction Damper	57
2.18	Components of the Damptech Friction Damper	59
2.19	Mechanism and Principle of Operation of the Friction Damper	59
2.20	Friction Spring Details.	60
2.21	External and internal views of the EDR	61
2.22	Pall Friction Damper	62
2.23	Deformation configuration of the Pall friction Damper	63

2.24	Friction damper concept in a cylindrical housing	64
2.25	Bladed disk with an underplatform damper	66
3.1	Schematic of a Maxwell Model and its Free Body Diagrams	71
3.2	Typical Displacement Response for three different Spring Stiffness levels for the Maxwell Model	75
3.3	Typical Velocity Response for three different Spring Stiffness levels for the Maxwell Model	75
3.4	Typical Acceleration Response for three different Spring Stiffness levels for the Maxwell Model	76
3.5	Schematic of a Kelvin Model and its Free Body Diagram	77
3.6	Displacement, Velocity and Acceleration Responses of a Sedan car using the Kelvin Model	81
3.7	Hybrid 1 Model and its Free Body Diagrams.	82
3.8	Displacement, Velocity and Acceleration Responses of the Hybrid 1 Model	85
3.9	Hybrid 2 Model and its Free Body Diagrams.	86
3.10	Displacement, Velocity and Acceleration Responses of the Hybrid 2 Model	89

3.11	Expected Response of a Barrier Crash Test	91
3.12	Range of Material Properties for the Study	93
3.13	Displacements for Maxwell Model at the various deign points.	94
3.14	Displacements for Kelvin Model at the various deign points.	95
3.15	Displacements for Hybrid 1 Model at the various deign points	95
3.16	Displacements for Hybrid 2 Model at the various deign points	96
3.17	Maximum Displacement at design points and effects of moving from one design point to the other for the Maxwell and Kelvin Models	98
3.18	Maximum Displacement at design points and effects of moving from one design point to the other for the Maxwell and Kelvin Models	98
3.19	Velocity for Maxwell Model at the various design points	101
3.20	Velocity for Kelvin Model at the various design points	102
3.21	Velocity for Hybrid 1 Model at the various design points	102

3.22	Velocity for Hybrid 2 Model at the various design points	103
3.23	Rebound Velocity at design points and effects of moving from one design point to the other for the Kelvin Model.	105
3.24	Rebound Velocity at design points and effects of moving from one design point to the other for the Hybrid 1 and Hybrid 2 Models	105
3.25	Acceleration for Maxwell Model at the various design points	108
3.26	Acceleration for Kelvin Model at the various design points	108
3.27	Acceleration for Hybrid 1 Model at the various design points.	109
3.28	Acceleration for Hybrid 2 Model at the various design points.	109
3.29	Maximum Acceleration at design points and effects of moving from one design point to the other for the Maxwell and Kelvin Models	112
3.30	Maximum Acceleration at design points and effects	

	of moving from one design point to the other for the	
	Hybrid 1 and Hybrid 2 Models	112
3.31	Duration of Pulse at design points and effects of	
	moving from one design point to the other for the	
	Maxwell and Kelvin Models	113
3.32	Duration of Pulse at design points and effects of	
	moving from one design point to the other for the	
	Hybrid 1 and Hybrid 2 Models	113
3.33	Schematic of the Bumper with Friction Damper Model	117
3.34	Free Body Diagram of the Friction Damper Model . . .	117
3.35	Simulation Results of Coefficient of Restitution and	
	the ratio of Residual to Dynamic Deformations against	
	the Residual Deformation	120
3.36	Test Results of Coefficient of Restitution and the	
	ratio of Residual Deformation to Dynamic Deformation	
	against the Residual Deformation from a test data . . .	120
3.37	Expression of a Second Order Differential Equation	
	in VisSim	123
3.38	Setting the Integrator Initial Conditions Externally . . .	124

3.39	Variable Deceleration and Displacement Response of the Model	125
3.40	Main Program for the complete Model	127
3.41	Program for Impact Force	128
3.42	Program for the Damping Force.	129
4.1	Normalized Response of a car to a Crash Pulse . . .	138
4.2	Relationship between Impact Velocity and Maximum Deceleration	140
4.3	Displacement for different Friction Elements.	141
4.4	Displacement of Bumper for different Impact Forces using Different Friction Elements	143
4.5	Impact velocity and corresponding Friction Force necessary to produce a deformation of 68 mm for the Material R	144
4.6	Threshold Impact Velocities for various Bumper Material Characteristics	146
4.7	Maximum displacement of five Bumper materials at different Impact Forces without a Friction Element	148
4.8	Maximum displacement of five Bumper materials at	

	different Impact Forces with 152 kN Friction Force from a Friction Element	149
4.9	Maximum displacement of five Bumper materials at different Impact Forces with 228 kN Friction Force from a Friction Element	150
4.10	Concept 1	157
4.11	Orthographic Views of Concept 1	158
4.12	Concept 2	159
4.13	Concept 3	160
4.14	Sectional View of Concept 3	160
4.15	Exploded View of Concept 3	161
4.16	Concept 4	162
4.17	Sectional View of Concept 4	162
4.18	Exploded View of Concept 4	163
4.19	Conceptual Model of a Friction Damper showing direction of Forces	172
4.20	Friction Pads with Compression Springs inside Friction Box.	173
4.21	Impact Test Machine with impact fixture (R) and	

	Hammer fixture (O)	174
4.22	Schematic of a simplified Pendulum Hammer of an Impact Test Machine	175
4.23	Schematic of the Experimental Setup without a Friction Damper: showing Impact Fixture (R) and Bumper Specimen (Q)	176
4.24	Schematic of the Experimental Setup with a Friction Damper showing Impact Fixture (R) and Bumper Specimen (Q)	177
4.25	Results for Bumper A without a Friction Element	181
4.26	Results for Bumper B without a Friction Element	182
4.27	Results for Bumper B with Friction Element Model 2	183
4.28	Results for Bumper C without a Damper	184
4.29	Results for test of Bumper C with Damper Model 1.	185
4.30	Results for Bumper C with and without a Damper	186
A-1	Hammer of Impact Test machine	199
A-2	Rectangular Area	200
A-3	Pendulum with mass m	203
D-1	Displacement of Spring A for Applied Loads	209

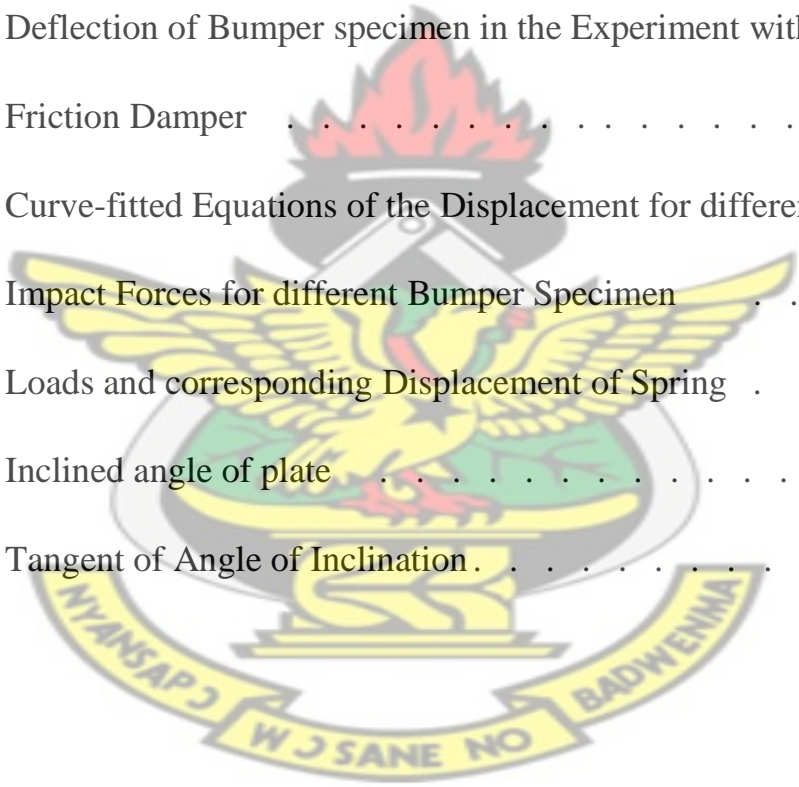
D-2	Displacement of Spring B for Applied Loads.	209
E-1	Experimental results of Bumper C	214

LIST OF TABLES

1.1	Road Crash Cost by Region	4
2.1	Number of Registered Vehicles in Ghana: 2000 to 2006 .	14
3.1	Maximum Displacement according to the various models	97
3.2	Time at Maximum Displacement according to the various Models	97
3.3	Rebound Velocity according to the various models . . .	104
3.4	Time at Rebound according to the various models . . .	104
3.5	Maximum Acceleration according to the various Models	110
3.6	Duration of Crash Pulse according to the various Models	111
3.7	Initial Acceleration According to the various Models	111
3.8	Values of Variables used	126
4.1	Bumper Design Material Parameters	145
4.2	Work Done by different Bumper Design Materials . . .	151

4.3	Extra Work done by different Bumper Design Materials compared with that done by the Design Material R without a Friction Element	152
4.4	Percentage Extra Work done by different Bumper Design Materials compared with that done by the Design Material R without a Friction Element . . .	153
4.5	Extra Work done by different Bumper Design Materials as a result of the introduction of Friction Element . . .	154
4.6	Extra Work done by different Bumper Design Materials as result a of the introduction of Friction Element Friction Element as a percentage	154
4.7	Production Cost Evaluation Scores	164
4.8	Shock Deflection Evaluation Scores	164
4.9	Friction Surface Area Evaluation Scores	164
4.10	Space Occupied by Damper Evaluation Scores	165
4.11a	Evaluation Table for Concepts One	165
4.11b	Evaluation Table for Concept Two	166
4.11c	Evaluation Table for Concept Three.	167
4.11d	Evaluation Table for Concept Four	168

4.12	Link Diameter, Width and Thickness of steel plate for the Damper	169
4.13	Link Diameter, Width and Thickness of steel plate for the Damper Model	171
4.14	Deflection of Bumper specimen in the Experiment without a Friction Damper.	178
4.15	Deflection of Bumper specimen in the Experiment with a Friction Damper	179
4.16	Curve-fitted Equations of the Displacement for different Impact Forces for different Bumper Specimen	180
D-1	Loads and corresponding Displacement of Spring	208
D-2	Inclined angle of plate	211
D-3	Tangent of Angle of Inclination	211

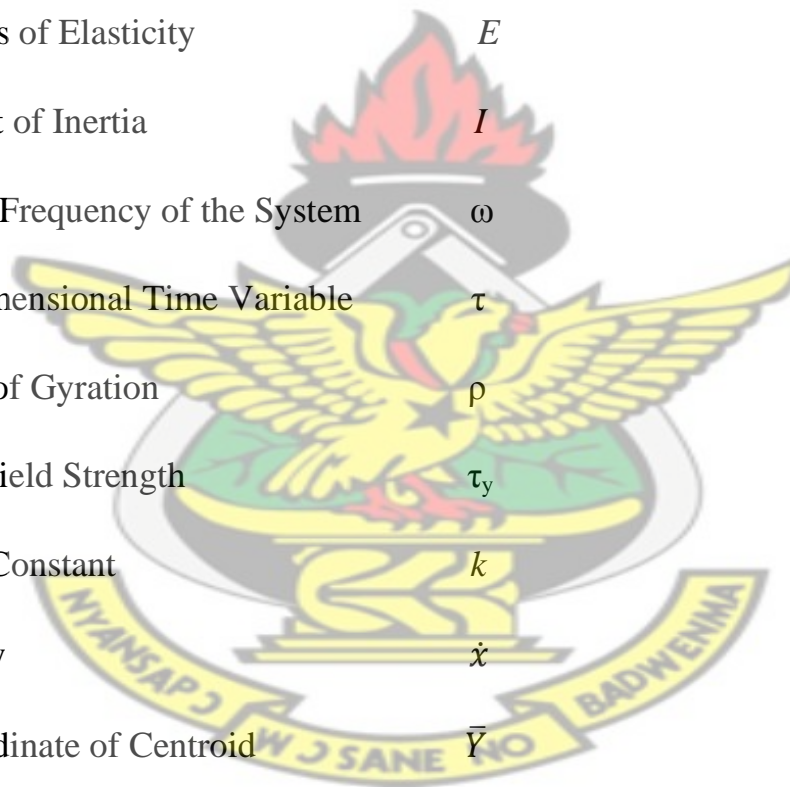


LIST OF SYMBOLS

Acceleration	\ddot{x}
Acceleration due to Gravity	g
Allowable Shear Stress	τ_{allow}
Allowable Stress	S_{allow}
Angular Acceleration	α
Angular Displacement	θ
Coefficient of Damping	c
Coefficient of Friction	μ
Critical Load	P_{cr}
Damping Factor	ζ
Derivative of Acceleration	$\ddot{\ddot{x}}$
Derivative with respect to time	s
Displacement	x
Dollar	\$
Euros	€
Factor of Safety	N

Force	F
Ghana Cedis	GHC
Impact Velocity	$V_i ; V_0$
Mass (mass of pendulum)	m
Mass (moving mass of vehicle	M
Mass (small mass)	M_D
Modulus of Elasticity	E
Moment of Inertia	I
Natural Frequency of the System	ω
Non-dimensional Time Variable	τ
Radius of Gyration	ρ
Shear Yield Strength	τ_y
Spring Constant	k
Velocity	\dot{x}
X-Coordinate of Centroid	\bar{Y}
Y-Coordinate of Centroid	\bar{X}
Yield Strength	S_y

KNUST



LIST OF ABBREVIATIONS

AASHTO	American Association of State Highway and Transportation Officials
ABS	Anti-Block System
ACRS	Air Cushion Restraint System
ASIC	Application Specific Integrated Circuit
BBD	Blade-to-blade Damper
BGD	Blade-to-Ground Damper
DALYs	Disability Adjusted Life Years
DMV	Division of Motor Vehicle
DOT	Department of Transportation
EDR	Energy Dissipation Restraint
EU	European Union
Gs	A Factor of Acceleration due to Gravity; $1G = 9.81 \text{ m/s}^2$
IIHS	Insurance Institute for Highway Safety
MEMS	Micro-Electromechanical System
NASA	National Aeronautics and Space Administration

NCAP	New Car Assessment Program
NHTSA	National Highway Traffic Safety Administration
NRTC	National Road Traffic Commission
ODE	Ordinary Differential Equations
PMVI	Periodic Motor Vehicle Inspection
SDI	Silicon Design Incorporated
SRS	Supplemental Restraint System
SUV	Sports Utility Vehicle



KNUST

To my wife Elizabeth, and my sons Kwabena, Kwasi and Kwabena Jr.



ACKNOWLEDGEMENTS

My gratitude goes to Dr. Jerome Antonio and Dr. Samuel Owusu-Ofori for their immense contribution, encouragements and support during the research and writing of the thesis.

My sincere thanks to Mr. E.E.K. Agbeko for his contribution, guidance and continuing encouragement for this thesis.

Furthermore I thank Dr. Kwasi Preko for his technical editing and for contributing yet more to the improvement of the thesis.

I wish to thank Mr. Winfred Arthur Keborni for his technical support in the experiments.

TABLE OF CONTENTS

ABSTRACT	i
LIST OF FIGURES	iii
LIST OF TABLES	xii
LIST OF SYMBOLS	xv
LIST OF ABBREVIATIONS	xvii
ACKNOWLEDGEMENTS	xx
TABLE OF CONTENTS	xxi
CHAPTER ONE	1
1.0 INTRODUCTION	1
1.1 Motivation and Justification	5
1.2 Goals and Objectives	7
1.3 Scope of the work	8
CHAPTER TWO	10
2.0 LITERATURE REVIEW	10
2.1 Influence of Road, Driver and Vehicle	10
2.2 Influence of the Interactions between the Road, Driver and Vehicle	20
2.3 Measures to Reduce Road Traffic Crashes and their Consequences	25
2.4 Energy Attenuation Devices	27

2.4.1	The Airbag	28
2.4.2	Collapsible Structures in the Vehicle's Body	33
2.4.3	The Bumper	43
2.4.4	Friction Elements	52
2.4.4.1	Slotted-bolted Connections	54
2.4.4.2	Sumitomo Passive Energy Dissipation Devices	55
2.4.4.3	Piezoelectric Friction Damper	56
2.4.4.4	Damptech Friction Damper	57
2.4.4.5	The Friction Spring Seismic Damper	60
2.4.4.6	Energy Dissipating Restraint	61
2.4.4.7	Pall Friction Damper	62
2.4.4.8	Vehicle Suspension Friction Damper	64
2.4.4.9	Blade-to-Blade and Blade-to-Ground Friction Dampers	65
2.5	Summary	67
CHAPTER THREE		69
3.0	Modelling, Simulation and Data Extraction	69
3.1	Modeling of Impact Attenuators	69
3.1.1	The Maxwell Model	70
3.1.2	The Kelvin Model	76
3.1.3	The Hybrid 1 Model	81
3.1.4	The Hybrid 2 Model	85
3.2	Simulation	90
3.2.1	Displacement Response	94
3.2.2	Velocity Response	101

3.2.3	Acceleration Response	107
3.2.4	Justification of High Speed Impact Attenuation Model	115
3.2.5	Modified Kelvin Model	116
3.3	Simulation and Post Processing Software	121
3.4	Solving Second Order nonlinear ODE with VisSim	122
3.5	Post Processing of Data	131
3.6	Summary	131
CHAPTER FOUR		137
4.0	Results and Discussion	137
4.1	Acceleration Change	139
4.2	Deformation	141
4.3	Work Done	147
4.4	Design Deductions from the Simulation	155
4.5	Friction Damper Design Concepts	157
4.6	Experimental Validation of Model	173
CHAPTER FIVE		188
5.0	Conclusion and Future Work	188
5.1	Challenges and Sources of Error	190
5.2	Future Work	190

KNUST



Appendix A	Calculations of Damper's lever Dimensions	191
Appendix B	Optimization Program in MATLAB™	194
Appendix C	Experimental Data – Equipment	199
Appendix D	Experimental Data – Components	208
Appendix E	Experimental Data – Work Done	214
References		217



CHAPTER ONE

1.0 INTRODUCTION

The rate of motor vehicle accidents globally is alarming and naturally increases as the number of vehicles on the roads increases. The trend in the rate of road accidents is the same in many countries in that it is growing. It is estimated that 1.2 million people are killed in road crashes and nearly 50 million are injured worldwide every year. In Ghana there are 1600 fatalities annually (Appiah, 2009). Road traffic injuries are currently ranked ninth globally among the leading causes of disease burden, in terms of Disability Adjusted Life Years (DALYs) lost (Odero, 2006). In the United States, the American Automobile Association estimates that road traffic accidents claim a life every thirteen minutes (Zheng, 2006). In Ghana 4 people get killed daily (Appiah, 2009).

In many developing countries, where there is a significant increase in vehicle traffic combined with poor road infrastructure, inadequate training of drivers, and a lack of good police control, the traffic injuring rates are enormous. Road traffic crashes are known to be a leading cause of deaths and injuries in Ghana in the past decade (Afukaar et al., 2003).

The majority of road traffic fatalities occurs on roads in rural areas. In Ghana about 58% more people die on roads in the rural areas than in urban

areas, and generally more severe crashes occur on rural roads compared with urban areas (Afukaar et al., 2003). Considering the fact that about 70% of the population in Ghana lives in rural areas, coupled with the fact that the majority of the rural residents are engaged in agricultural activities that supports the economy of the country, it is evident that these accidents and their consequences affect the food supply and the economy of the nation.

The problem of road traffic crashes and injuries is growing and this poses a serious developmental and public health problems. Generally, the poorer population groups in developing countries bear a disproportionate burden of avoidable consequences from road traffic injuries. Also within such countries, poor people account for a disproportionate portion of the ill health due to road traffic injuries. It is, however, expected because within poor countries, poorer people are usually pedestrians, cyclist and passengers in buses and trucks. In the case of rich countries, children from relatively lower socioeconomic classes also suffer a higher burden of morbidity and deaths from road crashes than their counterparts from high-income groups (Nantulya and Reich, 2003).

People, aged 15 to 44 years, who are the economically active adults, account for more than a half of the total road traffic deaths and about 30% to 86% of all trauma admissions as a result of road traffic crashes in some low-income and middle-income countries (Peden et al., 2004). Traumatic brain injury as a result of motor vehicle crashes is also a significant problem. Almost a quarter of all non-fatally injured victims requiring hospitalization sustain a traumatic brain injury (Peden et al., 2004).

The health, social and economic effects of road traffic crashes are substantial. They cost governments, on the average, between 1% and 2% of their Gross National Product (GNP). The GNP is the total value of all the goods and services produced in a nation, plus the value of goods and services imported, minus the goods and services exported. In economic terms, the cost of road crash injuries, that is the direct economic costs of global road crashes, has been estimated at US\$ 518 billion, with the costs in low-income countries – estimated at US\$ 65 billion (Peden et al., 2004). Road traffic accidents costs Ghana US\$ 165 million annually, which is about 1.6% of its Gross Domestic Product (GDP) (BRRI, 2006). The GDP of a country is the total market value of all final goods and services produced in the country in a given year, which is equal to the total consumer, investment and government spending, plus the value of exports, minus the value of imports. Table 1.1 shows the global road crash cost.

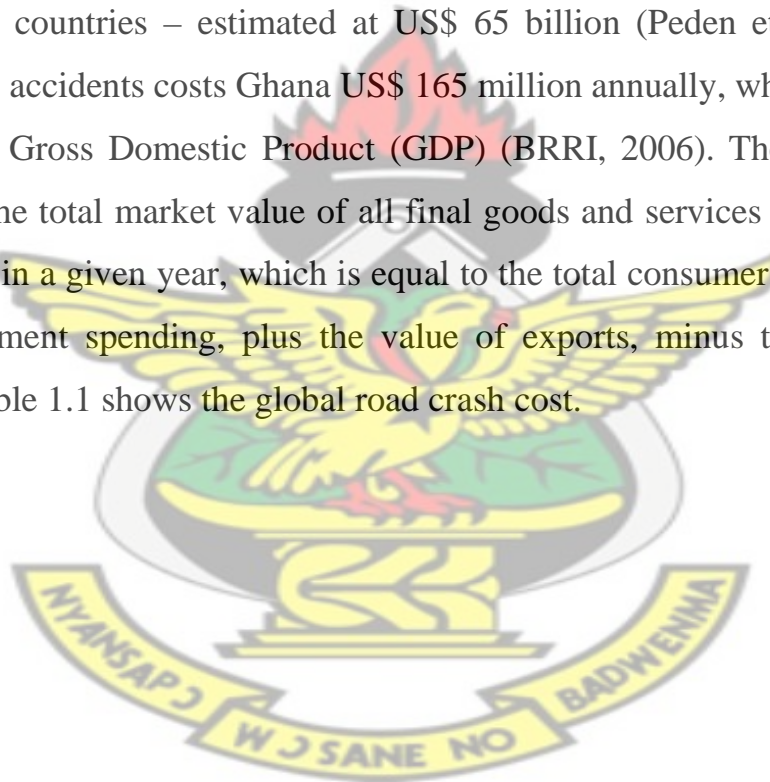


Table 1.1: Road Crash Cost by Region; (Peden et al., 2004)

Region	Gross National Product in 1997 (US \$ Billion)	Estimated Annual Crash Costs	
		As Percentage of Gross National Product	Costs (US \$ Billion)
Africa	370	1	3.7
Asia	2454	1	24.5
Latin America and Caribbean	1890	1	18.9
Middle East	495	1.5	7.4
Central and Eastern Europe	659	1.5	9.9
Subtotal	5615	-	64.5
Highly-motorized countries	22665	2	453.3
Total	-	-	517.8

A good number of people have become temporarily or permanently disabled as a result of road traffic crashes. Motor vehicle crashes cause many people to suffer serious psychological consequences for years after the incident. The social cost of motor vehicle crashes, which is very difficult to quantify, takes a heavy toll on victims, their families, friends and communities. For example, the death of a breadwinner through a crash most often pushes a family into poverty.

KNUST

These facts give a good indication that road traffic crashes are indeed a health, economic and social problem facing all mankind. There is, therefore, the need to study the causes of these crashes and to find remedies that will reduce trauma cases and fatalities.

1.1 Motivation and Justification

The effects of road crashes could be quite complicated and expensive. They may include all sorts of social costs, medical costs, loss of production, human costs, material costs, settlement costs and traffic jam costs. In monetary terms they may cost between 1% and 2% of the gross national product.

The estimated direct economic costs of global road crashes is about US\$ 518 billion. In the European Union (EU) countries alone, considering both direct and indirect costs of road crash injury, the cost exceeds €180 billion (US\$ 207 billion). In the United States of America, the human capital costs of road

traffic crashes in 2000 alone were estimated at about US\$ 230 billion (Peden et al., 2004). Road traffic accident costs Ghana US\$ 165 million annually, which is about 1.6% of its Gross Domestic Product (GDP) (BRRI, 2006). These amounts are huge and could be saved and used in development programs and projects to improve the quality of life.

Over a million people die worldwide every year as a result of road traffic crashes; and it is predicted that if no new or improved interventions are introduced, road traffic injuries will be the third leading cause of death by the year 2020 (Peden et al., 2004). In Ghana about 4 people get killed daily and there are 1600 fatalities annually (Appiah, 2009).

It appears the poor are the most affected by the problems associated with road crashes. About 90% of all road traffic deaths occur in the developing world, which makes up about two-thirds of the world's population; this implies that road crash fatalities have a more adverse effect on developing countries than the developed countries.

From Figure 1.1, males of age 15 to 44 years are more likely to be involved in road traffic crashes than females. In the developing world most of the breadwinners of families and communities are males. Since about 90% of all traffic deaths occur in the developing world, and the majority of these victims are in their most productive years. This implies that it is taking a big toll on the livelihood at majority of people on earth.

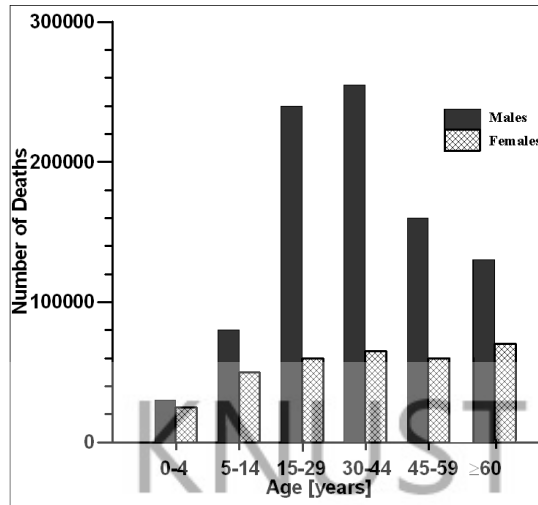


Figure 1.1 Global Road Traffic fatalities by sex and age, (Peden et al., 2004)

This is a cause for concern that needs to be addressed. This study aims at helping to solve part of this serious problem through the development of more effective crash attenuation systems.

1.2 Goals and Objectives

This mission of road safety research is to reduce the incidence of road traffic accidents and to minimize their effects once an accident has happened. In contrast, the goal of this dissertation is to reduce the effect of crash impact on passengers in collision of vehicles traveling at medium speeds (40 km/h to 56 km/h).

Automobile bumpers are designed to withstand impact energy equivalent to 4 km/h. This corresponds to rolling impact and it would be beneficial to improve upon this design criterion.

The specific objectives are to:

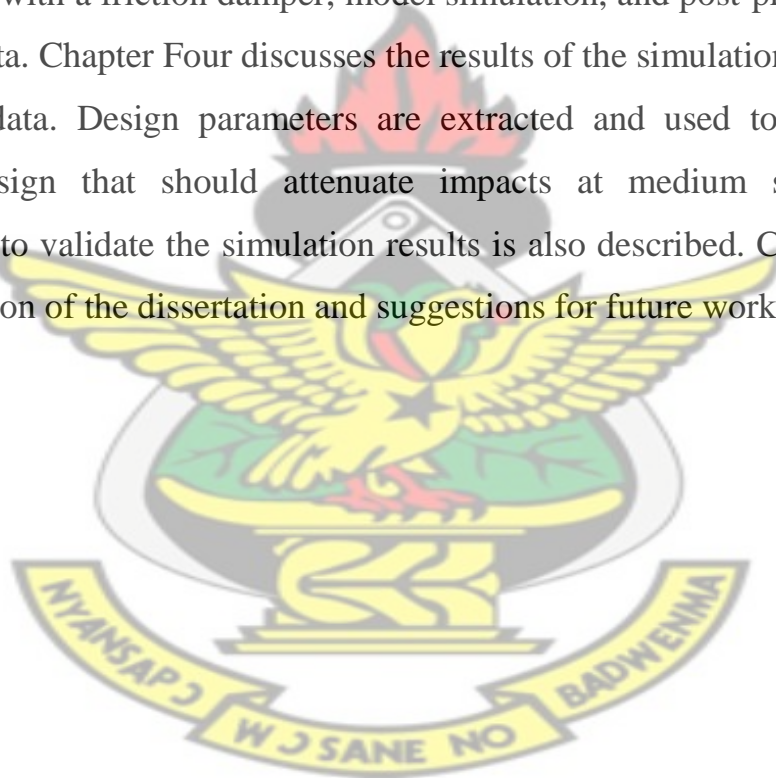
- i. Improve automobile bumpers to enable them withstand impact energy of vehicles traveling at several times the speeds conventional bumpers are designed for.
- ii. Model and simulate impact phenomenon in order to study crash dynamics.
- iii. Use information from the simulation to generate design parameters for better impact attenuation bumpers.
- iv. Propose designs of a bumper that could attenuate the impact energy of vehicles traveling at speeds several times the specified speeds for the design of a conventional bumper.

1.3 Scope of the work

The work involves a review of the literature on road traffic crashes and their causes. It also proposes a means of the attenuation of impact energy in a road traffic crash with a friction damper. The dissertation is divided into five chapters.

Chapter One introduces the work and gives the background information, and the objectives and justification of the work. Chapter Two deals with the

major factors contributing to road crashes. Among the factors considered are the road, the vehicle and the driver's performance. It also discusses the interaction of these factors and their possible contribution to road crashes. Different energy attenuation devices in the vehicle, such as the airbag, collapsible structures and the bumper, are also considered, but with more emphasis on the bumper. The friction damper is selected as the passive damper for this dissertation. Different friction dampers and their application are also discussed. Chapter Three deals with the mathematical modeling of the bumper with a friction damper, model simulation, and post-processing of acquired data. Chapter Four discusses the results of the simulations and post-processed data. Design parameters are extracted and used to propose a bumper design that should attenuate impacts at medium speeds. An experiment to validate the simulation results is also described. Chapter Five is a discussion of the dissertation and suggestions for future work.



CHAPTER TWO

2.0 LITERATURE REVIEW

This chapter describes the capabilities of the conventional bumper and investigates the characteristics of other impact attenuation devices and how they can be integrated into bumpers to improve their impact attenuation capabilities. It also discusses factors that contribute to road traffic accidents.

Road traffic crashes are attributed to a wide range of factors although some may play greater roles than others. These factors include the mood and behaviour of the driver, influence of substances taken in by the driver (food, drink, alcohol, medicine, drug, etc.), weather conditions, passengers' activities, conditions of road infrastructure, speed of vehicle, and the condition of the motor vehicle. Generally, road crashes are attributable to three main factors, namely the condition of the vehicle, the performance of the driver or the condition of the road. It could, however, also be caused by a combination of these factors. The influence of the interaction between these factors can be significant.

2.1 *Influence of Road, Driver and Vehicle*

Geometric road design elements that are important to road safety include cross section design (pavement width, shoulder width and type, lane width),

roadside design (width, slopes and roadside condition) and sight distance. Roadside design considers the width, slopes and roadside condition of the road. Roadside design affects the sight distance of the driver. Sight distance is a very important road design element. It is the length of roadway visible to a driver. According to AASHTO (2001) the three main types of sight distances in roadway design are intersection sight distance, stopping sight distance, and passing sight distance. All these need to be considered in the design of the road to improve safety.

In addition to road design, wear and damage to even well designed roads also affect road safety. Important factors and mechanisms that affect road conditions and cause road damage are (Cebon, 1993):

- (i) Fatigue cracking for all types of pavements;
- (ii) Permanent deformation (longitudinal rutting) for flexible and composite pavements; and
- (iii) Reduced skid resistance for flexible and composite pavements.

The extent and effect of these failure mechanisms listed above are influenced by many factors, including the roadway design and the construction methods, the material properties of each constituent layer, the traffic loading and the environmental conditions throughout the roadway service life.

The driver's driving ability, driving experience and the conditions under which he/she drives can also contribute to road traffic accidents. The driver's aptitude and performance are affected by his/her driving abilities and cultural background. Even though different classifications of factors leading to accidents are given, most researchers classify the causes of accidents in which drivers are the cause into three main categories. These are driving errors, general highway violations, and aggressive violations (Davey et al., 2007).

Driving errors are mainly associated with failures of observation and judgment, while general highway violations reflect a deliberate driving act that breaks social norms regarding driving behaviour(s). Aggressive violations consist of a mixture of emotion-oriented responses to driving situations and traditional Highway Code violations (Davey et al., 2007). Among drivers, the very old and the very young are the most vulnerable and this can be observed in their overrepresentation in crashes. The general trend indicates that young and old age groups are usually over-involved in crashes, as compared to their middle-age counterparts.

As people advance in age, many of their functional abilities decline and health conditions deteriorate. For example, some older drivers with visual impairment, such as declines in dynamic visual acuity, contrast sensitivity, peripheral vision, and conditions such as cataract, glaucoma and macular degeneration, can experience difficulty differentiating between details of

intersection features like kerbs, edge-lines and traffic islands, seeing other objects such as vehicles and pedestrians, difficulty perceiving the traffic environment for potential hazards, and difficulty seeing traffic signals (Oxley et al., 2006). Jennifer Oxley et al. also belong to this school of thought, that older drivers are currently over-represented in severe injury in road traffic crashes.

KNUST

The design of modern motor vehicles is typically handled by a large multi-disciplinary team of designers and engineers. Modern design has been leading in the direction of energy savings, comfort and safety. The use of motor vehicle has grown steadily, bringing with it higher rate of accidents. Table 2.1 gives the number of registered vehicles in Ghana from 2000 to 2006 and Figure 2.1 shows the trend of the growth in the production of the automobile.

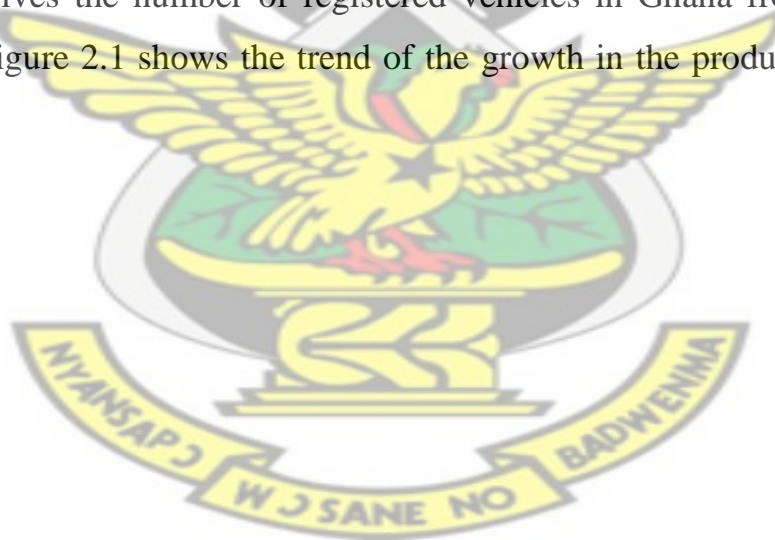
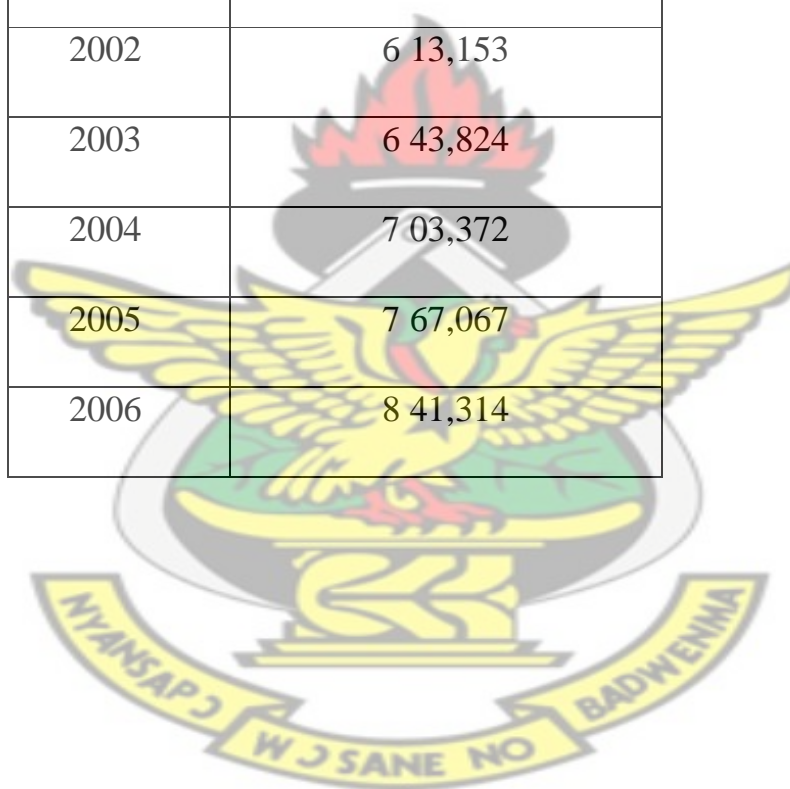


Table 2.1 Number of Registered Vehicles in Ghana: 2000 to 2006 (NRSC, 2010)

Year	Number of Registered Vehicles
2000	5 11,063
2001	5 67,780
2002	6 13,153
2003	6 43,824
2004	7 03,372
2005	7 67,067
2006	8 41,314



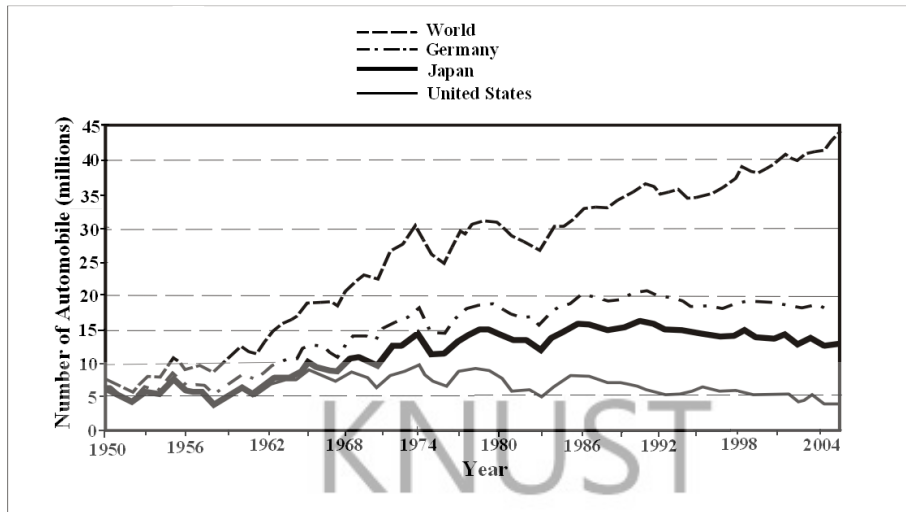


Figure 2.1 Automobile production by United States, Japan and Germany, (Hofsta-University, 2007)

The safety level of a motor vehicle may be very good after manufacture but it will have to be maintained with the use of the vehicle. This calls for regular maintenance to keep it free from defects that may make the vehicle unsafe to use. The level of roadworthiness could have different interpretations. Roadworthiness guidelines relevant to a vehicle or a component of a vehicle stipulates that the safe operation of the vehicle or the control of its emissions should not be impaired. That implies the component should be without a performance related defect that compromises the safety of the vehicle to pass the test.

A list of the applicable components of a vehicle that must be considered is as follows (NRTC, 1995): steering, suspension, structure and body, braking

equipment, wheels and tyres, lights and reflectors, tow couplings, seats and seat belts, mirrors, glazing and windscreen, engine, drive line and exhaust.

Some vehicle defects can contribute to the occurrence of crashes, but not all defects cause crashes. Factors that cause crashes are many and it may involve a chain of events, of which vehicle defects is just one. This implies that it is only in certain circumstances that defects are contributing factors in crashes (Rechnitzer et al., 2000). A study revealed that there was significant variation regarding the role of vehicle defects in crash causation and the effectiveness of Periodic Motor Vehicle Inspections (PMVI) programs in reducing defects and crashes. It appeared that vehicle defects are a contributing factor in only 6% of crashes. The effect of PMVI programs on accident rates was found to vary significantly, from no effect to decreasing the accident rate up to as much as 16%. Some studies suggest that periodic roadworthiness tests, in other words PMVI, could reduce the number of crashes caused by vehicle defects by about 50% (Rechnitzer et al., 2000).

A vehicle's age was found to be an important factor in the cause of an accident. In Australia it was found that the probability of a vehicle that is twenty-year-old or more being involved in a fatal single vehicle crash was 2.5 times greater than a newer vehicle. There are still significant methodological and statistical difficulties and shortcomings in many of the studies, including the difficulty of identifying and detecting defects in crashed vehicles and their contribution to a crash. These suggest that there

could be an under-reporting of the contribution of defects to crashes. Therefore to be assured of safety, it is important to aim at achieving and maintaining roadworthiness.

The number of times a vehicle is inspected does not necessarily establish its roadworthiness. To ensure that a vehicle remains roadworthy, one needs to perform a regular maintenance. Figure 2.2 shows 1999 roadworthiness test data from VicRoads, Victoria, Australia. It is evident from the data that defects were found in parts and components such as brakes, tyres and steering which are very critical with respect to safety (Brideson et al., 2001). From Figure 2.2, of all the vehicles that failed roadworthiness test in 1999, 65% had a defective body, 50% had defective brakes, 46% had a defective exhaust, 42% had defective lamps, 61% had defective seats or seat belts, 53% had defective steering, 53% had poor tyres and 42% had either a defective windscreen or wiper. It is interesting to note that the vehicles were being tested for certification and yet the percentages of defect were high. This makes the results quite alarming. This suggests that the maintenance of most vehicles was poor. The information, however, is not enough to suggest whether or not the defective items are over-represented in defect-related crashes.

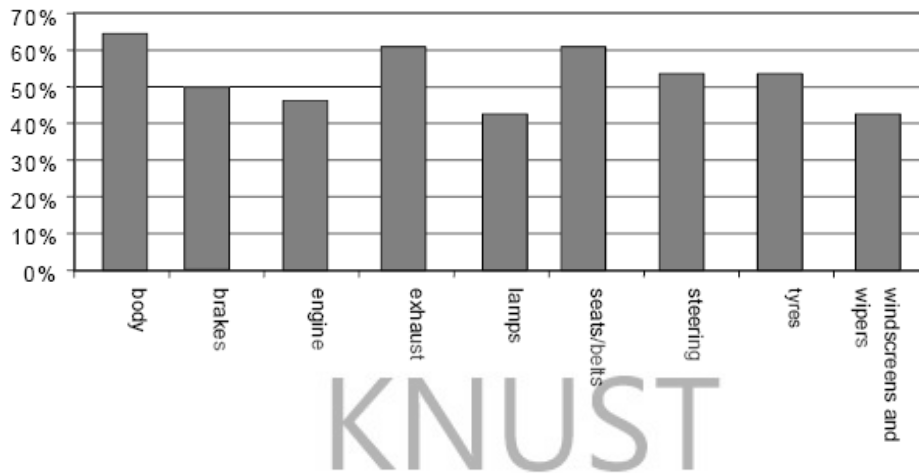


Figure 2.2 Light Vehicle Defects in 1999 Roadworthiness tests (Brideson et al., 2001).

Since defect-free vehicles cannot be guaranteed, it is necessary to stress the need for a vehicle condition considered to be safe in spite of possible defects. This calls for design of crashworthy vehicles. Crashworthiness is defined as a measure of the level of occupant protection offered by a vehicle (Brideson et al., 2001). Crashworthiness and safety, however, is not necessarily the same thing. Vehicles that are older than 24 years have a higher probability of being involved in accidents with severe injuries.

New vehicles are generally better designed and have sophisticated in-built safety features. These features tend to reduce the possible risk of fatal and serious injuries to their occupants in crashes. For example, ABS brakes and airbags have become standard requirements in most vehicles. Even though some old vehicles may not be technically roadworthy, with some additional

safety features a fatal or serious injury may be avoided. In a crash, the risk of serious injury is higher for occupants in an older vehicle than in new vehicles because the technology built into the old vehicle is not as advanced as the new one as far as safety and comfort are concerned (Brideson et al., 2001). A change of roadworthiness requirements may therefore not necessarily change this trend.

KNUST

Given their relatively cheaper prices, older light vehicles are more likely to be sold and therefore change owners. After change of ownership vehicles have to go through roadworthiness tests. This implies, older vehicles are more likely to be sent for testing and therefore, naturally, have the higher likelihood of showing defects at a test, (Brideson et al., 2001).

Even if vehicle defects could be ruled out, no conclusive evidence has been found that vehicle defects constitute a major issue in fatal or serious injury crashes. From evidence and submissions it was found that vehicle defects were not a significant cause or contributor to fatal or serious accidents (Brideson et al., 2001). The development of a fast roadside safety test that can be delivered on a consistent basis by Police Officers and Transport Safety Services personnel also would be helpful. It would not necessarily make the roadworthiness of vehicles any better, but it would influence drivers to do regular maintenance on their vehicle to make them safer; the objective being to encourage a culture among drivers to regularly inspect their vehicles and have possible defects repaired (Brideson et al., 2001).

Several causal factors may be present in a crash, but it is difficult to determine how much each factor contributes to an individual crash, (Brideson et al., 2001). Motor vehicle crashes are often attributed to driver's error or misjudgment on the part of the driver. These are caused usually as a result of impaired driving, inattention or over speeding. Should these be the only causes, something could be done by the driver to prevent a possible crash. In reality, not all vehicle crashes are necessarily caused by the driver. Some may be due to problems resulting from the driver's interaction with design elements of the road or with the vehicle itself and its components.

2.2 Influence of the Interactions between the Road, Driver and Vehicle

The driver's driving ability, driving experience and the conditions under which he/she drives may not account for all cases of crashes attributable to the driver. The driver interacts with road design elements, vehicle components and technological gadgets in the vehicle, some of which pose challenges to the driver and makes driving unsafe. These can also contribute to road traffic accidents. On the other hand the vehicle also may interact with the road and, in one way or the other, make driving unsafe.

In the United States, for example, about one-third of all fatal traffic accidents involving motor vehicles, happen at intersections (DMV, 2006). The most probable factors that must have been associated with the crashes are due to the drivers' interaction with the road condition. An innovative design element to improve intersection safety is the use of modern roundabouts to provide a safer environment for drivers (Lord et al., 2006).

KNUST

According to Oxley (2006), ten main factors were ascribed as primary causes across the crash sites in crashes attributable to the driver. They are:

1. Inappropriate free space selections in traffic,
2. High multi-task complexity,
3. High approach speeds of conflicting traffic
4. Limited and restricted sight distance
5. Inappropriate response to traffic signs and signals
6. Inadequate intersection definition
7. Inappropriate pavement markings
8. Poor canalization of water interfering with roads
9. High traffic volumes, and
10. Road width restrictions

The most significant finding of this study for crash involving drivers was the selection of safe and free space in conflicting traffic when crossing at intersections. It was noted that the problem of gap selection as a factor was the case in over three-quarters (76%) of the crashes. This problem manifests

itself especially at intersections controlled by 'stop' or 'give-way' signs, or at signalized intersections that provided either no control or partial-control of left-turn (in a Right-Hand Traffic System). Restricted sight distance also was a major issue. It was also observed that crashes occurred often when traffic volumes and speeds were high; where there were nearby upstream signals, where seeing signals was difficult, and when drivers had to negotiate wide multi-lane carriageways.

KNUST

The following recommendations were made from the study of Oxley et al., 2006,:

1. The replacing of intersections controlled by 'stop' or 'give-way' signs, with roundabouts could greatly enhance safety for drivers of all ages. Negotiating in a roundabout is a fundamentally simpler and safer task than choosing a coincident gap in two streams of traffic. In the event of a crash at the roundabout, the injury consequences will be less severe because of the greatly reduced impact speeds and more favourable collision angles experienced under this form of intersection control. Roundabouts are less expensive to implement as compared to a fully controlled intersection. Some sites studied have been improved with the installation of a roundabout, and crash records indicated elimination or reduction of injury crashes after installation.

2. Introduction of fully controlled turning signals to assist drivers to make safe left-turns at intersections controlled partially by traffic signals.

3. Improvement in sight distances, with those with less than 2.5 s perception–reaction time.
4. Designing of roads to suit all categories of drivers, which indirectly mean a safer environment for the vulnerable group of road users as well.

In a study of the reaction of a driver as he/she interacts with the systems in the vehicle, three dependent variables describing the driver's braking response and two dependent variables describing driver trust in the system and perception of alarm timing were observed. The results revealed that if alarms are presented at the mean value of alarm time for relatively early alarms in short headway driving, then these alarms may decrease braking reaction compared to the no alarm condition. But on the other hand, if alarms are presented at the mean value of alarm time for relatively early alarms in long headway driving these alarms have no potential to decrease braking reaction. It was observed that, with respect to the overall effects of alarms on driver behaviour, the presentation of alarms at the mean value of alarm time for relatively early alarms for all driving conditions may lead to more consistent braking reaction to imminent collision situations as compared to the situation when no alarms are provided (Abe and Richardson, 2006). This may be positive and can help to reduce the incidence of road crashes. A limitation of the study was the drivers' anticipation of the need to brake repeatedly while driving in the simulator which may prompt faster alarm response times than would have been obtained in a real driving environment. On the other hand, operating of radios, mobile phones and other modern navigation technologies like

computers and GPS systems, may distract the driver and can impact negatively on the prevention and reduction of road traffic crashes.

Concerning the interaction between the Road and Vehicle, poorly designed roads and poorly maintained roads can cause deterioration in the vehicle and compromise their safety. That is, interaction of poor roads with vehicles can cause damage to some vehicle components. On the other hand, vehicles interacting with roads can also cause deterioration to the road conditions with time. Research into the interaction between the vehicle and roads have revealed that tyre road contact forces, especially those generated by heavy vehicles, influence road surface deterioration and damages it to an appreciable extent.

The vertical force applied by the tyre of vehicles can be separated into two components, namely the static load, and dynamic wheel load or forces. The static load is due to the weight of the vehicle and depends on the geometry and mass distribution of the vehicle as well as the static load sharing characteristics of the suspension system. The dynamic tyre forces on the other hand are caused by vibration of the vehicle when it is excited by the roughness of the road surface. This occurs, normally, at frequencies below 20 Hz. Thus, the interaction of the road with the vehicle can cause damage to the road condition which in turn can cause damage to the vehicle and thus render the vehicle unsafe to its occupants and may consequently cause road traffic accidents.

2.3 Measures to Reduce Road Traffic Crashes and their Consequences

Considering the impact of road traffic crashes, it is important that certain measures be taken to prevent road traffic crashes and to minimize their eventual consequences. To minimize the occurrences of crashes and their effects, many measures can be taken to help but they cannot completely rule out crashes. Road design through the use of good technical design principles and well marked roads with a good number of road signs can help reduce crashes attributed to roads. Even for a well designed road there could be damage and even failure of road infrastructure materials due to many factors, including the roadway design, the construction methods used, the material properties of each constituent layer, the traffic loading and the environmental conditions throughout the service life of the road. This possible damage and failure of road infrastructure materials can compromise the safety of the roads.

The causes of accidents in which drivers are the cause are classified as either driving errors, general highway violations, or aggressive violations (Davey et al., 2007). Gaining driving experience through education and training, is essential to develop safe driving habits, but this can only help reduce the incidence of crashes due to the first cause only; namely, driving errors. General highway violations and aggressive violations, however, are human

behavioural tendencies making it difficult to influence them to reduce vehicle crashes. The focus of attention in reducing crashes should therefore be on the vehicle.

Concerning the vehicle, improving the safety standards can help reduce incidence of crashes. Satisfactory vehicle safety standards may only be met at the time of the inspection. Roadworthiness may not necessarily make a vehicle safe. Other causal factors may be present in a crash but it is difficult to determine how much each factor contributes to an individual crash, (Brideson et al., 2001). This makes it difficult to come up with any solution to reducing or eliminating crashes due to the vehicle.

Concerning causes due to the interactions of the various factors, most of them will be difficult to eliminate completely. This implies that crashes cannot be eliminated completely. It would therefore be good to think about how to reduce the effects of the impact due to these crashes to the barest minimum to save lives and property. In the light of this, it is essential to focus on safety components that will help reduce the effect of crashes when they occur, since eliminating crashes is very difficult if not impossible. Crashworthiness of the vehicle therefore becomes the vital issue to deal with.

Most drivers take evasive and counter measures when they realize that a crash is going to occur. There is often a deceleration prior to the impact. As

a result most impacts occur at medium speeds. The speed limit in most towns and cities is pegged at 50 km/h. A medium speed of about 50 km/h has therefore been selected for this research to investigate into crashes at high speed (about 70 km/h) that decelerate to medium speeds before impact, and impacts at a city's speed limit.

The energy possessed by the vehicle at the 50 km/h needs to be attenuated. Some component(s) of the vehicle should be designed in such a way that they could reduce the impact of crashes when they occur; and it should be possible to use these in older vehicles as well. Examples of such components in the vehicle are the energy attenuation devices and components discussed in the next section.

2.4 *Energy Attenuation Devices*

Important energy attenuation devices and components in a typical vehicle include airbags, bumpers and collapsible structures of the vehicle. Each of these is discussed here with respect to its energy attenuation capacities and possible implementation in a vehicle.

2.4.1 The Airbag

Airbags are used in the absorption of impact energy in different applications. It was initially used to cushion the landing of some space vehicles and their instruments, and recently in automobiles as an impact attenuation device.

The airbag in the automobile is an inflatable cushion designed to protect occupants of the vehicle from serious injury in the case of a collision. It is also known as air cushion restraint system (ACRS) or an air bag supplemental restraint system (SRS), designed to supplement the protection offered by seat belts.

A typical air bag system is made up of an air bag module – which consists of an inflator or gas generator and a sewn, woven nylon fabric air bag – crash sensors, a diagnostic monitoring unit, a steering wheel connecting coil, and an indicator lamp. These components are networked by a wiring harness and powered by the vehicle's battery. Air bag systems are designed to store a reserve charge after the ignition has been turned off or after the battery has been disconnected. To ensure reliability, the air bag circuitry performs an internal "self-test" during each engine startup, usually indicated by a light on the instrument panel that glows briefly at each startup.

The driver's-side air bag material is coated with a heat shield coating to protect the woven nylon fabric from scorching, especially near the inflator

assembly, during deployment. Talcum powder or corn starch is also used to coat the air bag as a form of lubrication. Newer designs with silicone and urethane coated air bag materials require little or no heat shield coating. The inflator body or canister is made from either stamped stainless steel or cast aluminum. Inside the inflator canister is a filter assembly, made up of a stainless steel wire mesh with ceramic material sandwiched in between. The filter assembly is surrounded by metal foil seal that prevents propellant contamination. The propellant, in the form of pellets, is primarily sodium azide combined with an oxidizer. It is typically located inside the inflator canister between the filter assembly and the initiator or igniter.

Air bags inflate very rapidly and therefore come out of the steering wheel hub or instrument panel with considerable force, generally at a speed of about 322 km/h (200 mph). As a result of this initial force, contact with a deploying air bag may cause injury. The sound of air bag deployment is very loud, in the range of 165 to 175 decibels for 0.1 of a second.

While airbags can protect a person under the right circumstances, they can also injure or even kill. New airbag control units recognize if a belt is used and set the trigger time accordingly. Newer airbags trigger at a lesser speed; nonetheless, passengers must remain at least 25 centimeters (10 in) from the bag to avoid injury from the bag in a crash. Injuries such as abrasion of the skin, hearing damage (from the sound during deployment), head injuries, eye damage for spectacle wearers and breaking the nose, fingers, hands or arms

may occur as the airbag deploys. Airbags can detonate long after the initial crash. It could therefore injure rescue workers who may be inside the car.

Air bags are usually designed to deploy in frontal and near-frontal collisions. That is equivalent to approximately hitting a fixed barrier at about 13 to 23 km/h (8 to 14 mph) or roughly, equivalent to striking a parked car of similar size across the full front of each vehicle at about 45 km/h (28 mph).

Air bag sensors are triggered when the level of deceleration exceeds a set value. Its sensors are Micro-electromechanical System (MEMS) accelerometers. MEMS accelerometer is an integrated circuit chip that is usually made with nickel- or silicon-base and integrated micromechanical elements.

The microscopic mechanical element moves in response to rapid deceleration which causes a change in capacitance or resistance, depending on the technology used, and prompts the chip to send a signal to trigger the airbag if the set maximum deceleration value is exceeded. Figure 2.3a shows a diagram of the airbag module and Figure 2.3b shows the deployed airbag.

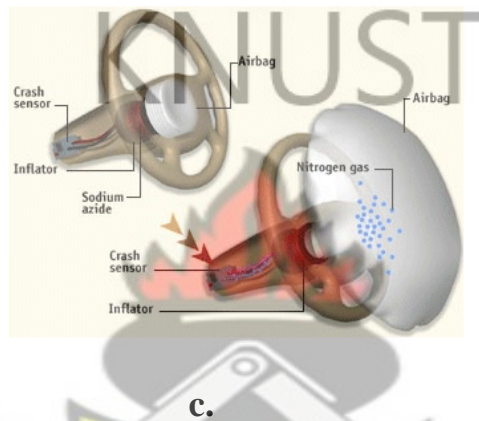
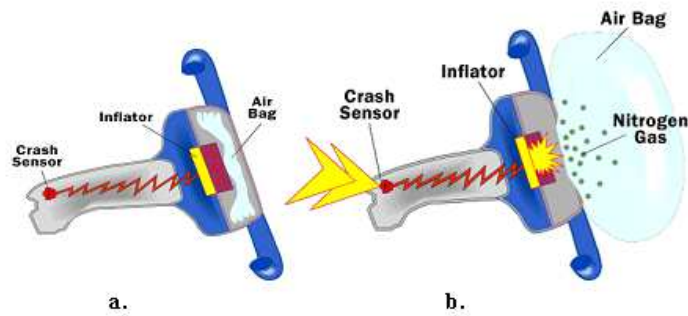


Figure 2.3 Deployment of an airbag a. and b. (How-Stuff-Works, 2007),
c. (CarPros, 2009)

Most air bags automatically deploy in the event of a vehicle fire when temperatures reach about 150 to 200 °C (300 to 400 °F). This safety feature ensures that such temperatures do not cause an explosion of the inflator unit within the air bag module.

The sensor of the airbag is an accelerometer. The accelerometer uses either capacitance change or resistance change due to acceleration pulse as the

sensed parameter and depending on whether it is resistive sensing (as in piezoelectric type of accelerometers) or capacitive sensing (as in capacitance accelerometers). Unlike the piezoelectric type which requires a dynamic input of some minimum frequency to generate a response, the capacitive sensing allows for response to DC (steady state) accelerations as well as dynamic vibration (SDI, 2007).

KNUST

The accelerometer unit is basically made up of two parts: the micro-machined sense element or sensor chip and the integrated electronics or Application Specific Integrated Circuit (ASIC) chip. They are attached together using a die attachment and gold wire bonding techniques and the whole package is solder sealed to provide a simple device.

In the process of airbag deployment, the expanding nitrogen gas undergoes a process that reduces the temperature in the system and also helps in removing most of the combustion residue or ash. The nitrogen gas inflates the nylon bag in less than 0.05s, splitting open its plastic module cover and inflating in front of the occupant. As the occupant comes in contact with the bag, the nitrogen gas is vented through openings in the back of the bag. The bag is fully inflated for only 0.1s and is nearly deflated by 0.3s after impact.

Many new vehicles are equipped with side air bags. They are designed to reduce the risk of injury in moderate to severe side impact crashes and are generally located in the outboard edge of the back of the seat, in the door or

in the roof rail above the door. Seat and door-mounted air bags provide upper body protection. Some airbags extend upwards to provide head protection. Two types of side air bags, called inflatable tubular structures and inflatable curtains, are specially designed to reduce the risk of head injury and/or help keep the head and upper body inside the vehicle.

Apart from the traditional way of using airbags to attenuate impacts inside the vehicle, one can also think about introducing external airbags at the front of vehicles such that the bags could be deployed during a crash to absorb part of the impact shock. In this case the bag could be placed behind the bumper and inflate to cushion the vehicles and prevent direct contact at impact, but deflate just after impact as the traditional air bags do. This could be a new concept to attenuate impact energy after a crash.

2.4.2 Collapsible Structures in the Vehicle's Body

In a vehicle crashes, the kinetic energy of the vehicle will be dissipated. Energy dissipation comes primarily from the deformation of the vehicle or by friction. There are two types of collisions. The first is the collision between the vehicle and external objects; be they barriers or other vehicles. The second are the internal collisions such as between occupant(s) and the interior of the vehicle. Good vehicle design seeks to protect occupants in the 'first' collision, which deforms the vehicle structure, and changes the velocity of the vehicle, but also seeks to reduce injury risk to occupants in the

'second' collision. The effects of a collision on the occupants of a vehicle depends on the crashworthiness of the vehicles.

Crashworthiness is the ability of a structure to withstand the effects of a crash and protect its occupants during an impact. Crashworthiness design of a vehicle aims at designing the vehicle structure for optimum impact energy absorption, and to design the restraint system (seatbelts, airbags, bolsters, etc.) for optimum occupant protection (Nripen, 1993). The vehicle's body is designed to help absorb energy by deforming in a controlled manner during a collision. Vehicle components like front side rails, rear rails, door structure and pillars undergo considerable amounts of deformation to assist in mitigating the effects of impact in a crash (Nripen, 1993).

It is desired that in an impact a major part of the impact energy is absorbed by the vehicle structure; the restraint components should then provide protection of occupants against the remaining crash energy. The deformation should not intrude in the passenger compartment. A safety cage is designed to surround the passenger compartment to help provide protection. Systems that help protect occupants during the secondary collision include the safety belt system, different types of air bags, and seat design including head restraints. They can also include other restraints for cargo and concepts that discourage placement of cargo likely to become projectiles on the cage.

Engine/suspension cradles are used by designers to better control this deformation and to by-pass very rigid components such as engine blocks which are not effective energy absorbers and could cause greater impulse force on the occupants (Paine et al., 1998). Some Sport Utility Vehicles (SUVs) and pick-up trucks have high bumpers and frame rails. The trend in design today is lowering the bumpers and frame rails, which are designed to deform to protect the passenger cabin. Lowering the bumpers and frame rails help to align them to meet car bumpers and frame rails during a crash so that the vehicles can absorb as much of the energy in an accident as possible.

Figure 2.4 shows a car indicating the area of a vehicle that absorbs crash energy upon impact. This crumple zone has materials that are relatively weaker in a car's structure to enable the structure work to collapse in a controlled manner. As a result the collapse is controlled, and energy from the impact can be directed away from the passenger area, and channeled for example to the floor, bulkhead, roof, or hood. In effect energy from the impact is used up in deforming the materials in the crumple zone, often converting some of it into heat and sound energy.

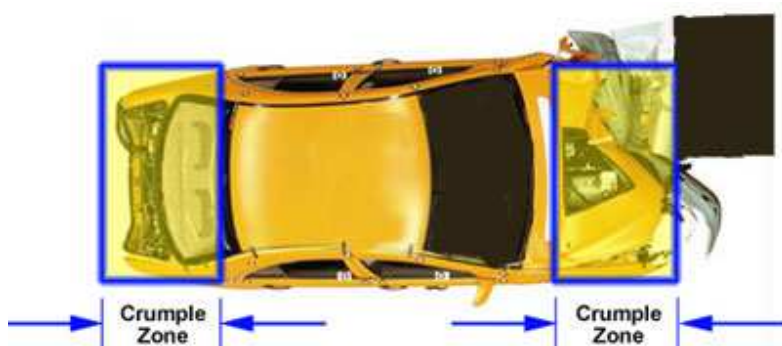


Figure 2.4 A crushed car showing the crumple zone

Crumple zones slow the time it takes for a vehicle to come to a complete stop in the deformation process, and through that spread the impact of force over a longer period of time, with less potential for injury. By making the time of impact longer the deceleration is reduced. The deceleration of a vehicle in a crash can be enormous. At the height of a frontal crash the front of the vehicle comes to a halt but the remainder of the vehicle may continue to undergo a high deceleration - typically around 40g's (up to 60g's with some four-wheel-drive vehicles). (Paine et al., 1998).

The properties of the material used in the crumple zone affect the crashworthiness of a vehicle. If the vehicle (along with the other objects involved) were perfectly rigid it would stop instantly in a crash, subjecting its occupants to deceleration loads mitigated only slightly by their human response dynamics. Steel is usually used in this design, but there is the tendency today to use aluminium for the design of the crumple zone. Corrosion is another factor that favors the use of aluminium. Rust attacks any exposed steel, but many aluminum alloys are corrosion-resistant. The

energy absorption capacity of longerons of new vehicles exceeds that of old vehicles. This could be linked to corrosion. It has been observed that corrosion of longerons could decrease the value of energy absorption by 1.6 times (Griškevičius and Žiliukas, 2003). Aluminum is also easier to recycle, since it melts at a much lower temperature than steel.

Good vehicle design tends to produce vehicles that perform well at protecting their occupants in a crash while apparently having low aggressivity towards the occupants of other vehicles. Evidently this may be achieved by efficiently absorbing crash energy in the front structure while retaining the integrity of the passenger compartment (Paine et al., 1998).

The front rail is the main deformable component dissipating energy in a frontal impact. In a frontal impact these rails have the greatest influence on vehicle crash performance. The design of the front rail, usually consisting of a thin walled prismatic column, requires definition of the geometry. Dent initiators are introduced into the front rails to facilitate a controlled deformation of the structure. Rectangular dent-type crush initiator absorbs more crash energy than the circular dent-type crush initiator (Cho et al., 2006).

Different designs for crash energy absorption that use adaptive concepts have been proposed. One of them is an adaptive vehicle structure that could change the stiffness in real time for optimal energy absorption in different

crash situations (Witteman, 2005). Figure 2.5 shows the assembly of a proposed conceptual design which tends to reduce the resulting crash pulse of the vehicle. In the proposed conceptual design by Witteman, the right amount of energy could be absorbed by means of friction generated by hydraulic brakes on two rigid backwards moving beams. In case of an offset or oblique crash, a mounted cable system moves the missed beam backwards. Figure 2.6 shows the cable system. By combining this design with possible interactive controlled hydraulic brakes (by regulating a normal force), an optimal vehicle deceleration pulse could be found for each crash velocity independent of the struck vehicle position (Witteman, 2005). Figure 2.7 shows a conceptual sketch of the controlled friction device.

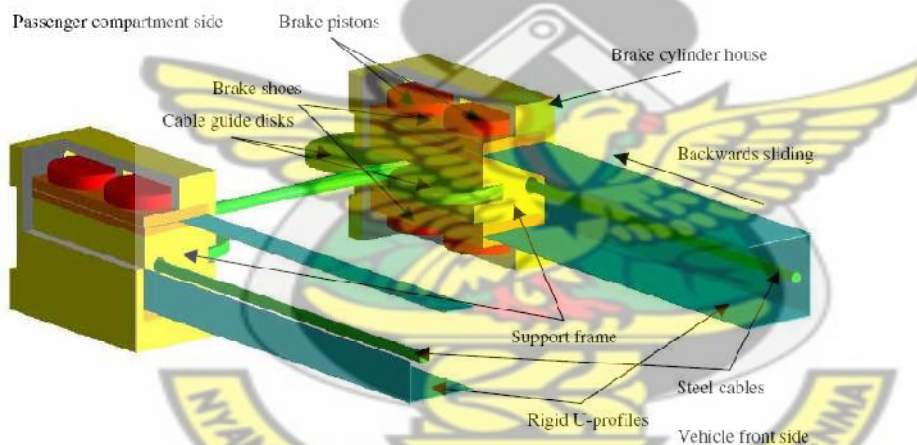


Figure 2.5 An assembly of the frontal structure showing the cable and brake system (Witteman, 2005)

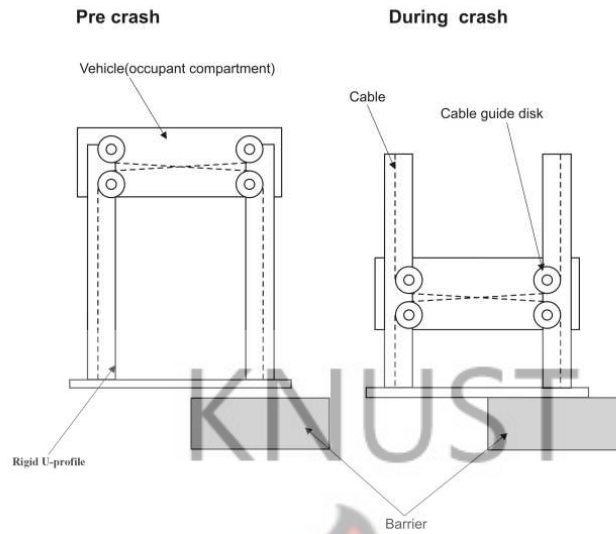


Figure 2.6 Frontal structure with cable system to involve the not directly loaded beam in an offset crash (Witteman, 2005)

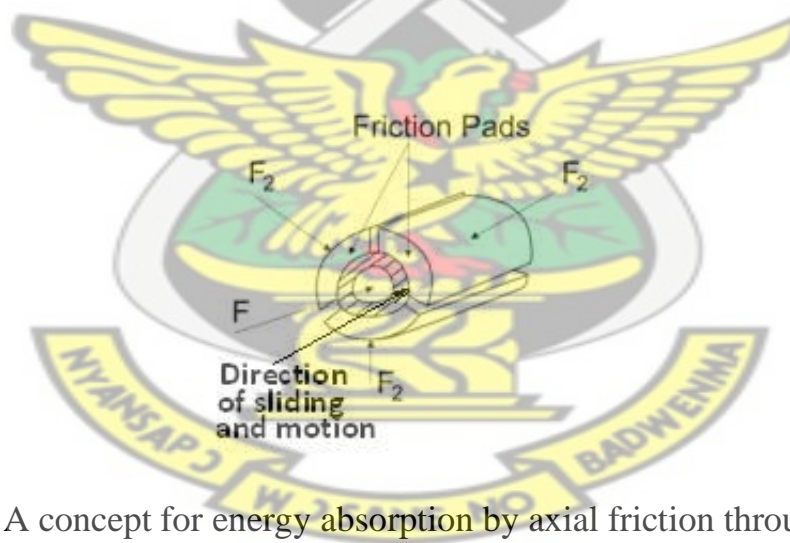


Figure 2.7 A concept for energy absorption by axial friction through an applied normal force F_2 (Witteman, 2005)

Another design concept for crash energy absorption also uses an adaptive concept. A frontal structure consisting of two special longitudinal members,

combine a higher bending resistance with stiffness; without increasing the axial stiffness. The longitudinal members are supported by a cable connection system for symmetric force distribution. If only one of the longitudinal members is loaded during a partial overlap crash, a cable connection system will force the other longitudinal member also to be engaged and crumple as well. This results in normal energy absorption by both members (Witteman and Kriens, 1998).

This concept proposes a design with almost the same stiffness for all overlap percentages and impact angles, resulting in one crash pulse which can be optimized for minimal injury of the occupants. The new concept is based on the design philosophy that an optimal longitudinal member must be functionally distinguished into two separate systems. The first, called the crushing part, guarantees the desired stable and efficient energy absorption. The other, called the supporting part or enveloping tube, guarantees the desired stiffness in the transverse direction. The latter allows enough energy absorption during an off-axis collision and gives enough support with a sliding wall to protect the crushing part against a possible bending collapse. The components' square tubes are designed to slide into each other well (Witteman and Kriens 1998).

Figure 2.8 shows a drawing of the longitudinal member and Figure 2.9 shows its interior view. The dimensions used are based on a popular compact class car and both ends of the longitudinal member, the two

functional components are joined with a rigid plate. Two squared rings are used to support and prevent a bending collapse of the crushing part in the larger rear parts of the telescope (Witteman and Kriens, 1998).

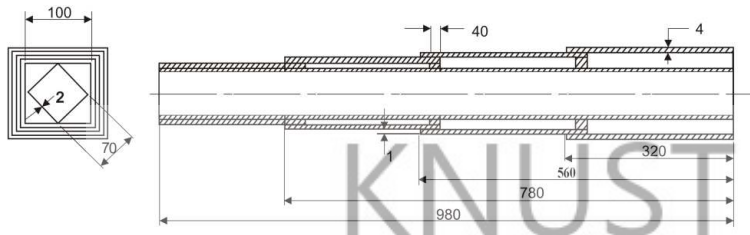


Figure 2.8 Longitudinal member of the Telescopic Structure (Witteman and Kriens, 1998)



Figure 2.9 Interior view of the longitudinal member of the Telescopic Structure (Witteman and Kriens, 1998)

During deformation the first part of the supporting structure with the smallest inner dimensions slides together with the folding front to the rear. After a full deformation all the folds would be packed in the first supporting part (Witteman and Kriens, 1998).

A structure consisting of two stiff sliding bars and two cables form the cable connection system. It connects the rear of one bar inside one longitudinal member to the front of the other longitudinal member to transmit the crushing force from a loaded to an unloaded longitudinal member (Witteman and Kriens, 1998). Figure 2.10 and Figure 2.11 show the cable connection system while Figure 2.12 shows the cross-section of the cable and its guide.

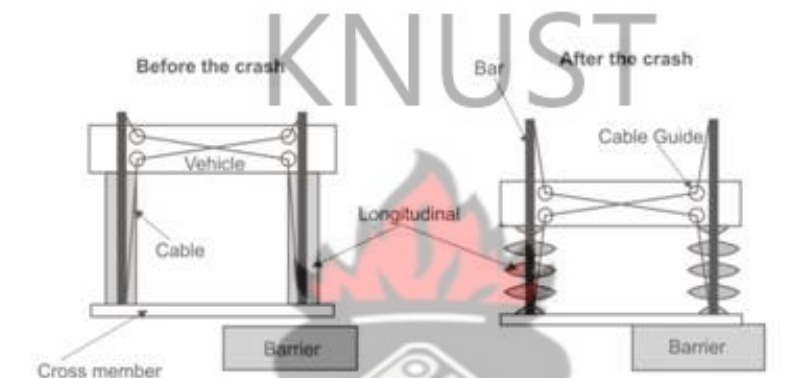


Figure 2.10 Principle sketch of a cable-supported longitudinal structure (Witteman and Kriens, 1998)

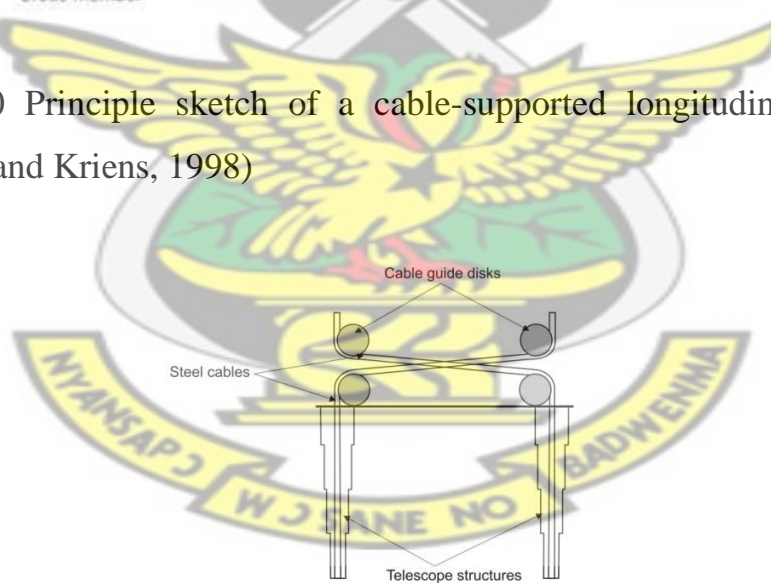


Figure 2.11 Top view of the cable-supported longitudinal structure (Witteman and Kriens, 1998)

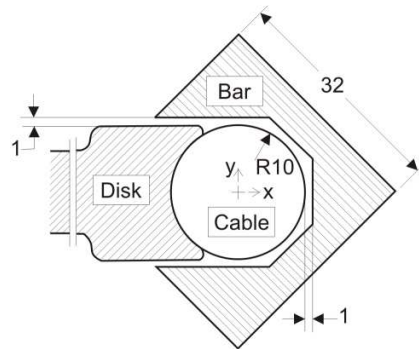


Figure 2.12 Cross-section of the cable and the cable guide disk inside the bar (Witteman and Kriens, 1998)

Witteman's telescopic design concept could also be implemented by fitting it behind the bumper, such that on an impact, the bumper-telescopic collapsible structure could absorb the impact, and through deformation of the longitudinal structure, absorb the kinetic energy involved to reduce the impact on the occupant of the vehicle. Its length is the only disadvantage in this proposed application, since the space behind the bumper is rather limited.

2.4.3 The Bumper

A bumper of an automobile is designed to absorb shock loads at low speeds in order to mitigate the effects of the impact. The bumper is meant to reduce damage to the vehicle at low speeds. The bumpers of vehicles are required to pass an impact test at 2.5 mph (4 km/h) with no visible damage to the body.

Bumpers keep safety-related equipment such as headlights and taillights, hoods, fenders, exhaust and cooling systems, away from damage.

When bumpers are poorly designed, these car body parts sustain damage even in parking-lot collisions and other low-speed impacts. Replacement costs of such components are very high. It is therefore essential to equip passenger vehicles with bumpers that effectively reduce damage in low-speed collisions.

Passenger vehicles are designed to absorb crash energy in frontal crashes through deformation of energy-absorbing structures forward of the occupant compartment. This is basically the bumper. In collisions between cars and light trucks, however, possible mismatches in height can cause the capacity of energy-absorption structures not be fully utilized (Baker et al., 2007).

There are benefits from enhancing the compatibility between cars and light trucks in serious front-to-front crashes. If the bumpers of different vehicles are made compatible, fatality risks for car occupants in front-to-front crashes with light trucks could be reduced by about 8 percent for lighter SUVs and pickups weighing between 2400 and 2500 pounds, and by about 28 percent for car occupants in front-to-front crashes with heavier trucks weighing 4,000 lbs or higher (O'Neill and Kyrychenko, 2003).

Front and rear bumpers generally consist of a plastic cover over a reinforcement bar made of steel, aluminum, fiberglass composite, or plastic. They are designed as a bumper bar and its attachment brackets to crush in a low-speed crash to absorb energy. Polypropylene foam or plastic honeycomb, also called "eggcrate," is sometimes used instead of crushable brackets and bar. In some designs both are used. Sometimes the foam's main purpose is to serve as a spacer between the bar and the bumper cover and not necessarily as an energy absorber. Figure 2.13 shows a bumper's reinforcement bar, with the plastic cover removed.

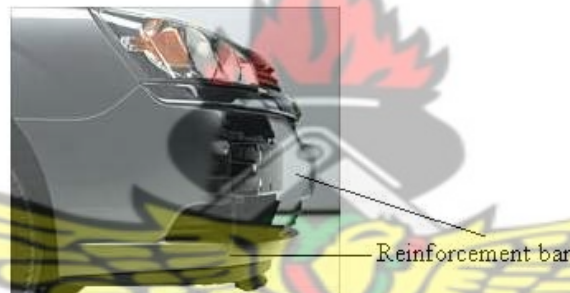


Figure 2.13 A bumper reinforcement bar, shown without the plastic bumper cover

During a collision impact, the bumper absorbs impact energy by going through a sacrificial deformation thereby increasing the body crush or deceleration distance in order to minimize the G-loads on the vehicle and passenger compartment during head-on and oblique frontal and rear collisions. The bumper distributes kinetic energy over a wide area through predetermined force transmission paths into the stronger and heavier parts of the vehicle inner body and chassis structure.

The trend in the design is to make pedestrian-friendly bumpers. Two general approaches to reducing the severity of pedestrian lower limb impacts can be identified. They are the provision of cushioning and support of the lower limb in the bumper and a new lower stiffener; as well as the integration of impact sensors and exterior airbags (Schuster, 2004). The main method proposed for *cushioning* the lower limb in an impact uses an energy absorber in front of a semi-rigid beam. Energy absorbers proposed include plastic foams (single or multi-density), molded plastic ‘egg-crates’, ‘spring-steel’, composite steel-foam, and crush-can energy absorbers (Schuster, 2004).

The most common beams used in the proposed pedestrian-friendly bumper designs are rolled steel or extruded aluminum. Other designs propose the use of molded plastic beams or plastic-steel composite structures. There are also designs that involve deploying bumpers that either move or change stiffness in response to the impact. The typical design proposed for *supporting* the lower limb in an impact is with a secondary lower beam, also called a ‘stiffer’ or ‘spoiler’. Plastic plates or metal beams appear to be the most recommended types of lower stiffeners (Schuster, 2004). Exposed steel bumpers that involve frontal airbags design are also alternative design concepts that appear to be adaptable to meet the pedestrian’s safety requirements but these may be costly and require advanced sensors to function efficiently (Schuster, 2004).

For passenger cars in USA, the law specifies 10 bumper tests, including pendulum tests and crashes into a fixed flat barrier. This is in line with the bumper standards that stipulates the impact resistance of vehicles in low speed front and rear collisions. The purpose of this standard is to reduce physical damage to the front and rear ends of a passenger motor vehicle from low speed collisions (NHTSA, 1977).

KNUST

Bumpers are tested using pendulum and fixed barrier tests. Apart from pendulum tests at 2.4 km/h (1.5 mph), bumpers must pass the fixed barrier tests. The fronts and rears of the vehicles crash into a flat barrier at 4 km/h (2.5 mph). To pass these barrier and pendulum tests, unlimited damage is allowed to the bumper, but none is allowed to other parts of the vehicle. Hood and trunk doors, propulsion, suspension, steering, and braking systems must all operate normally after the test. There should be no broken headlights or fuel, cooling, or exhaust leaks or constrictions after the tests. The bumper should be within the test zone of 40.64 to 50.8 cm (16-20 inches) from the ground. SUV's and vans are excluded from such bumper standards. Even though most pickups and SUV's do have bumpers, their heights often vary from the USA federally specified test zone for cars.

The Insurance Institute for Highway Safety (IIHS) in USA uses a series of four tests to better reflect real vehicle-to-vehicle collisions and the kinds and amounts of damage they cause. Instead of a flat barrier, it uses a test barrier shaped like a bumper of a vehicle with a deformable surface. Figure 2.14

shows a test barrier of the Insurance Institute for Highway Safety (IIHS). It is a steel barrier with a plastic absorber and flexible cover to simulate a typical cars' energy absorbers and plastic bumper covers. In these tests, vehicles strike this barrier in 4 tests — full-front and full-rear at 6 mph, plus front and rear corner impacts at 3 mph.

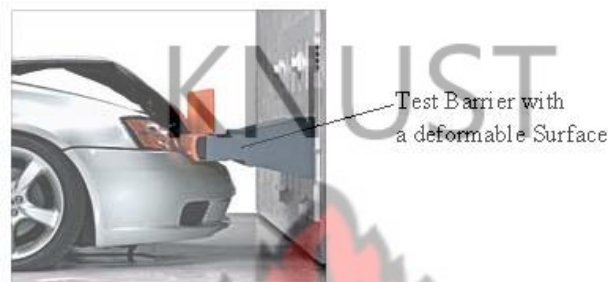


Figure 2.14 An IIHS test barrier with a steel barrier and a plastic absorber and flexible cover

The barrier is set at 45.7 cm (18 inches) off the ground in the front and rear full-width crash tests, and 40.64 cm (16 inches) in the corner impacts. Test results indicate not only the strength of car bumpers but also how well they engage, and then stay engaged with the bumpers on other vehicles with which they collide. These test configurations produce and reflect the kinds and amounts of damage that commonly result from actual low-speed collisions.

Three major components of good bumper design that are lacking on many current passenger vehicles are compatible geometry, stability during

impacts, and effective energy absorption (Aylor et al., 2005). Compatible geometry implies bumpers must be located and sized so they engage the bumper systems on other vehicles with sufficient overlap to account for variations in ride height due to occupant and cargo loading and braking. The stability requirement expects that once engaged, bumper systems offer a stable interface and remain engaged throughout the impact. Apart from meeting the geometry and stability requirements, bumpers still must have sufficient energy absorption capabilities to limit damage to the bumper system itself. Bumper stability is mainly influenced by bumper cover geometry, bumper reinforcement bar shape and strength, and energy absorber design (Aylor et al., 2005).

In economic terms, eighty-one percent of vehicle damage repair estimates are for front or rear impacts, and 65 percent of these entail costs less than \$2,500 (Aylor et al., 2005). Vehicle bumpers could be expected to play a major role in preventing or limiting the damage.

In many cases, vehicles involved in front-into-rear crashes sustained significant damage to safety equipment like lights and cosmetic parts like hoods, fenders, and grilles, with only minor damage to the bumper itself. This is often as a result of underride, either because the bumpers failed to match up or because the bumpers did not remain engaged during the impact (Aylor et al., 2005). To reduce the risk of override/underride, tall bumper beams should be designed such that they will be in alignment with other

vehicles within a specified zone. Research shows that bumpers with deep bumper beams that are aligned with other vehicles, can reduce the risk of underride/override in low speed crashes and lower associated repair costs (Avery and Weekes, 2006).

Bumpers could be designed to absorb more energy than they usually do with some modification of the design and possibly with the use of additional energy absorption devices. Impacts due to vehicle accidents could be attenuated by introducing damping control systems. There are different types of control systems used to attenuate vibrations as a result of an impact. These include active control, semi-active control, and passive control. A combination of two or more of these, called a hybrid control system, also finds itself in some applications.

The Active Control System consists of active mass dampers, active mass drivers, active tendon systems, pulse thrusters and active variable stiffness systems (Lametrie, 2001). Active control is effected through the use of an external energy supply. It uses sensors to detect system response and send information to actuators to apply force to damp vibrations. It requires substantial power and may have instability problems in heavy impacts due to possible power fluctuations and activation response time of the control signal. Active control systems use computer controlled actuators (Lametrie, 2001). The computer processes information according to an algorithm and sends the appropriate signal to the actuator. The actuator then reacts by

applying inertial control forces to the structure to reduce the structural responses in a desired manner.

The Semi Active Control System includes control systems that use relatively low input power to attenuate or damp vibrations. It uses the system's response and a feedback feature to develop control forces and vary the damping properties. With lack of power it still retains its damping properties. Examples of semi-active control systems are Magneto-Rheological Fluid Damper, Variable-Orifice Damper and Controllable Tuned Liquid Damper (Lametrie, 2001).

Passive Control Systems are uncontrolled dampers which require no input power to operate. They attenuate or absorb vibrations automatically without the need of an electrical control system. They are simple and generally low in cost, but are unable to adapt to changing needs after installation. The passive control system was selected for this dissertation because of its stability, simplicity and low cost in its application. Passive systems include base isolation systems, viscoelastic dampers, bracing systems and friction dampers (Lametrie, 2001). *Base Isolation* systems are used to isolate the dynamic force transfer from the structure to the base; *Viscoelastic dampers* attenuate the force due to external loads using their natural damping properties; *Bracing systems* are usually made up of brace frames and are usually used to permanently stabilize buildings from external forces such as wind loads and earthquakes by stiffening the structural components; and

lastly *Friction elements* consist of dampers that use dry friction to dissipate energy. They are also referred to as Coulomb Damping Systems.

The Friction Element was selected for this dissertation mainly due to the fact that it does not need external energy, it is robust, and low cost. Even though viscous damping shares most of these advantages, the friction damper's dryness and therefore no risk of leakages during operation makes it preferable. Other advantages of Coulomb damping compared with viscous damping were observed by (Inman, 1996); they include the following:

1. In damping with Coulomb friction the amplitude decays linearly while in that with a viscous damper it is exponential
2. The motion under Coulomb damping comes to a complete stop at a different equilibrium position than when initially at rest, whereas in a viscous damped system, it oscillates around a single equilibrium.
3. The frequency of oscillation of a system with Coulomb damping is the same as that of the undamped frequency; unlike in viscous damping where the frequency of oscillation is decreased.

2.4.4 Friction Elements

The application of coulomb friction has been useful in different technical products. They are currently used in various applications such as turbines of aircraft engines and power plants, in the protection of buildings against earthquake effects, and generally in applications to reduce vibrations. In

friction dampers, they are generally used to effect and enhance energy dissipation. The purpose of considering them is to identify a friction element that can withstand impact forces equivalent to the collision force.

In most cases friction elements have been studied and used in a passive context. Damping performance of friction elements may be greatly improved by controlling the normal force applied at the friction damper. This notion of producing a damping force by controlling a secondary variable is termed semi-active control (Dupont et al., 1997). Friction dampers have been widely used in turbomachinery applications for a considerable period of time in order to provide mechanical damping to reduce resonance stresses (Sanliturk et al., 2001). Friction dampers find their application also in the attenuation of seismic impacts.

Friction dampers are good at shock and impact attenuation. In this study friction elements that are available will be considered and the ones that would satisfy some design requirements for implementation with a bumper would be considered and modified to be used in the friction damper design concept. This design concept should make use of a passive friction element that makes use of sticking friction to dissipate energy. Among the dampers that have practical applications and were considered are:

1. Slotted-Bolted Connections
2. Sumitomo Passive Energy Dissipation Devices
3. Piezoelectric Friction Damper

4. DAMPTECH™ Friction Devices
5. The Friction Spring Seismic Damper
6. The Energy Dissipating Restraint (EDR)
7. Pall Friction Damper
8. Vehicle Suspension Friction Damper, and
9. Blade-to-Blade and Blade-to-Ground Friction Dampers

These dampers are briefly described in the next section.

2.4.4.1 Slotted-bolted Connections

Slotted-bolted Connections are one of the simplest forms of friction dampers. They consist basically of slotted connecting plates bolted together as shown in Figure 2.15. It is designed to allow slippage of the device to occur before a possible buckle or yield of compressed braces in order to dissipate energy by friction.

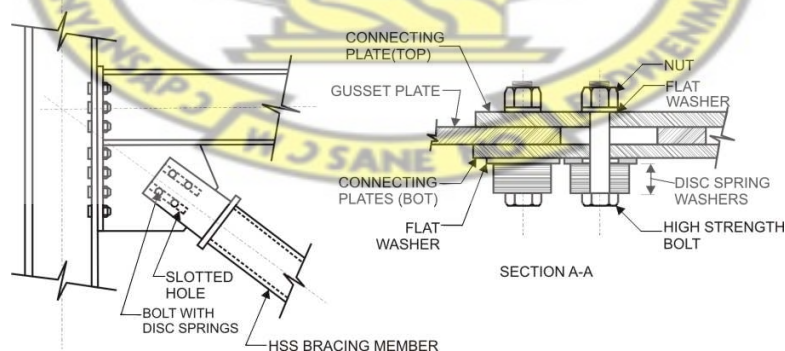


Figure 2.15 Slotted Bolted Connection Assemblage (Tremblay and Stierner, 1993)

Tremblay and Stiemer (1993) found in their study that the sliding connections can exhibit a very high energy dissipation capability under extreme loading conditions, provided appropriate materials and bolt clamping forces are used. This friction damper dissipates energy through the sliding action of two surfaces. That is, it makes use of sliding friction. This makes it not suitable, since it does not meet the design requirement for the concept for this study given in section 2.4.4.

2.4.4.2 Sumitomo Passive Energy Dissipation Devices

The Sumitomo passive energy dissipation device as shown in Figure 2.16 is made up of a cylindrical steel tube casing fitted with friction pads that slide against the inner wall. The sliding surface consists of a bronze friction pad sliding against the steel casing that produces the normal force. The steel casing also has a graphite coating to ensure an even frictional force and to help prevent corrosion. It has a spring connected to the caps of the tube that causes the pads to be pressed against the inner wall and by so doing dissipate energy by friction when there is a relative motion. The friction force may be varied by increasing the stiffness of the cup spring which is done during calibration by the manufacturer. It is used in the railway industry and in seismic applications and are often installed on top of modified chevron braces between adjacent floors in buildings in seismic applications (Ruiz et al., 2005).

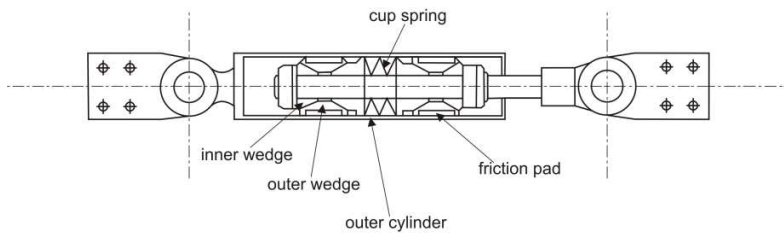


Figure 2.16 Sumitomo Friction Damper (Ruiz et al., 2005)

The Sumitomo Friction Damper concept makes use of passive damping and the relative movements of the steel tube and the friction surfaces can be prevented by selecting a high normal force during manufacture so that sticking friction results. This damper meets the design requirement for this study and can therefore be considered.

2.4.4.3 Piezoelectric Friction Damper

The piezoelectric friction damper consists of several moving and stationary components. Figure 2.17 shows a schematic diagram of the damper. It is made of a shaft fixed to the base. A flex-tensional mechanical amplifier is attached to the shaft. The outer housing and the air bearing make up the moving components. As it vibrates, the outer housing comes into contact with the friction pads. The normal force provided between the friction pads and the outer housing induces a frictional force which retards the motion of the outer housing; thereby dissipating energy. Within the damper is also a spring which connects the moving housing to the stationary base (Unsal et al., 2002).

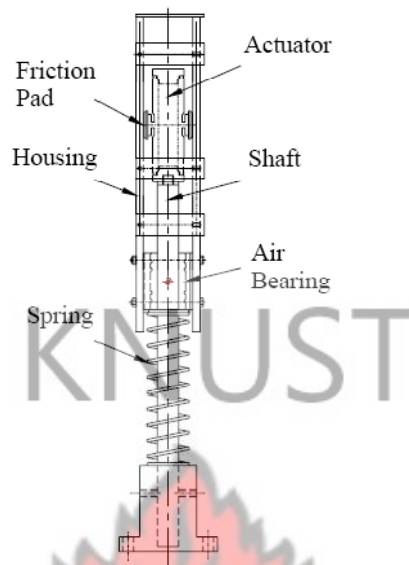


Figure 2.17 Piezoelectric Friction Damper (Unsal et al., 2002)

The piezoelectric friction damper operates by relative motion of the outer moving housing with the friction pads on the stationary central shaft, and through that dissipates energy by sliding friction. This concept does not meet the design requirement for this study. The friction should be static or sticking friction for maximum friction force.

2.4.4.4 Damptech Friction Damper

The damper is made up of a central (vertical) plate, two side (horizontal) plates, and two circular friction pads placed between the steel plates as shown in Figure 2.18. The central plate is attached to the girder mid-span in a frame structure by a hinge. The hinge allows some relative rotation

between the central and side plates, which in turn enhances the energy dissipation in the system. The ends of the two side plates are connected to the members of inverted V-brace at some distance from the friction damper's centre. The bracing makes use of pre-tensioned bars in order to avoid compression stresses which could cause buckling. The bracing bars are pin-connected at both ends to the damper and also to the column bases (Mualla and Belev, 2002).

KNUST

The two side plates and one central plate are so designed to increase the frictional surface area and provide the symmetry needed for obtaining plane action of the device. A pre-tightened adjustable bolt connects the three plates of the damper to one another. This adjustable bolt is used to control the compression force applied on the interfaces of the friction pad discs and steel plates. Several discs of the spring washers (Belleville washers) are used. Hardened washers are placed between these springs and the steel plates to protect the plate surface from any marks and scratches when the springs are under compression (Mualla and Belev, 2002).

The device configuration is very simple. It can be arranged in different bracing configurations to obtain a complete damping system. Figure 2.19 shows the mechanism and principle of operation of the friction damper. When a lateral force excites a frame structure, the girder tends to displace horizontally. The bracing system and the forces of friction developed at the

interface of the steel plates and friction pads then tend to resist the horizontal motion (Mualla and Belev, 2002).

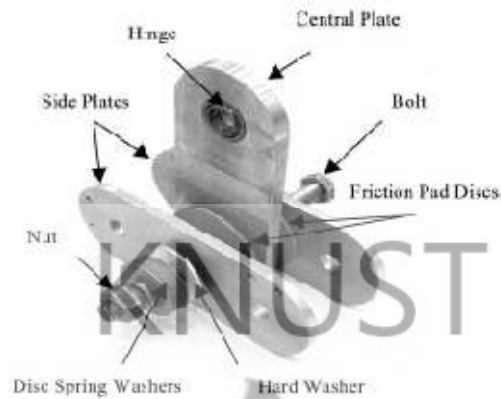


Figure 2.18 Components of the Damptech Friction Damper

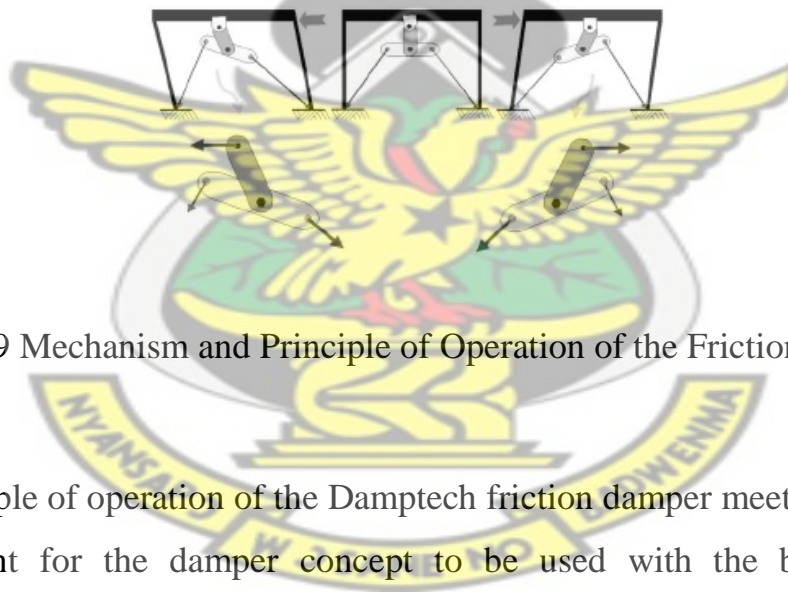


Figure 2.19 Mechanism and Principle of Operation of the Friction Damper

The principle of operation of the Damptech friction damper meets the design requirement for the damper concept to be used with the bumper. It dissipates energy by a passive means and the compression force on the friction surfaces can be increased to avoid sliding.

2.4.4.5 The Friction Spring Seismic Damper

The SHAPIA seismic damper, also known as the friction spring damper, uses ring springs, also called friction springs, to dissipate seismic-induced energy. It is based on a self-centering friction mechanism and is used in seismic applications (Filiatrault et al., 2000). A section through a typical ring spring assembly, as shown in Figure 2.20, consists of outer and inner rings that have tapered mating surfaces. When the spring column is loaded in compression, the axial displacement induces the sliding of the rings on the conical friction surfaces. The outer rings are subjected to circumferential tension (hoop stress), and the inner rings to compression. The ring springs are designed to remain elastic during a seismic impact so that no repair or replacement of parts is required, and the structure is protected against aftershocks and future earthquakes (Filiatrault et al., 2000).

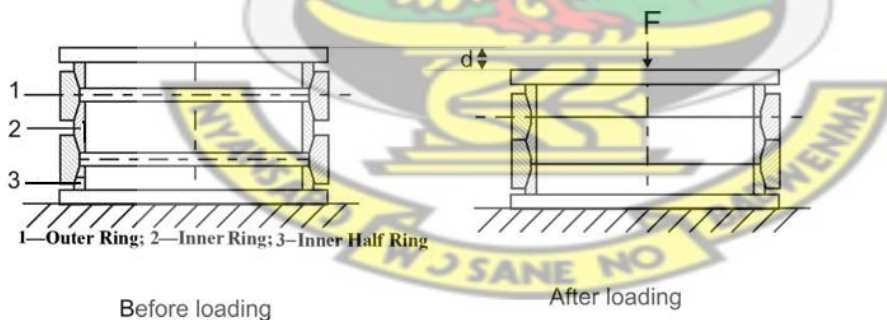


Figure 2.20 Friction Spring Details, (Filiatrault et al., 2000).

The principle of operation of the friction spring damper meets the design requirement for the damper concept to be used with the bumper. It

dissipates energy by a passive means and the principle of operation can prevent sliding.

2.4.4.6 Energy Dissipating Restraint

The Energy Dissipating Restraint (EDR) was originally designed and developed as a seismic restraint device for the support of piping systems in nuclear power plant. Figure 2.21 shows a drawing of the damper. The mechanism of the EDR consists of sliding friction through a range of motion with a stop at the end of its range of motion. The device is self-centering and the frictional force is proportional to the displacement. Depending on the spring constant of the core, the initial slip load, the configuration of the core, and the gap size, several different types of hysteretic behaviour of the damper are possible (Aiken et al., 1993).

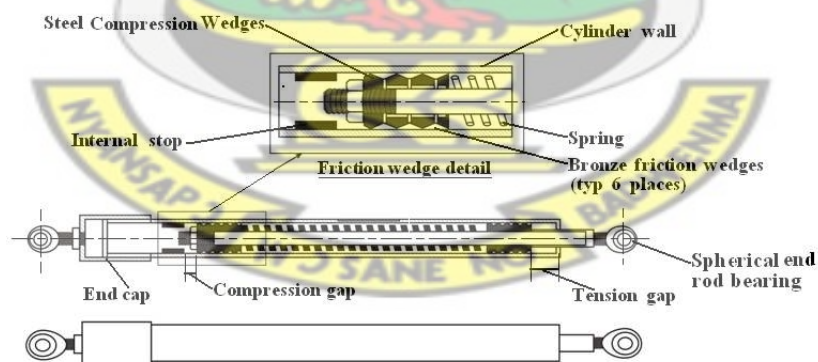


Figure 2.21 External and internal views of the EDR (Aiken et al., 1993)

The mode of operation of the EDR consists of sliding friction through a range of motion with a stop at the end of its range of motion, as a result it does not meet the design requirement needed for the concept for this study.

2.4.4.7 Pall Friction Damper

The Pall friction dampers are made up of a series of specially treated steel plates, clamped together with high strength steel bolts. They have friction interfaces at their intersection points. Figure 2.22 shows a schematic diagram of the friction damper, and Figure 2.23 its deformation configuration. The Pall friction damper is designed to develop constant and stable friction. They are designed not to slip during impacts like windstorms, service loads and minor earthquakes. During a major earthquake, the friction dampers slip at a predetermined optimum load before yielding begins in other structural members, and they dissipate a good portion of the seismic energy to protect the buildings (Malhotra et al., 2004).

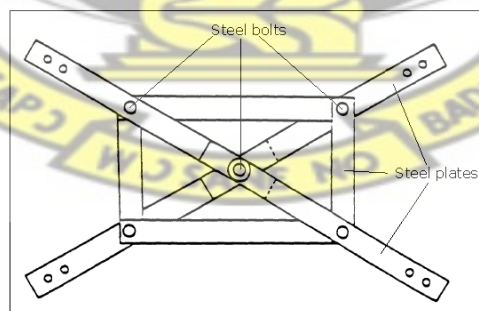


Figure 2.22 Pall Friction Damper

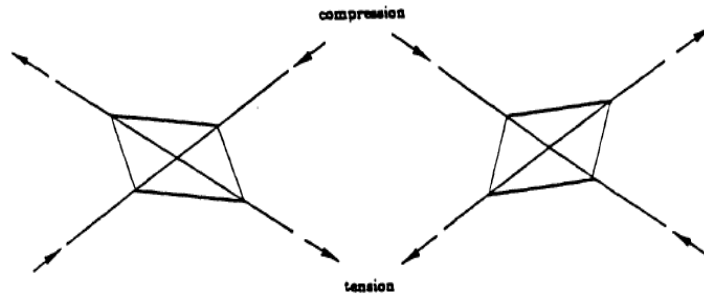
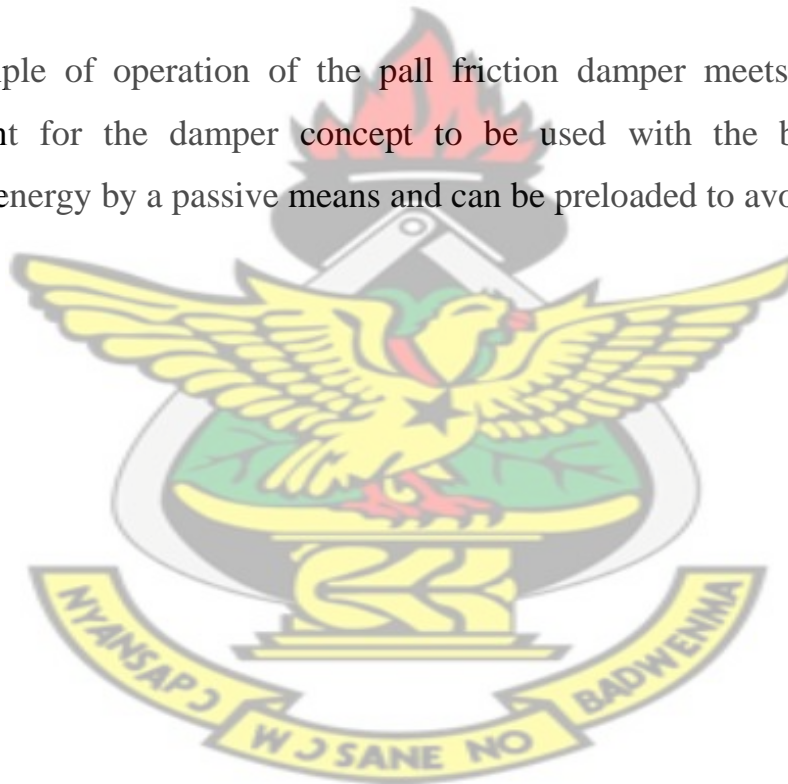


Figure 2.23 Deformation configuration of the Pall friction Damper

The principle of operation of the pall friction damper meets the design requirement for the damper concept to be used with the bumper. It dissipates energy by a passive means and can be preloaded to avoid sliding.



2.4.4.8 Vehicle Suspension Friction Damper

Friction dampers can be designed for different purposes to dissipate energy by coulomb friction. For their experimental studies, Guglielmino and Edge constructed a single friction damper in such a manner as to be able to replace a conventional viscous damper in a vehicle. Figure 2.24 shows drawing of the damper. The design concept was a piston in a cylindrical housing which contains two diametrically-opposed pistons with friction pads bonded to them such that the pistons are controlled with hydraulic oil through the centre of the piston rod with the control valve mounted remotely (Guglielmino and Edge, 2004).

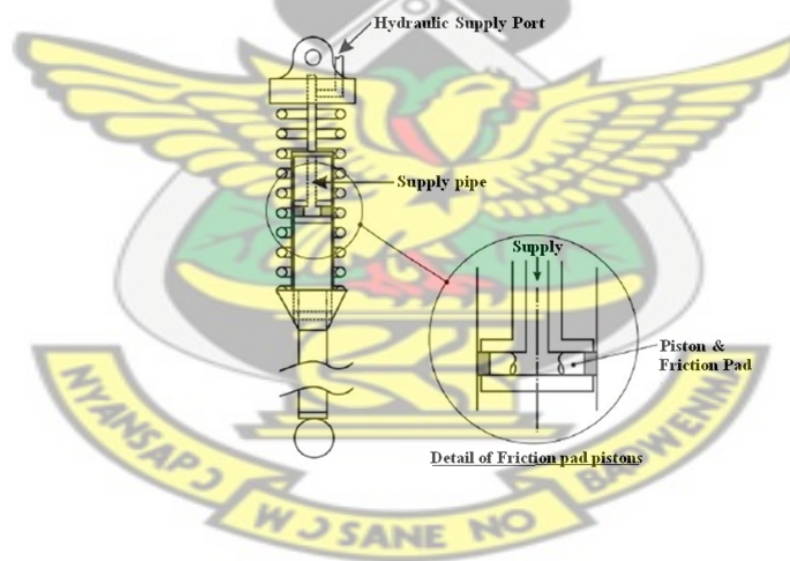


Figure 2.24 Friction damper concept in a cylindrical housing (Guglielmino and Edge, 2004)

The principle of operation of the vehicle suspension friction damper is not passive. Hydraulic oil will have to be pumped into the damper to control the pistons with the friction pads. There could be the risk of a leakage and also external power or energy is needed to pump the hydraulic oil. Therefore it does not meet the design requirement of the damper needed for this study.

2.4.4.9 Blade-to-Blade and Blade-to-Ground Friction Dampers

Special friction dampers are used in turbo-machinery applications to avoid undesired large vibration amplitudes that could lead to blade damage and fracture. Such dampers are designed as either blade-to-blade (BB or underplatform) or blade-to-ground (BG) dampers. Underplatform dampers, are pressed against the platforms of adjacent blades, as shown in Figure 2.25, at the reference points OL and OR by centrifugal forces (Ciğeroğlu and Özgüven, 2006). It is generally designed as a small piece of metal with friction surface, which usually is wedge-like (or sometimes other shapes), and is located underneath the blade platforms. Dissipation of vibration energy into thermal energy starts when blade displacements reach a certain level (Petrov and Ewins, 2007). Relative displacements between the blade platforms and the damper generate friction forces to dissipate energy as desired (Panning et al., 2003).

The blade-to-ground on the other hand is realized by placement of dry friction dampers between the blades and the cover plate (Ciğeroğlu and Özgüven, 2006).

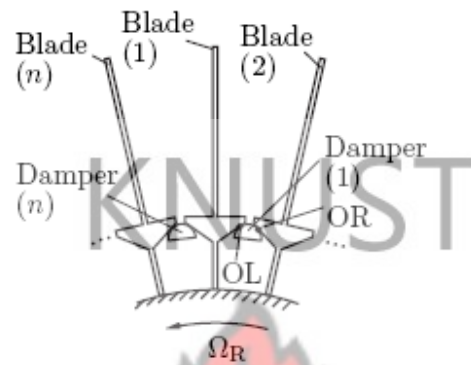


Figure 2.25 Bladed disk with an underplatform damper (Ciğeroğlu and Özgüven, 2006)

Both types of dampers have similar effects in terms of vibration damping; however, low frequency behaviour of the system changes if BG dampers are used since the system changes from positive semi-definite to positive definite. These dampers dissipate energy in the form of heat due to the rubbing motion of the contacting surfaces resulting from relative motion.

The blade-to-blade and blade-to-ground friction damper concepts dissipate energy in the form of heat due to the rubbing motion of the contacting surfaces resulting from relative motion. This is possible through sliding friction. This damper therefore does not meet the design requirement necessary for this study, which should be sticking friction.

2.5 *Summary*

In this chapter the capabilities of the traditional bumper was considered. Different impact attenuation devices were investigated to see how they could be integrated into bumpers to improve their capability of impact attenuation. Factors that contribute to road traffic accidents were also discussed. Generally, road crashes are attributable to three main factors, namely the condition of the vehicle, the performance of the driver or the condition of the road. It could, however, also be caused by a combination of these factors as well. Roads, depending on their design and condition, can contribute to road traffic accidents. A road could be considered as a properly designed roadway if it takes into consideration efficient mobility and safety.

The effect of Periodic Motor Vehicle Inspections (PMVI) programs on accident rates was found to vary significantly, from no effect to decreasing the accident rate up to as much as 16%. A USA study found out that PMVI was associated with a reduction of 2.5%. Some studies suggest that periodic roadworthiness tests, in other words PMVI, could reduce the number of crashes caused by vehicle defects by about 50% (Rechnitzer et al., 2000).

Bumpers could be designed to absorb more energy than they usually do with some modification of the design and, possibly, with the use of additional energy absorption devices. Impacts due to vehicle accidents could be attenuated by introducing damping control systems. The Active Control

Systems are effected through the use of an external energy supply. They make use of sensors to detect system response and send information to actuators to apply force to damp vibrations and require substantial power. The actuator then reacts by applying inertial control forces to the structure to reduce the structural responses in a desired manner. The Semi Active Control System includes control systems that use relatively low input power to attenuate or damp vibrations. It uses the system's response and a feedback feature to develop control forces and vary the damping properties. With lack of power it still retains its damping properties. The Passive Control Systems are uncontrolled dampers, which require no input power to operate. They attenuate or absorbs the vibrations automatically without the need of an electrical control system. They are simple and generally low in cost, but are unable to adapt to changing needs after their installation.

The passive control system with a friction element was selected for this dissertation because of its stability, simplicity and low cost in its application. Among the friction dampers studied, the friction dampers that meet the design requirements as far as this study is concerned are the Sumitomo, DamptechTM, friction spring seismic, and the pall friction dampers. They use a passive control concept and can work on the principle of sticking friction. These will be considered and modified to get some design concepts for the friction damper to be used in the Bumper-Damper System to attenuate impact energy due to crashes. The next chapter will discuss the modeling and simulation of the attenuation system in order to evaluate and select an appropriate friction element for the design.

CHAPTER THREE

3.0 Modelling, Simulation and Data Extraction

This chapter deals with modelling a friction damper, the simulation of the damper response and data extraction from the simulation for design purposes. The chapter presents the Maxwell, Kelvin and two Hybrid Models for the bumper. It also presents a visual simulation software and discusses how it was used to program and simulate the friction damper. It then focuses on how the simulation software was used to generate the relevant information. MATLAB™ is also used to post-process the data generated from the visual simulation.

3.1 Modeling of Impact Attenuators

The bumpers of most vehicles are made basically of visco-elastic materials (Huang, 2002). Properties of visco-elastic materials include:

- Creep: increase in strain with time when the applied stress is kept constant.
- Relaxation: decrease in stress with time when the applied strain is kept constant.

- Dependence of the effective stiffness on the strain rate.
- Loss of energy due to hysteresis and
- Coefficient of restitution that is less than one.

In modelling the bumper, there is the need to address these behaviour. The loss and storage of energy as well as creep and relaxation phenomena are usually modelled with spring and dashpot elements. The two main simple models that can address these are known as the Maxwell and Kelvin Models. Both models make use of a spring and a viscous damper. On the other hand a hybrid of the two, called the Solid or the Hybrid Model is also used to model this behaviour. The elements of the model can be arranged in two different ways, giving two types of Hybrid models; the Hybrid 1 and Hybrid 2 models (Huang, 2002).

3.1.1 The Maxwell Model

The Maxwell Model consists of a spring and a damper connected in series. Figure 3.1(a) shows the Maxwell model and Figure 3.1 (b) and (c) the free body diagrams of the Maxwell model. The elements of the model are considered to be massless and uni-axial.

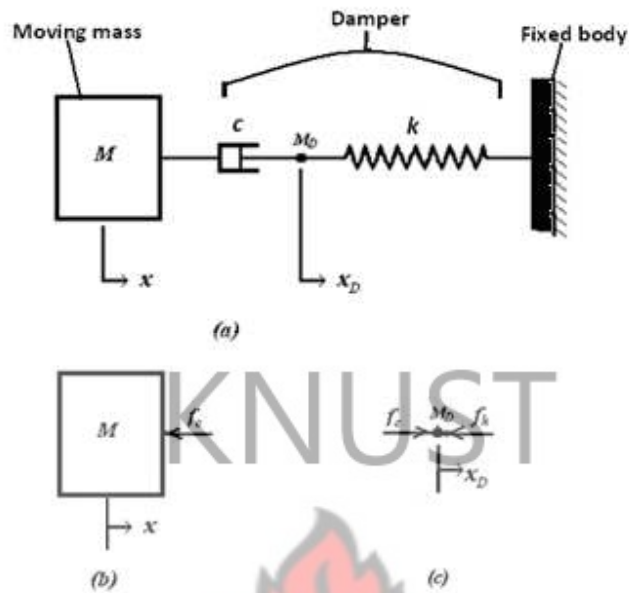


Figure 3.1 Schematic of a Maxwell Model and its Free Body Diagrams

Equations of motion for the damper deflection and the total deflection are derived next:

Let:

Force on the viscous damper at impact = f_c

Force on the spring at impact = f_k

Deflection of the mass = x

the small mass $M_D = 0$

deflection of $M_D = x_D$

spring constant = k

damping coefficient of the damper = c

Then consider the mass M ,

$$M\ddot{x} = -f_c = -c(\dot{x} - \dot{x}_D) \quad (3.1)$$

and considering the mass M_D

$$\sum F = M_D a_D = M_D \ddot{x}_D$$
$$M_D \ddot{x}_D = f_c - f_k = c(\dot{x} - \dot{x}_D) - kx_D \quad (3.2)$$

Differentiating (3.1) and (3.2) with respect to t , and setting $M_D = 0$

$$M\ddot{x} = -c(\ddot{x} - \ddot{x}_D) \quad (3.3)$$

$$M_D \ddot{x}_D = 0 = c(\ddot{x} - \ddot{x}_D) - k\dot{x}_D \quad (3.4)$$

Substituting (3.3) into (3.4) and rearranging:

$$\dot{x}_D = -\frac{M}{k}\ddot{x} \quad (3.5)$$

substituting (3.5) into (3.1)

$$M\ddot{x} = -c\left(\dot{x} + \frac{M}{k}\ddot{x}\right)$$

Rearranging gives $\ddot{x} + \frac{k}{c}\ddot{x} + \frac{k}{M}\dot{x} = 0$ (3.6)

with the characteristic equation:

$$s\left(s^2 + \frac{k}{c}s + \frac{k}{M}\right) = 0 \quad (3.7)$$

where $s = \frac{d}{dt}$.

For the Maxwell model the mass may or may not have a rebound. The differential equation can be solved for the two situations.

Case I : Real roots; $\left(\frac{k}{c}\right)^2 > 4\frac{k}{M}$. The solution is (Huang, 2002):

with initial conditions:

at $t = 0$: $x = 0, \dot{x} = v, \ddot{x} = 0$.

$s_0 = 0$, and two negative real roots, $s_1 = a + b$ and $s_2 = a - b$. where $a = \frac{-k}{2c}$

and $b = \sqrt{\left(\frac{k}{2c}\right)^2 - \frac{k}{M}}$

$s_1 > s_2$ or $s_1 - s_2 > 0$

To simplify the expression of the solution, let d_0, d_1 and d_2 be defined such that:

$$d_0 = \frac{v(s_1 + s_2)}{s_1 s_2}, d_1 = \frac{v s_2}{s_1 (s_1 - s_2)}, d_2 = \frac{-v s_1}{s_2 (s_1 - s_2)}, \dot{x}(t=0) = v$$

$$x = d_0 e^{-s_0 t} + d_1 e^{-s_1 t} + d_2 e^{-s_2 t}, \quad (3.8)$$

$$\dot{x} = -d_0 s_0 e^{-s_0 t} - d_1 s_1 e^{-s_1 t} - d_2 s_2 e^{-s_2 t} \text{ and} \quad (3.9)$$

$$\ddot{x} = d_0 s_0^2 e^{-s_0 t} + d_1 s_1^2 e^{-s_1 t} + d_2 s_2^2 e^{-s_2 t} \quad (3.10)$$

Case II : $\left(\frac{k}{c}\right)^2 < 4\frac{k}{M}$. The solution is (Huang, 2002):

$s_0 = 0$, and two complex roots, $s_1 = a + ib$ and $s_2 = a - ib$. where $a = \frac{-k}{2c}$ and

$$b = \sqrt{\frac{k}{M} - \left(\frac{k}{2c}\right)^2}$$

For $d_0 = -d_2$, $d_1 = \frac{v - ad_2}{b}$, $d_2 = \frac{2av}{a^2 + b^2}$

$$x = d_0 e^{s_0 t} + e^{at} [d_1 \sin(bt) + d_2 \cos(bt)] \quad (3.11)$$

$$\dot{x} = e^{at} [(ad_1 - bd_2) \sin(bt) + (bd_1 + ad_2) \cos(bt)] \quad (3.12)$$

$$\ddot{x} = e^{at} [(a^2 - b^2)d_1 - 2abd_2] \sin(bt) + [(a^2 - b^2)d_2 + 2abd_1] \cos(bt) \quad (3.13)$$

With the initial conditions: at $t=0, x=0, \dot{x}=v, \ddot{x}=0$. x could also be solved using numerical integration.

Typical transient response of the displacement, velocity and acceleration for the Maxwell model at an impact velocity of 4.5 m/s are shown in Figures 3.2, 3.3 and 3.4 respectively. Each Figure shows the response for a given damping coefficient ($c = 52.54$ kN-s/m) and three different levels of spring stiffness, referred to as stiff (35,027 kN/m), regular (5,254 kN/m) and soft (525.4 kN/m), (Huang, 2002). Different values for the spring constant and

damping coefficients were used to study the responses for evaluation and selection of an appropriate model for the study in Section 3.2.

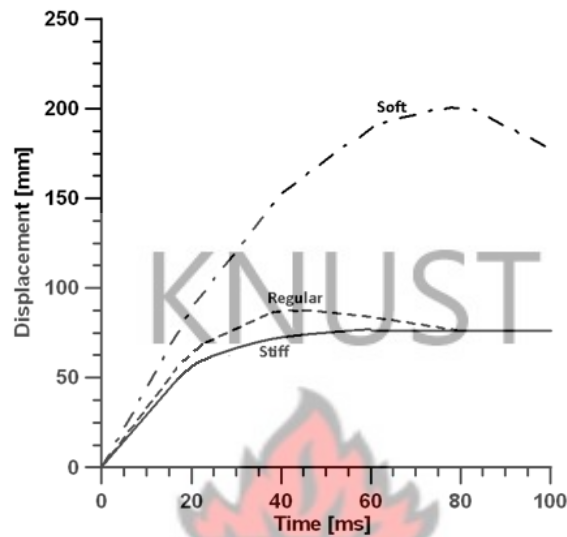


Figure 3.2 Typical Displacement Response for three different Spring Stiffness levels for the Maxwell Model

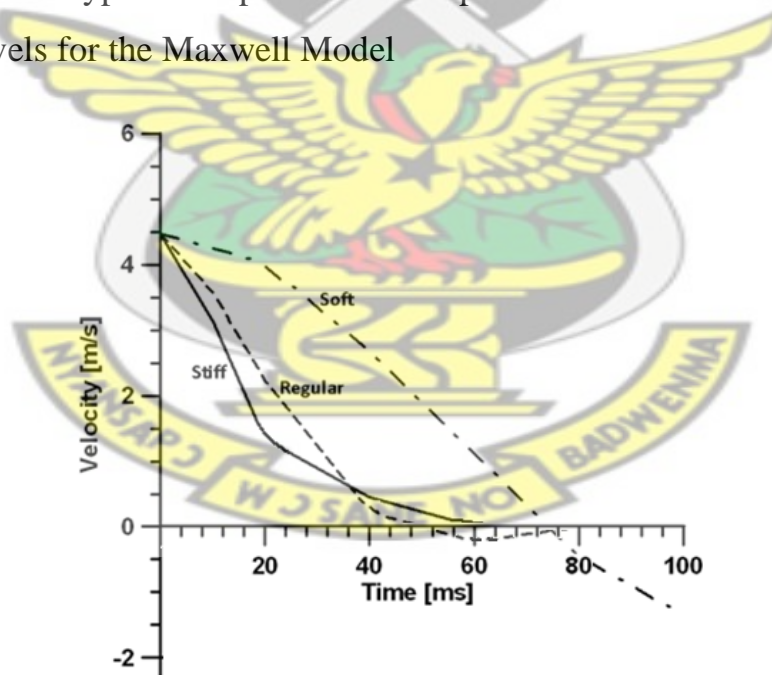


Figure 3.3 Typical Velocity Response for three different Spring Stiffness levels for the Maxwell Model

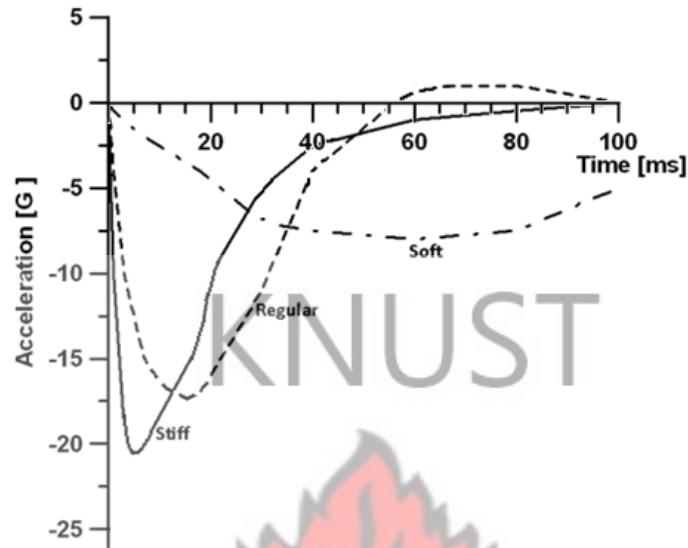


Figure 3.4 Typical Acceleration Response for three different Spring Stiffness levels for the Maxwell Model

3.1.2 The Kelvin Model

The Kelvin model (Huang, 2002) consists of two elements; a spring and a dashpot connected in parallel. Figure 3.5(a) shows a schematic diagram of the Kelvin model and Figure 3.5(b) shows its free body diagram. The differential equation representing the model can be obtained.

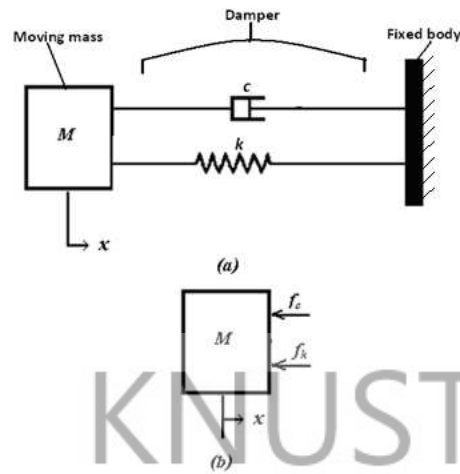


Figure 3.5 Schematic of a Kelvin Model and its Free Body Diagram

Let:

Force on the viscous damper at impact = f_c

Force on the spring at impact = f_k

deflection of the mass = x

deflection of the damper = deflection of the spring = x

spring constant = k

damping coefficient of the damper = c

For the mass, M ,

$$\sum F = Ma = M\ddot{x} \quad (3.14)$$

$$\text{Therefore } M\ddot{x} = -f_c - f_k \quad (3.15)$$

$$f_c = c\dot{x}$$

$$f_k = kx$$

which implies that: $M\ddot{x} = -c\dot{x} - kx$ (3.16)

The equation of motion (3.16) can be re-written using

$$\omega_e = \sqrt{\frac{k}{M}}; \zeta = \frac{c}{2M\omega_e} \text{ as}$$

$$\ddot{x} + 2\zeta\omega_e\dot{x} + \omega_e^2 x = 0; \tag{3.17}$$

where ζ is the damping factor and ω_e is the natural frequency of the system.

This can be rewritten as $s^2 + 2\zeta\omega_e s + \omega_e^2 = 0$; where $s = \frac{d}{dt}$, and with initial

conditions $x(t=0) = 0$, $\dot{x}(t=0) = v_0$

and $\ddot{x}(t=0) = 0$. The solution of the second order differential equation is (Huang, 2002):

Underdamped system: $1 > \zeta > 0$

Roots of the characteristic equation are: $s_1 = a + ib$ and $s_2 = a - ib$

where: $a = -\zeta\omega_e$; $b = \omega_e\sqrt{1 - \zeta^2}$

General solution: $x = e^{at}\{c_1 \sin(bt) + c_2 \cos(bt)\}$, where c_1 and c_2 are constants (3.18)

Critically damped system: $\zeta = 1$

Roots of the characteristic equation are: $s_1 = a + ib$ and $s_2 = a - ib$

From the general solution: $x = e^{at} \{c_1 \sin(bt) + c_2 \cos(bt)\}$ applying the conditions:

$$as: \zeta \rightarrow 1; bt = \omega_e t \sqrt{1 - \zeta^2} \rightarrow 0; \text{and}, s_1 = s_2 = a$$

For $t \ll 1$; $\sin(bt) \rightarrow bt, \cos(bt) \rightarrow 1$ therefore $x = e^{at} [c_1 + c_2 t]$

but with n repeated roots, $s_1 = s_2 = \dots = s_n = a$; $x = e^{at} [c_1 + c_2 t + \dots + c_n t^{n-1}]$

Overdamped system: $\zeta > 1$

General solution: $x = c_1 e^{at} + c_2 e^{at}$

$$\text{where: } a = \omega_e (-\zeta + \sqrt{\zeta^2 - 1}) < 0; b = \omega_e (-\zeta - \sqrt{\zeta^2 - 1}) < 0$$

The constants c_1 and c_2 can be found by using the initial conditions. The closed form solution for the transient responses of an overdamped system using the initial conditions is as follows:

$$x(t) = \frac{v_0 e^{-\zeta \omega_e t}}{\omega_e \sqrt{1 - \zeta^2}} \sin(\omega_e t \sqrt{1 - \zeta^2}) \quad (3.19)$$

$$\dot{x}(t) = v_0 e^{-\zeta \omega_e t} \left[\cos(\omega_e t \sqrt{1 - \zeta^2}) - \frac{\zeta}{\sqrt{1 - \zeta^2}} \sin(\omega_e t \sqrt{1 - \zeta^2}) \right] \quad (3.20)$$

$$\ddot{x}(t) = v_0 \omega_e e^{-\zeta \omega_e t} \left[-2\zeta \cos(\omega_e t \sqrt{1 - \zeta^2}) + \frac{2\zeta^2 - 1}{\sqrt{1 - \zeta^2}} \sin(\omega_e t \sqrt{1 - \zeta^2}) \right] \quad (3.21)$$

The response can be normalized using factors of an undamped system. The aim is to make the relationship between the normalized responses and time

independent of undamped natural frequency, ω_e and impact velocity v_0 . Factors used are v_0/ω_e for displacement, v_0 for the velocity and $v_0\omega_e$ for acceleration. The time t is normalized by multiplying it by ω_e (the angular natural frequency of the system) to obtain the non-dimensional time variable, τ .

The normalized transient responses are therefore:

$$\frac{x(t)\omega_e}{v_0} = \frac{e^{-\zeta\tau}}{\sqrt{1-\zeta^2}} \sin(\tau\sqrt{1-\zeta^2}) \quad (3.22)$$

$$\frac{\dot{x}(t)}{v_0} = e^{-\zeta\tau} \left[\cos(\tau\sqrt{1-\zeta^2}) - \frac{\zeta}{\sqrt{1-\zeta^2}} \sin(\tau\sqrt{1-\zeta^2}) \right] \quad (3.23)$$

$$\frac{\ddot{x}(t)}{v_0\omega_e} = e^{-\zeta\tau} \left[-2\zeta \cos(\tau\sqrt{1-\zeta^2}) + \frac{2\zeta^2-1}{\sqrt{1-\zeta^2}} \sin(\tau\sqrt{1-\zeta^2}) \right] \quad (3.24)$$

Similarly the critically damped transient responses are:

$$x(t) = v_0 t e^{-\omega_e t} \quad (3.25)$$

$$\dot{x}(t) = v_0 (1 - \omega_e t) e^{-\omega_e t} \quad (3.26)$$

$$\ddot{x}(t) = v_0 \omega_e (\omega_e t - 2) e^{-\omega_e t} \quad (3.27)$$

This can be normalized using the same normalizing factors as in the underdamped system, which gives:

$$\frac{x(t)\omega_e}{v_0} = \tau e^{-\tau} \quad (3.28)$$

$$\frac{\dot{x}(t)}{v_0} = (1 - \tau) e^{-\tau} \quad (3.29)$$

$$\frac{\ddot{x}(t)}{v_0 \omega_e} = (\tau - 2)e^{-\tau} \quad (3.30)$$

The transient response of the displacement, velocity and acceleration for a typical Sedan car of mass 1590 kg, with spring constant, $k = 433280$ N/m and coefficient of damping, $c = 7303$ N-s/m for Kelvin model at an impact velocity, $v_0 = 14$ m/s, are shown in Figure 3.6.

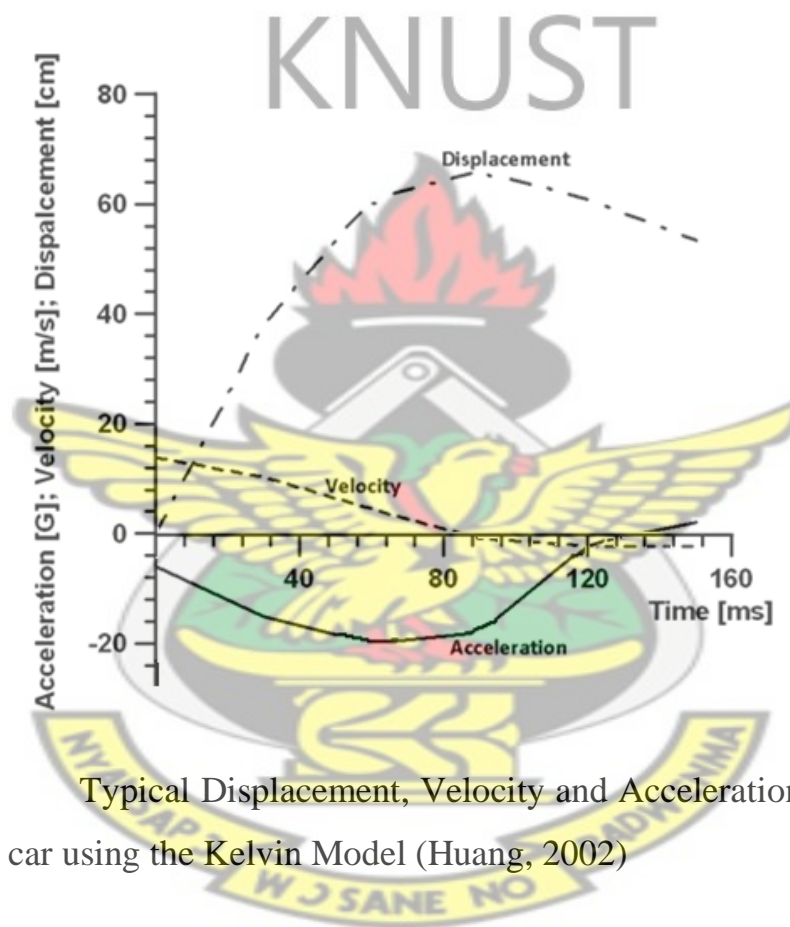


Figure 3.6 Typical Displacement, Velocity and Acceleration Responses of a Sedan car using the Kelvin Model (Huang, 2002)

3.1.3 The Hybrid 1 Model

Two types of hybrid models were considered, Hybrid 1 model and Hybrid 2 model. The Hybrid models combine the Kelvin and Maxwell models making use of two springs and a dashpot. Hybrid 1 model combines a spring k_1 in

parallel with the Maxwell model. Figure 3.7 (a) shows the model and Figure 3.7 (b) and (c) its free body diagrams.

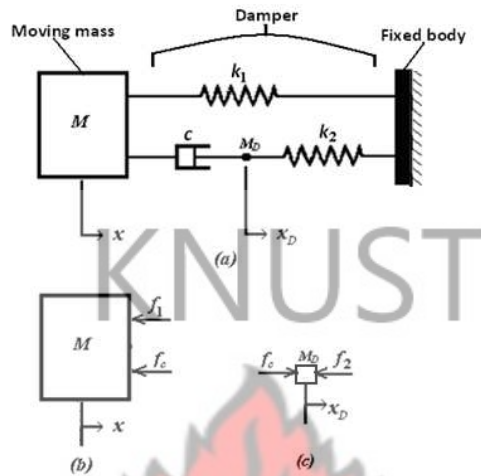


Figure 3.7 Hybrid 1 Model and its Free Body Diagrams

Let :

force on the damper c at impact $= f_c$

spring constant for spring one $= k_1$

spring constant for spring two $= k_2$

damping coefficient of the damper $c = c$

Then:

$$f_1 = k_1 x$$

$$f_2 = k_2 x_D$$

$$f_c = c(\dot{x} - \dot{x}_D)$$

$$\sum F = Ma = M\ddot{x}$$

Therefore for a mass, M , $M\ddot{x} = -f_1 - f_c = -k_1x - c(\dot{x} - \dot{x}_D)$ and (3.31)

$$\sum F = M_D a_D = M_D \ddot{x}_D$$

Therefore $M_D \ddot{x}_D = f_c - f_2 = c(\dot{x} - \dot{x}_D) - k_2 x_D$ (3.32)

$$M_D \ddot{x}_D = f_c - f_2 = c(\dot{x} - \dot{x}_D) - k_2 x_D$$

Setting the small mass to zero ($M_D = 0$) gives $f_c = f_2$ (3.33)

Substituting (3.33) into (3.31) gives:

$$M\ddot{x} = -k_1x - k_2x_D$$

Rearranging: $x_D = \frac{-M\ddot{x} - k_1x}{k_2}$ (3.34)

Differentiating (3.34) with respect to t gives

$$\dot{x}_D = \frac{-M\ddot{x} - k_1\dot{x}}{k_2}$$
 (3.35)

substituting (3.35) into (3.31)

$$M\ddot{x} = -k_1x - c\dot{x} + c\left(\frac{-M\ddot{x} - k_1\dot{x}}{k_2}\right)$$

rearranging gives

$$\frac{cM\ddot{x}}{k_2} + M\ddot{x} + \left(c + \frac{ck_1}{k_2}\right)\dot{x} + k_1x = 0$$
 (3.36)

multiplying equation (3.36) by $\frac{k_2}{cM}$ gives the final differential equation for the model:

$$\ddot{x} + \frac{k_2}{c}\dot{x} + \left(\frac{k_1 + k_2}{M}\right)x + \frac{k_1 k_2}{cM}x = 0 \quad (3.37)$$

Then substituting $s = \frac{d}{dt}$, the characteristic equation of the Hybrid 1 model becomes:

$s^3 + ws^2 + us + v = 0$ with the following definitions for w , u and v :

let $\omega_e = \sqrt{\frac{k_1}{M}}$ undamped (angular) natural frequency

$\zeta = \frac{c}{2M\omega_e}$, the damping factor, and $R = \frac{k_2}{k_1}$

Then $w = \frac{k_2}{c} = \frac{-R\omega_e}{2\zeta}$, $u = \frac{k_1 + k_2}{M} = (1+R)\omega_e^2$, $v = \frac{k_1 k_2}{cM} = \frac{-R\omega_e^3}{2\zeta}$

Let $\varepsilon = \frac{u + \frac{v}{\beta}}{2\beta}$ and $\omega = \sqrt{\left(\varepsilon^2 + \frac{v}{\beta}\right)}$ with β , ε and ω in radians

Then the roots of the differential equation are: $\beta, \varepsilon + i\omega$ and $\varepsilon - i\omega$ (one real and two complex roots); the solution of the differential equation is given by the following equations (Huang, 2002):

let $p' = \frac{-2\varepsilon}{(\beta - \varepsilon)^2 + \omega^2}$, $q' = \frac{\beta^2 - \varepsilon^2 + \omega^2}{\omega[(\beta - \varepsilon)^2 + \omega^2]}$, then $p = p'\dot{x}$, $q = q'\dot{x}$

$$x = -pe^{-\beta t} + e^{-\varepsilon t}(p \cos \omega t + q \sin \omega t) \quad (3.38)$$

$$\dot{x} = p\beta e^{-\beta t} + e^{-\varepsilon t} [\omega(-p \sin \omega t + q \cos \omega t) - \varepsilon(p \cos \omega t + q \sin \omega t)] \quad (3.39)$$

$$\ddot{x} = -p\beta^2 e^{-\beta t} + e^{-\varepsilon t} [(\varepsilon^2 - \omega^2)(p \cos \omega t + q \sin \omega t) + 2\varepsilon\omega(p \sin \omega t - q \cos \omega t)] \quad (3.40)$$

A typical transient response of the displacement, velocity and acceleration against time for the Hybrid 1 model are shown in Figure 3.8.

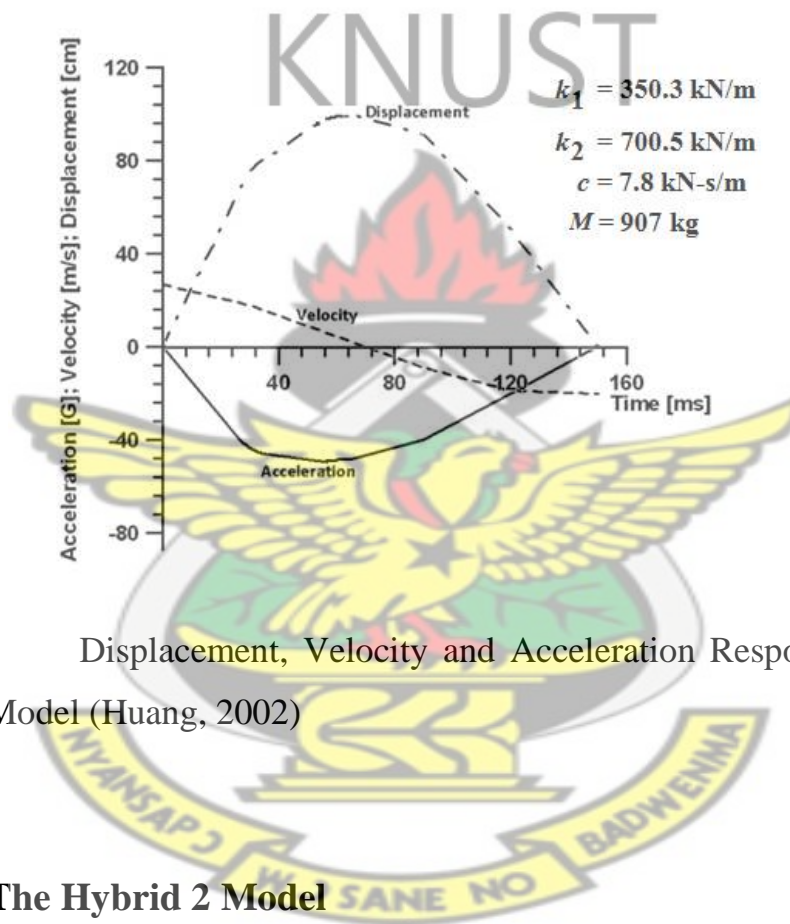


Figure 3.8 Displacement, Velocity and Acceleration Responses of the Hybrid 1 Model (Huang, 2002)

3.1.4 The Hybrid 2 Model

The second hybrid model, Hybrid 2 model also combines two springs with a dash pot. It combines the Kelvin model in series with a spring. Figure 3.9 (a) shows the model and Figure 3.9 (b) and (c) its free body diagrams.

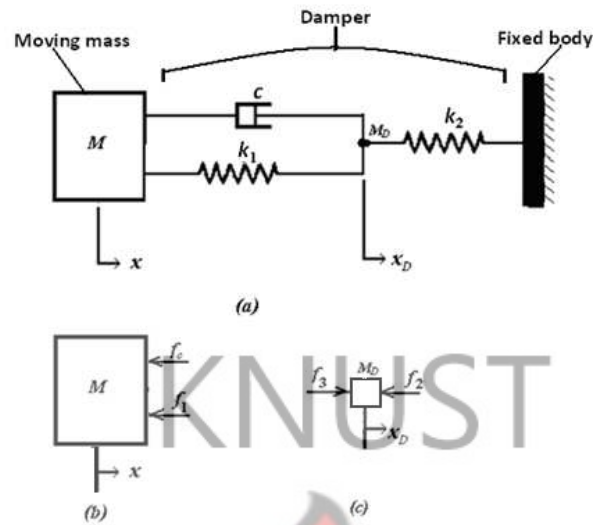


Figure 3.9 Hybrid 2 Model and its Free Body Diagrams

Let :

force on the damper c at impact $= f_c$

force on the spring k_1 at impact $= f_1$

force on the spring k_2 at impact $= f_2$

Then:

$$(3.41)$$

$$f_c = c(\dot{x} - \dot{x}_D)$$

$$f_1 = k_1(x - x_D)$$

$$(3.42)$$

$$f_2 = k_2 x_D$$

$$(3.43)$$

$$f_3 = f_1 + f_c$$

$$(3.44)$$

But

$$\sum F = Ma = M\ddot{x}$$

Therefore $M\ddot{x} = -f_1 - f_c = -k_1(x - x_D) - c(\dot{x} - \dot{x}_D)$ (3.45)

and

$$\sum F = M_D a_D = M_D \ddot{x}_D$$

Therefore

$$M_D \ddot{x}_D = -f_2 + f_3 = -f_2 + f_1 + f_c$$

$$M_D \ddot{x}_D = -k_2 x_D + k_1(x - x_D) + c(\dot{x} - \dot{x}_D)$$

Setting the small mass to zero ($M_D = 0$) gives

$$0 = -k_2 x_D + k_1(x - x_D) + c(\dot{x} - \dot{x}_D)$$

$$k_2 x_D = k_1(x - x_D) + c(\dot{x} - \dot{x}_D)$$
 (3.46)

Substituting (3.45) into (3.46) gives:

$$k_2 x_D = -M\ddot{x}$$

Rearranging: $x_D = \frac{-M\ddot{x}}{k_2}$ (3.47)

Differentiating (3.47) with respect to t gives

$$\dot{x}_D = \frac{-M.\ddot{x}}{k_2}$$
 (3.48)

substituting (3.47) and (3.48) into (3.45)

$$M\ddot{x} = -k_1\left(x + \frac{M\ddot{x}}{k_2}\right) - c\left(\dot{x} + \frac{M.\ddot{x}}{k_2}\right)$$

rearranging gives

$$\frac{cM.\ddot{x}}{k_2} + \left(M + \frac{Mk_1}{k_2}\right)\ddot{x} + c\dot{x} + k_1x = 0$$
 (3.49)

multiplying equation (3.49) by $\frac{k_2}{cM}$

$$\ddot{x} + \frac{k_2}{cM} \left(M + \frac{k_1 M}{k_2} \right) \ddot{x} + \frac{ck_2}{cM} \dot{x} + \frac{k_1 k_2}{cM} x = 0$$

Which reduces to

$$\ddot{x} + \left(\frac{k_1 + k_2}{c} \right) \ddot{x} + \frac{k_2}{M} \dot{x} + \frac{k_1 k_2}{cM} x = 0 \quad (3.50)$$

Then substituting $s = \frac{d}{dt}$, the characteristic equation of the Hybrid 2 model becomes:

$$s^3 + qs^2 + us + v = 0 \quad (3.51)$$

with the following definitions for q , u and v :

Let $\omega_e = \sqrt{\frac{k_1}{M}}$ undamped (angular) natural frequency

$\zeta = \frac{c}{2M\omega_e}$, the damping factor, and $R = \frac{k_2}{k_1}$

Then for Hybrid 2 model:

$$q = \frac{(k_1 + k_2)}{c} = \frac{-(1+R)\omega_e}{2\zeta}, u = \frac{k_2}{M} = R\omega_e^2, v = \frac{k_1 k_2}{cM} = \frac{-R\omega_e^3}{2\zeta}$$

With $\varepsilon = \frac{u + \frac{v}{\beta}}{2\beta}$ and $\omega = \sqrt{|\varepsilon^2 + \frac{v}{\beta}|}$ with β , ε and ω in radians.

The roots are: $\beta, \varepsilon + i\omega$ and $\varepsilon - i\omega$ (one real and two complex roots)

The solution of the differential equation is given by the following equations (Huang, 2002):

$$\text{let } p' = \frac{-2\varepsilon}{(\beta - \varepsilon)^2 + \omega^2}, \quad q' = \frac{\beta^2 - \varepsilon^2 + \omega^2}{\omega[(\beta - \varepsilon)^2 + \omega^2]}, \text{ then } p = p'\dot{x}, \quad q = q'\dot{x}$$

$$x = -pe^{-\beta t} + e^{-\varepsilon t}(p \cos \omega t + q \sin \omega t) \quad (3.52)$$

$$\dot{x} = p\beta e^{-\beta t} + e^{-\varepsilon t}[\omega(-p \sin \omega t + q \cos \omega t) - \varepsilon(p \cos \omega t + q \sin \omega t)] \quad (3.53)$$

$$\ddot{x} = -p\beta^2 e^{-\beta t} + e^{-\varepsilon t}[(\varepsilon^2 - \omega^2)(p \cos \omega t + q \sin \omega t) + 2\varepsilon\omega(p \sin \omega t - q \cos \omega t)] \quad (3.54)$$

A typical transient response of the displacement, velocity and acceleration for the Hybrid 2 model are shown in Figure 3.10.

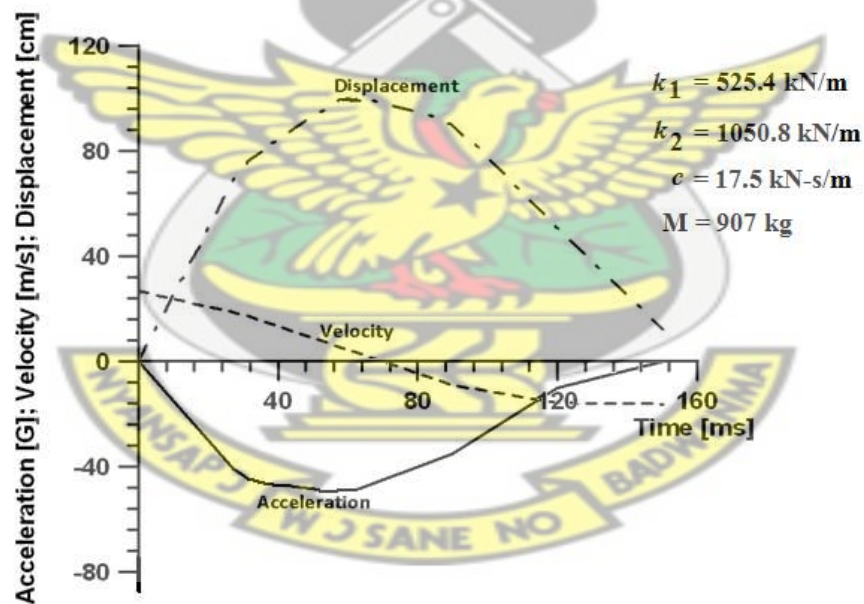
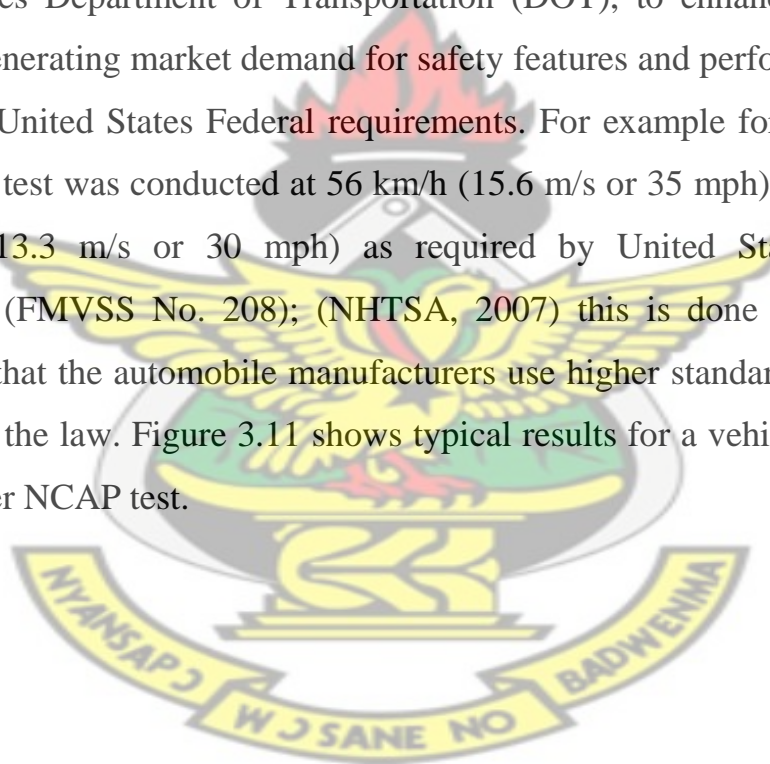


Figure 3.10 Displacement, Velocity and Acceleration Responses of the Hybrid 2 Model (Huang, 2002)

3.2 *Simulation*

This section discusses the responses of displacement, velocity and acceleration of the four models in line with desired behaviour to evaluate them, and select the most appropriate one for further analysis. These graphs are compared with a plot of a standard crash test data used by U.S. automobile manufacturers, the New Car Assessment Program (NCAP) test, for evaluation. NCAP was established by the United States National Highway Traffic Safety Administration (NHTSA), an integral part of the United States Department of Transportation (DOT), to enhance occupant safety by generating market demand for safety features and performance that go beyond United States Federal requirements. For example for the barrier test, NCAP test was conducted at 56 km/h (15.6 m/s or 35 mph), rather than 48 km/h (13.3 m/s or 30 mph) as required by United States federal regulations (FMVSS No. 208); (NHTSA, 2007) this is done to prove to consumers that the automobile manufacturers use higher standards than that required by the law. Figure 3.11 shows typical results for a vehicle in a Full width barrier NCAP test.



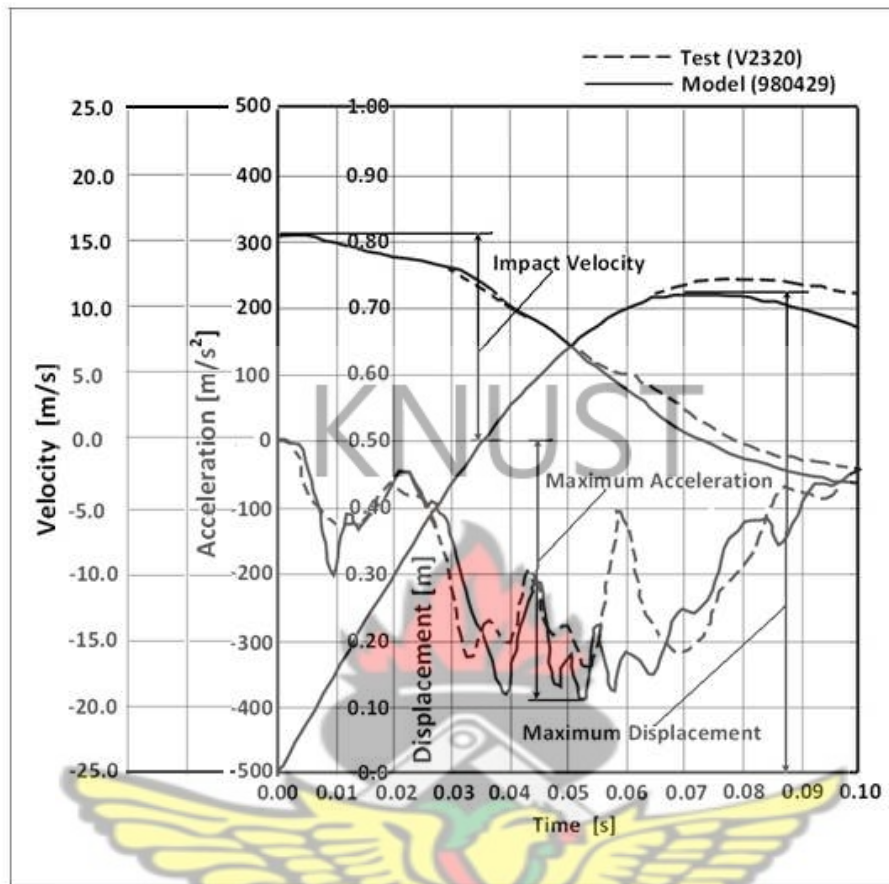


Figure 3.11 Expected Response of a Barrier Crash Test (Leneman et al., 2004)

These plots will be compared with the response of the various models to help in their evaluation. Some terms that will be used in the discussion are defined here. A crash pulse (or acceleration pulse) has a zero initial acceleration value and ends when the acceleration turns zero again. The maximum displacement occurs when the velocity is zero. The rebound velocity is the velocity at the separation time after the crash, that is, when acceleration is equal to zero. In Figure 3.11 the maximum displacement is

0.725 m, the impact velocity is 15.5 m/s and the maximum acceleration is - 390 m/s².

A range of material properties was considered in this study. The material properties under consideration here were the spring constant and the damping coefficient. The spring constant ranges from a low stiffness value of k_1^* to a high stiffness value of k_2^* while the damping coefficient ranges from a low damping value of c_1^* to a high damping value of c_2^* . The choice was made based on practical values of the material properties of a small car (Sedan Car) and a relatively bigger car (SUV). The general material properties considered were as follows (Huang, 2002):

SUV: $k = 4339$ lb/in and $c = 83.2$ lb-s/in

Passenger Car: $k = 3099$ lb/in and $c = 65.7$ lb-s/in

Sedan Car: $k = 2474$ lb/in and $c = 41.7$ lb-s/in

In order to evaluate the models to cover the range of k 's and c 's, a high value of $k_2^* = 5000$ lb/in and low value of $k_1^* = 2000$ lb/in were selected. Also the range of damping coefficients selected was from $c_1^* = 40$ lb-s/in to $c_2^* = 85$ lb-s/in. In SI units, $c_1^* = 7005.3$ N-s/m, $c_2^* = 14886$ N-s/m, $k_1^* = 350270$ N/m, and $k_2^* = 875670$ N/m. This range of material properties defines the region under study. Figure 3.12 shows the region or range of material properties considered in this study. The behaviour of the responses of the four models is evaluated within this spectrum of material properties. In the evaluation, $k_n^*c_n^*$ implies a combination of spring constant k_n^* and damping coefficient c_n^* ; where $n = 1, 2$. Thus, the combination $k_1^*c_1^*$ corresponds to

design point 1 at the bottom left corner of the region under study. The combination $k_1^*c_2^*$ corresponds to design point 2 at the bottom right corner of the region under study; while $k_1^*c_1^*$ corresponds to design point 3 at the top left corner and $k_2^*c_2^*$ corresponds to design point 4 at the top right corner of the region under study as shown in Figure 3.12. These points are used in the simulation processes.

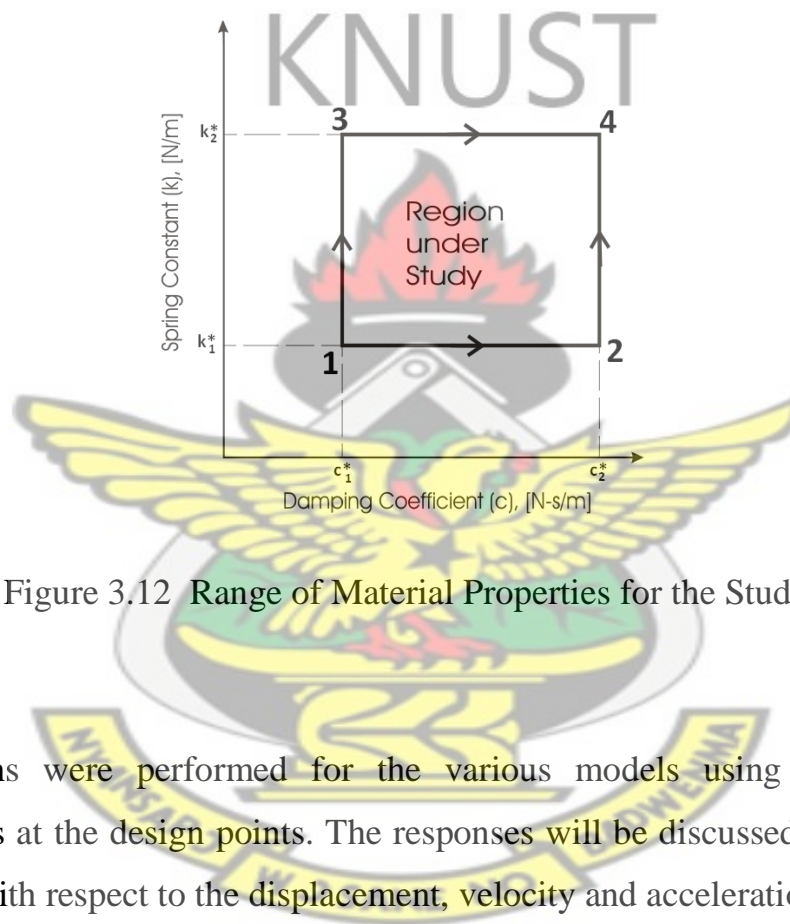


Figure 3.12 Range of Material Properties for the Study

Simulations were performed for the various models using the design parameters at the design points. The responses will be discussed in the next sections with respect to the displacement, velocity and acceleration.

3.2.1 Displacement Response

Figures 3.13 to 3.16 give the displacement responses of the various models. Equations 3.8, 3.11, 3.19, 3.38 and 3.52 were used in the simulation. Information from these plots is summarized in Tables 3.1 and 3.2.

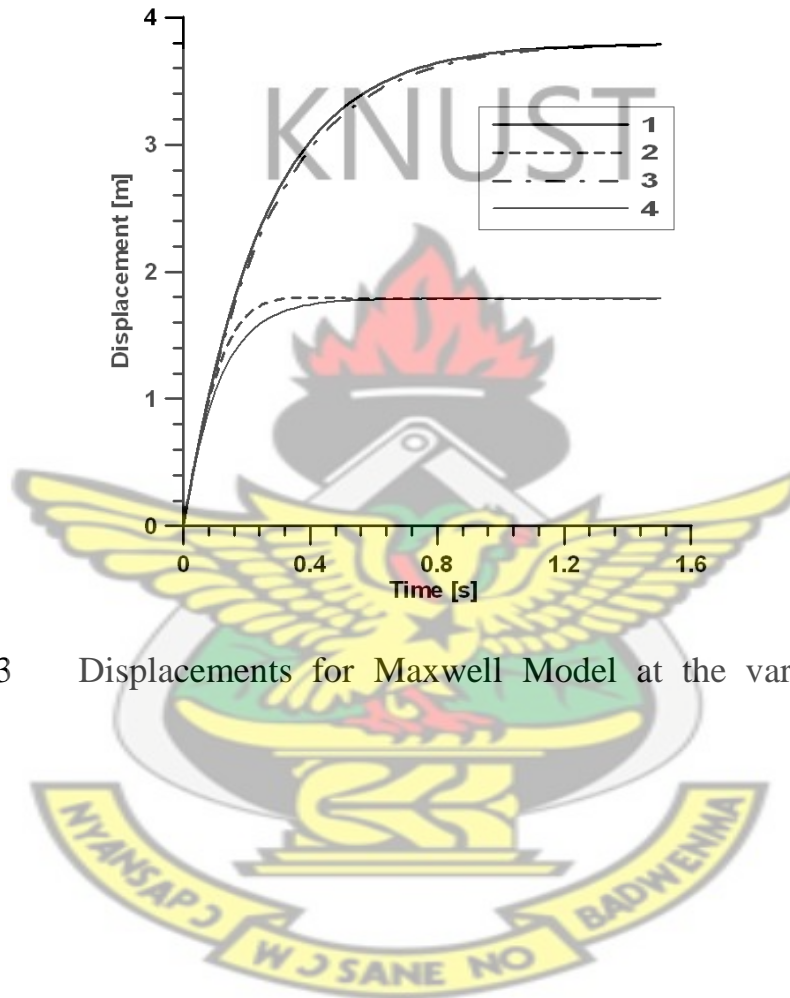


Figure 3.13 Displacements for Maxwell Model at the various design points

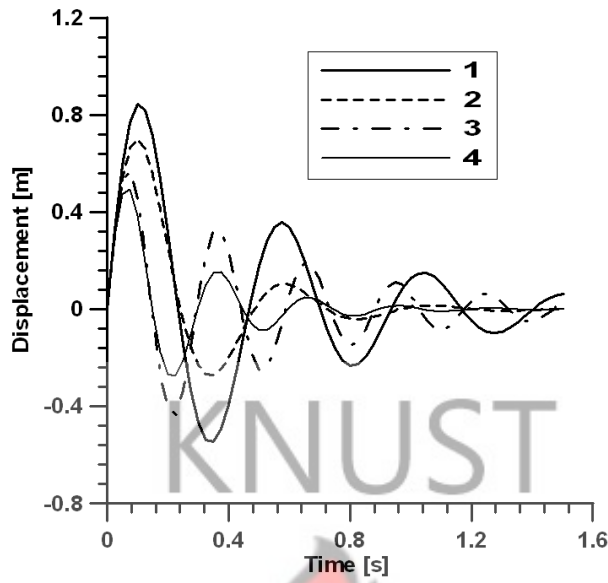


Figure 3.14 Displacements for Kelvin Model at the various design points

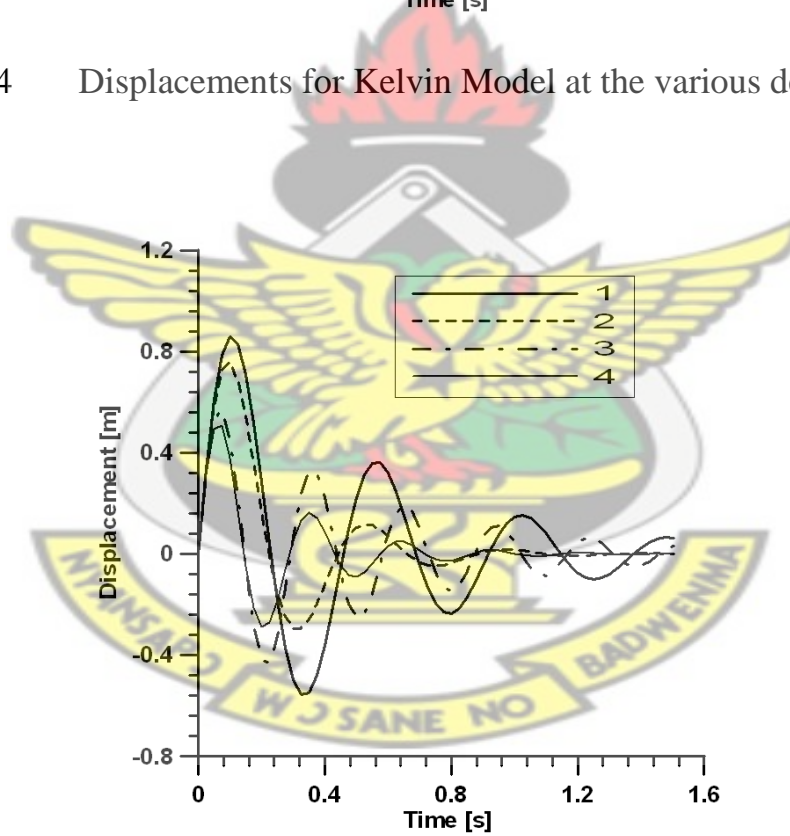


Figure 3.15 Displacements for Hybrid 1 Model at the various design points

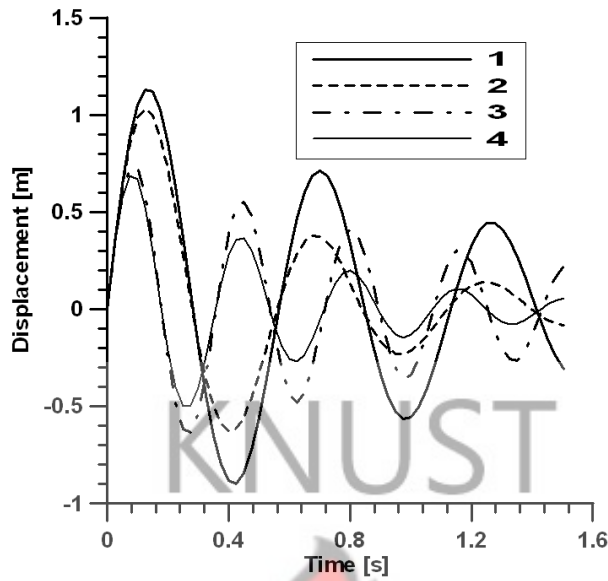


Figure 3.16 Displacements for Hybrid 2 Model at the various design points

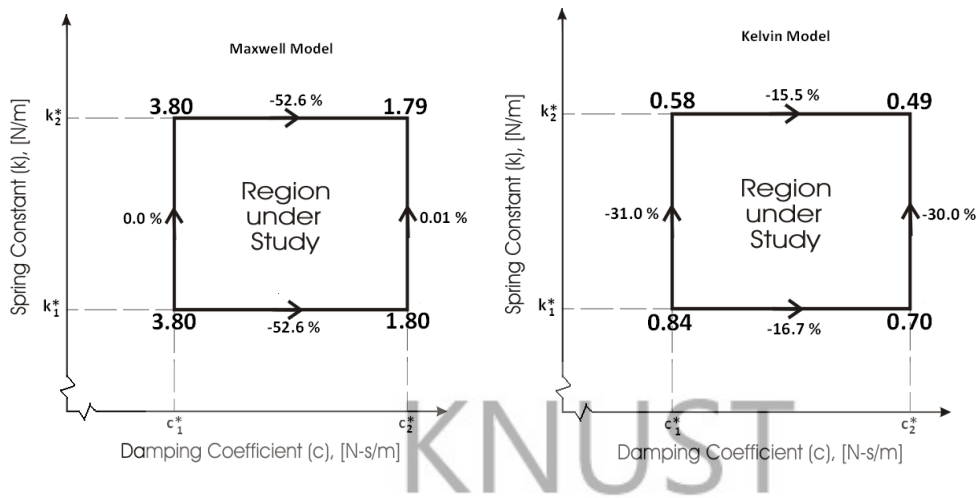
Tables 3.1 and 3.2 contain the respective information on the maximum displacements and the time they occurred, while the change in the maximum displacement as a result of changes in material properties are shown in Figure 3.17 for the Maxwell and Kelvin models, and Figure 3.18 for the Hybrid 1 and Hybrid 2 models. Maximum Displacements at design points are given at the respective corners of the region under study and the effects of moving from one design point to the other are given as % on the arrows.

Table 3.1 Maximum Displacement according to the various models

Maximum Displacement (m)				
Design Point	Maxwell Model	Kelvin Model	Hybrid 1 Model	Hybrid 2 Model
1	3.80	0.84	0.86	1.13
2	1.80	0.70	0.76	1.04
3	3.80	0.58	0.58	0.73
4	1.79	0.49	0.51	0.70

Table 3.2 Time at Maximum Displacement according to the various models

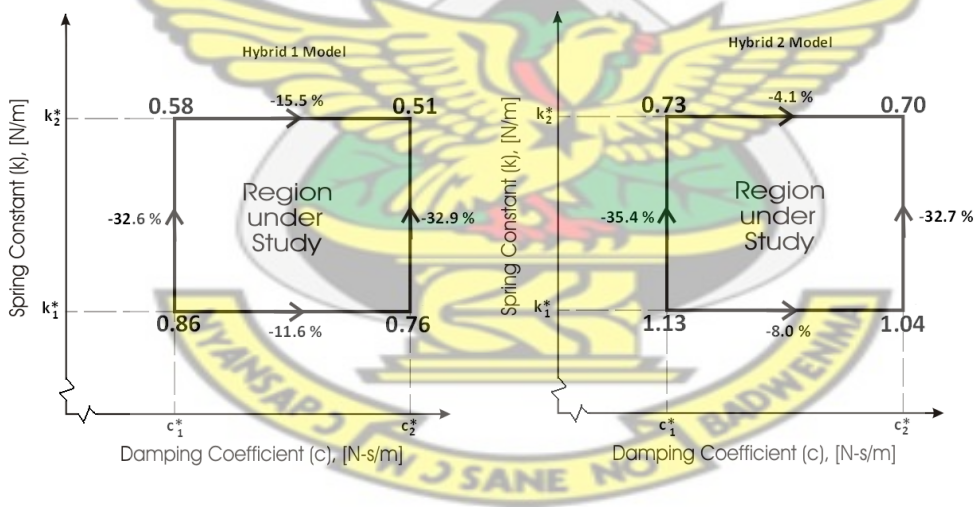
Time at Maximum Displacement (s)				
Design Point	Maxwell Model	Kelvin Model	Hybrid 1 Model	Hybrid 2 Model
1	1.50	0.11	0.11	0.14
2	0.40	0.10	0.09	0.13
3	1.50	0.06	0.06	0.08
4	0.58	0.06	0.06	0.08



(a)

(b)

Figure 3.17 Maximum Displacement at design points and effects of moving from one design point to the other for the Maxwell and Kelvin Models.



(a)

(b)

Figure 3.18 Maximum Displacement at design points and effects of moving from one design point to the other for the Hybrid 1 and Hybrid 2 Models.

The following observation can be made from the resulting responses:

- i. The displacement response of the Maxwell model (Figure 3.13) rises to an asymptotic maximum value.
- ii. The displacement behaviour of the Maxwell model (Figure 3.13) is different from the NCAP test crash plot in Figure 3.11. The deviation is quite high and therefore the Maxwell model is not good to be used to model as far as the displacement response is concerned.
- iii. The Kelvin, Hybrid 1 and Hybrid 2 models (Figures 3.14, 3.15 and 3.16 respectively) are damped sinusoidal curves. The first half cycle of the plots (which is the relevant part of the graphs) are similar to the behaviour of the NCAP test plot in Figure 3.11.
- iv. The Kelvin, and the two Hybrid models show reduction in maximum displacement with increase in stiffness.
- v. From Table 3.1 the Kelvin model and Hybrid 1 model have very close values; a difference of between 0.00 m (for design point 3) to 0.06 m (for design point 2). Hybrid 2 model, however deviates quite remarkably from Kelvin model values; a difference of from 0.15 m (for design point 3) to 0.34 m (for design point 2).
- vi. From Figure 3.17 (a), unlike the other three models, the Maxwell model is less responsive to changes in stiffness (0.0% and 0.01%) compared to changes in damping coefficient (-52.6%). For a given damping coefficient, a change in stiffness appears to have very little or no effect on the maximum displacement for the Maxwell model.
- vii. From Figures 3.17 (b), 3.18 (a) and 3.18 (b), at constant damping coefficient a change in stiffness causes a change of displacement

between -30.0% (for Kelvin) and -35.4% (for Hybrid 2) in the Kelvin, Hybrid 1 and Hybrid 2 models, but only little change, i.e. between -4.1% (for Hybrid 2) and -16.7% (for Kelvin) for a change in damping coefficient at constant stiffness. This shows that a change in stiffness has a greater effect (about three times more) than a change in damping coefficient for all three models.

- viii. The Maxwell model does not show any remarkable change in maximum displacement due to the asymptotic behaviour of the curves. The model behaves this way because the transition damping coefficient (c_T) is greater than the damping coefficient (c) except in the case of point 2; i.e. when $c_T = \frac{\sqrt{Mk}}{2} > c$ (Huang, 2002).

The transition damping coefficient (c_T) is the minimum value of damping coefficient c , for which there is a dynamic crush at a finite time; and then the body rebounds afterwards (Huang, 2002).

Here c_T values for k^*_1 and k^*_2 are 12898.8 N-s/m and 20394.7 N-s/m respectively.

Since $c^*_1 = 7005.3$ N-s/m and $c^*_2 = 14886$ N-s/m, there will be no rebound except at point 2 and the model's displacement responses are asymptotic as expected. The Maxwell model is therefore not good for this study as far as displacement response is concerned.

- ix. Comparatively the Kelvin model shows much higher responsiveness to change in c at a constant spring constant k^* of the material by a difference of 5.1 % and 0.0 % for Hybrid 1 model at spring constants k^*_1 and k^*_2 respectively, and a difference of 8.7 % and 11.4 % for

Hybrid 2 model at k^*_1 and k^*_2 respectively. However, the two hybrid models show slightly better responsiveness to change in spring constant at constant damping coefficient, c^* . That is a difference of only 1.6 % and 2.9 % for Hybrid 1 at constant c^*_1 and c^*_2 respectively; and 4.4 % and 2.7 % for Hybrid 2 model at constant c^*_1 and c^*_2 respectively.

KNUST

3.2.2 Velocity Response

Figures 3.19 to 3.22 give the velocity response of the various models. Equations 3.9, 3.12, 3.20, 3.39 and 3.53 were used in the simulation. Information from these plots is summarized in Tables 3.3 and 3.4.

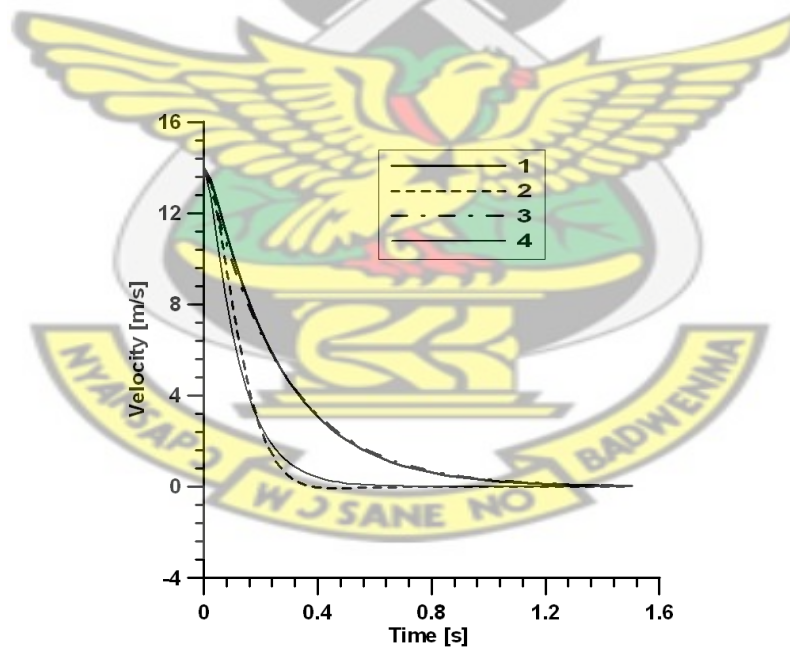


Figure 3.19 Velocity for Maxwell Model at the various design points

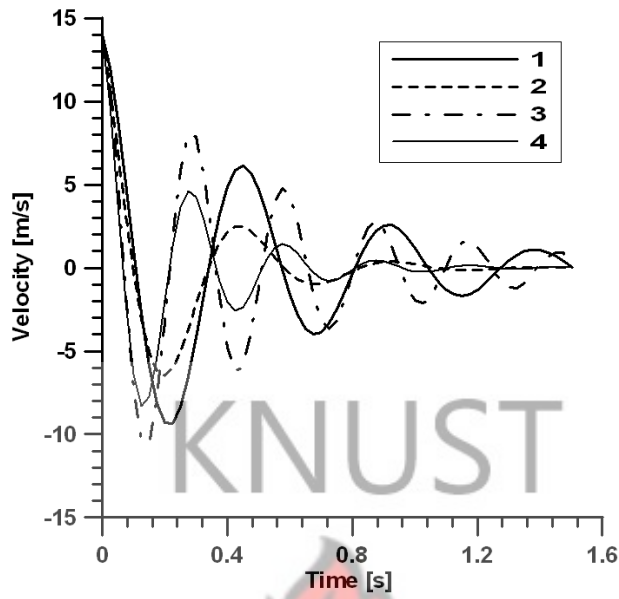


Figure 3.20 Velocity for Kelvin Model at the various design points

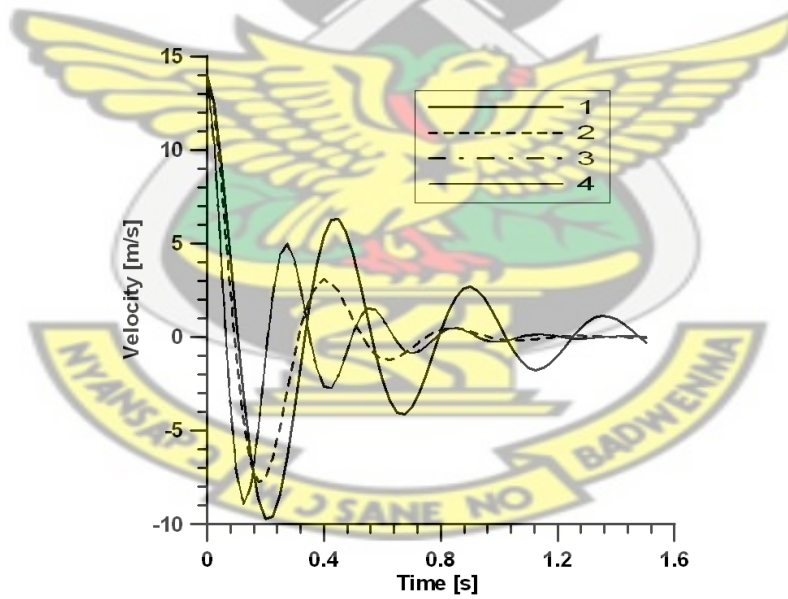


Figure 3.21 Velocity for Hybrid 1 Model at the various design points

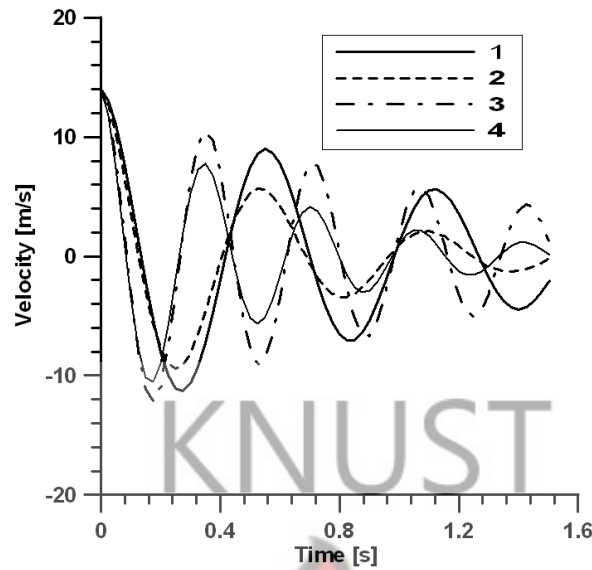


Figure 3.22 Velocity for Hybrid 2 Model at the various design points

Tables 3.3 and 3.4 contain the respective information on the rebound velocity and the time they occurred, while the change in the rebound velocity as a result of changes in material properties are shown in Figure 3.23 for the Kelvin model and Figure 3.24 for the Hybrid 1 and Hybrid 2 models. Rebound velocities at design points are given at corners of the region under study and the effects of moving from one design point to the other are given as % on arrows.

Table 3.3 Rebound Velocity according to the various models

Rebound Velocity (m/s)				
Design Point	Maxwell Model	Kelvin Model	Hybrid 1 Model	Hybrid 2 Model
1	–	-9.3	-9.6	-11.4
2	-0.1	-6.4	-7.5	-9.5
3	–	-10.5	-10.7	-12.0
4	–	-8.2	-8.9	-10.5

Table 3.4 Time at Rebound according to the various models

Time at Rebound (s)				
Design Point	Maxwell Model	Kelvin Model	Hybrid 1 Model	Hybrid 2 Model
1	–	0.21	0.21	0.26
2	0.50	0.19	0.18	0.25
3	–	0.14	0.13	0.17
4	–	0.13	0.13	0.16

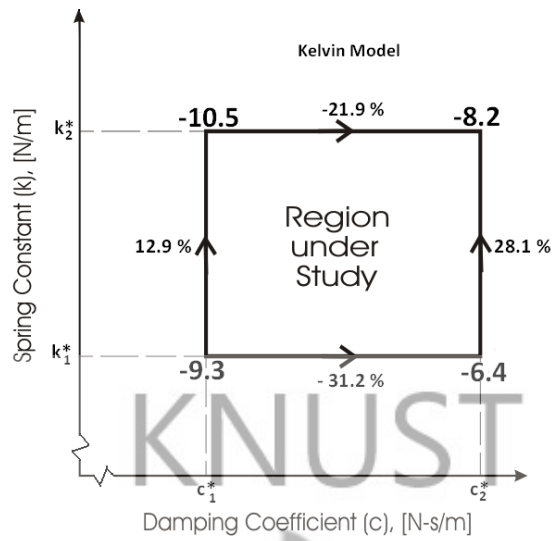
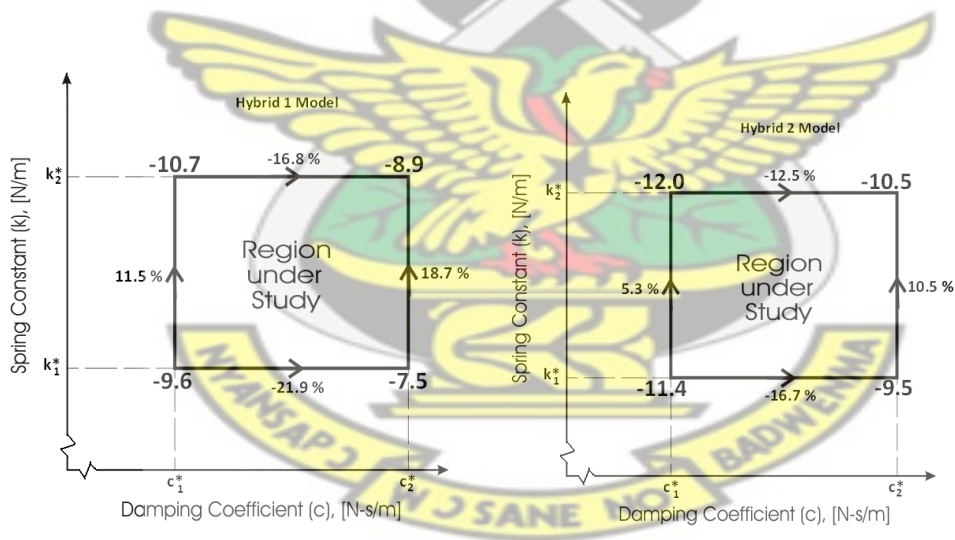


Figure 3.23 Rebound Velocity at design points and effects of moving from one design point to the other for the Kelvin Model.



(a)

(b)

Figure 3.24 Rebound Velocity at design points and effects of moving from one design point to the other for the Hybrid 1 and Hybrid 2 Models.

The following can be observed from the plots and tables:

- i. The velocity response of the Maxwell model (Figure 3.19) also deviates drastically from the typical crash response of the NCAP test plots. The velocity starts with the impact velocity of 14 m/s, as usual for all the models, but reduces exponentially to zero as the time tends to infinity.
- ii. The Kelvin, Hybrid 1 and Hybrid 2 models (Figures 3.20, 3.21 and 3.22 respectively) are damped sinusoidal curves. The first half cycle of the plots (which are the relevant part of the graphs) are similar to the shape of the NCAP test plot in Figure 3.11.
- iii. The velocity response of the Maxwell model is not similar to that of the NCAP crash test plot in Figure 3.11. It does not show any rebound except for design point 2. This is expected since the damping coefficients used are below the transition damping coefficient (c_T) except in the case of design point 2.
- iv. From Table 3.3 the Hybrid 1 model has velocities that are very close to those of the Kelvin model; a minimum difference of 0.2 m/s (for design point 3) to a maximum difference of 1.1 m/s (for design point 2). On the other hand the Hybrid 2 model deviates from the Kelvin model by a minimum of 1.5 m/s (for design point 3) to a maximum difference of 3.1 m/s (for design point 2).
- v. From Table 3.4 the Kelvin and Hybrid 1 models have almost the same times for rebound (with a maximum difference of 0.01 s); while the times for the Hybrid 2 rebound velocities deviates only slightly from that of the Kelvin's model; from a minimum difference of 0.03 s (for

- design point 3 and design point 4) to a maximum of 0.06 s (for design point 2). That is, the differences in the rebound times for the Kelvin and Hybrid models are not very significant.
- vi. From Figure 3.23, 3.24 (a) and 3.24 (b) the Kelvin, Hybrid 1 and Hybrid 2 models all show an increase in rebound velocity for an increase in stiffness at constant damping; and a decrease in rebound velocity for an increase in damping coefficient at constant stiffness.
 - vii. From Figure 3.23, 3.24 (a) and 3.24 (b) the Kelvin, Hybrid 1 and Hybrid 2 models all show a higher responsiveness to a change in damping coefficient at low stiffness (k^*_1) than at high stiffness (k^*_2).
 - viii. The Kelvin, Hybrid 1 and Hybrid 2 models all show a higher responsiveness to a change in stiffness at higher damping coefficient (c^*_2) than at low damping coefficient (c^*_1).
 - ix. Comparatively the Kelvin model shows the highest level of responsiveness to changes in the damping coefficients and stiffness of the material, followed by the Hybrid 1 model and then the Hybrid 2 model as far as rebound velocity is concerned.

3.2.3 Acceleration Response

Figures 3.25 to 3.28 give the velocity response of the various models. Equations 3.10, 3.13, 3.21, 3.40 and 3.54 were used in the simulation. Information from these plots is summarized in Tables 3.5 and 3.6.

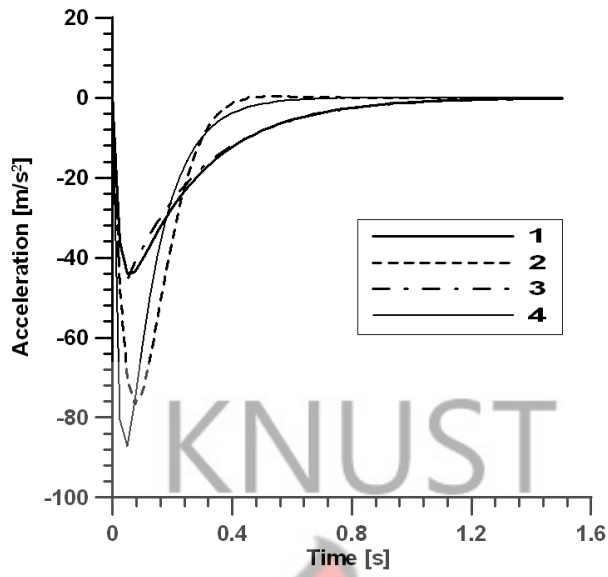


Figure 3.25 Acceleration for Maxwell Model at the various design points

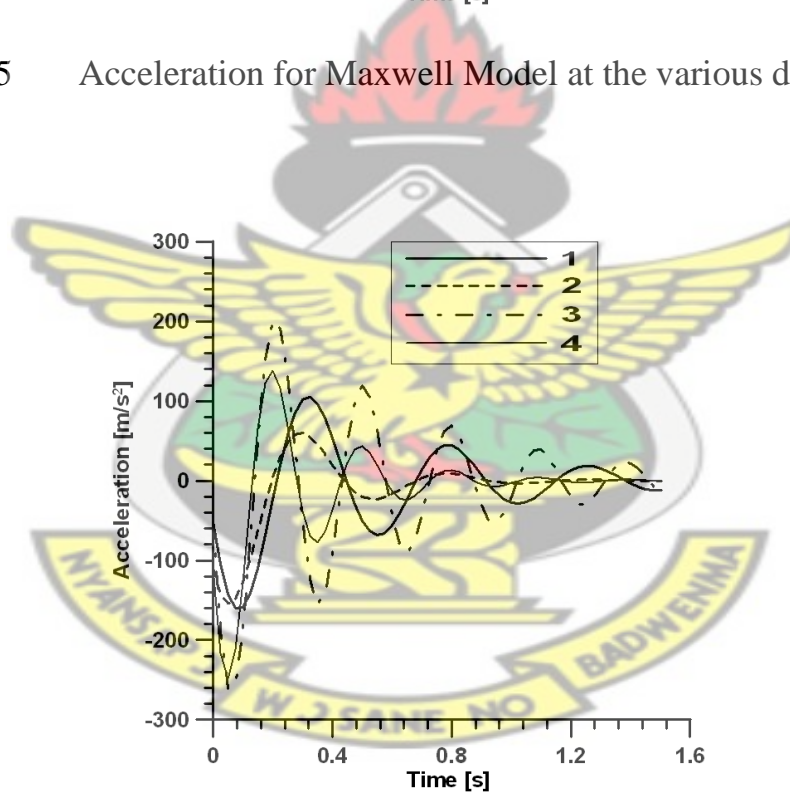


Figure 3.26 Acceleration for Kelvin Model at the various design points

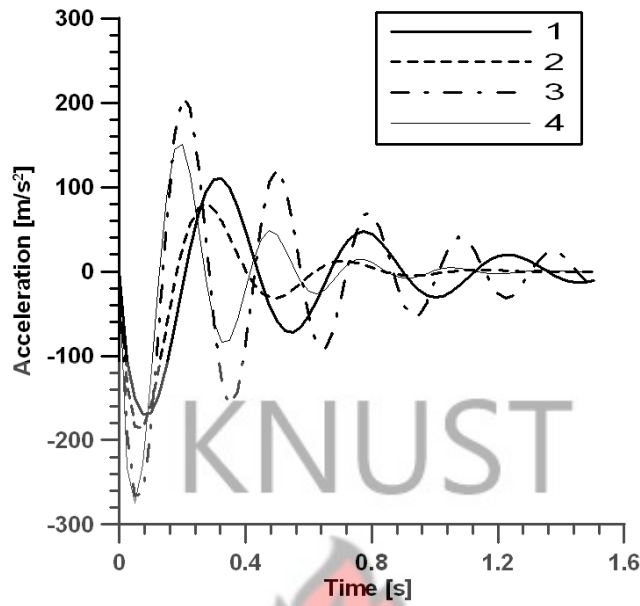


Figure 3.27 Acceleration for Hybrid 1 Model at the various design points

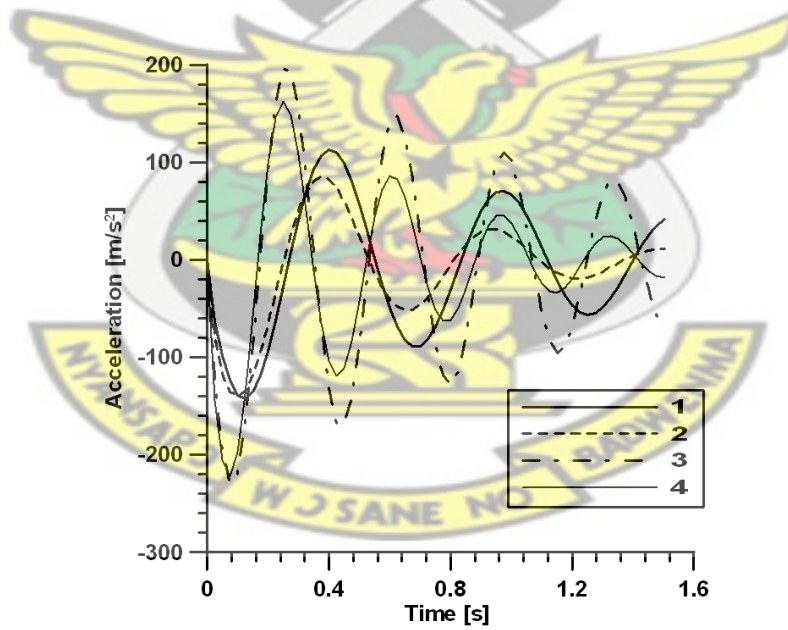


Figure 3.28 Acceleration for Hybrid 2 Model at the various design points

Tables 3.5, 3.6 and 3.7 contain the respective information on the maximum acceleration, the duration of the crash pulse and the initial acceleration at time zero, while the change in the maximum acceleration as a result of changes in material properties are shown in Figure 3.29 for the Maxwell and Kelvin models, and Figure 3.30 for the Hybrid 1 and Hybrid 2 models. Maximum acceleration at design points are given at corners of the region under study and the effects of moving from one design point to the other are given as % on arrows.

Table 3.5 Maximum Acceleration according to the various Models

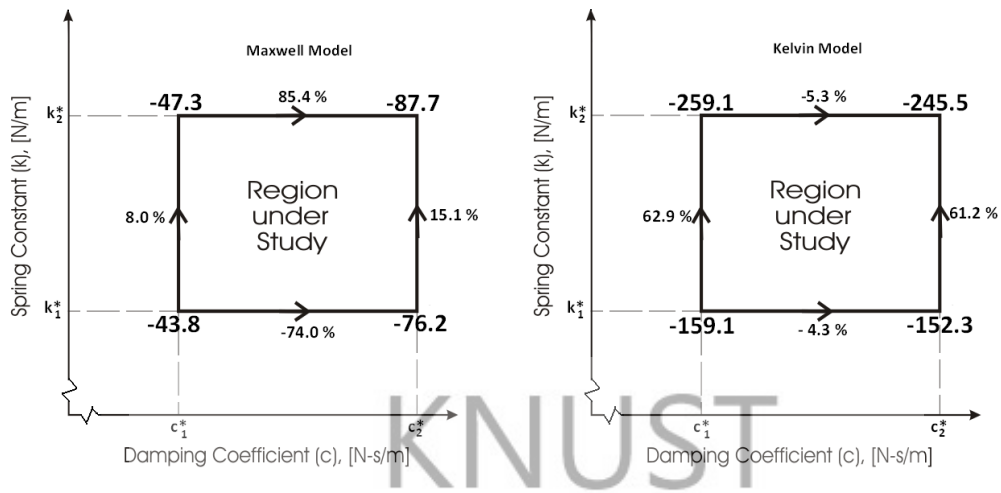
Maximum Deceleration (m/s²)				
Design Point	Maxwell Model	Kelvin Model	Hybrid 1 Model	Hybrid 2 Model
1	-43.8	-159.1	-168.2	-140.0
2	-76.2	-152.3	-186.4	-136.7
3	-47.3	-259.1	-263.6	-226.7
4	-87.7	-245.5	-272.7	-223.3

Table 3.6 Duration of Crash Pulse according to the various Models

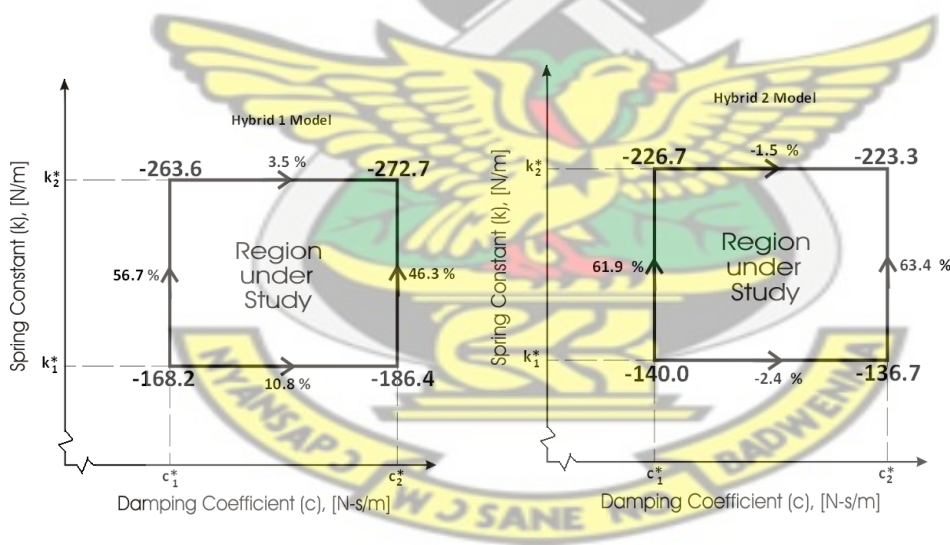
Duration of Crash Pulse (s)				
Design Point	Maxwell Model	Kelvin Model	Hybrid 1 Model	Hybrid 2 Model
1	1.5	0.21	0.21	0.26
2	0.5	0.19	0.18	0.25
3	1.5	0.14	0.13	0.17
4	0.75	0.13	0.13	0.16

Table 3.7 Initial Acceleration According to the various Models

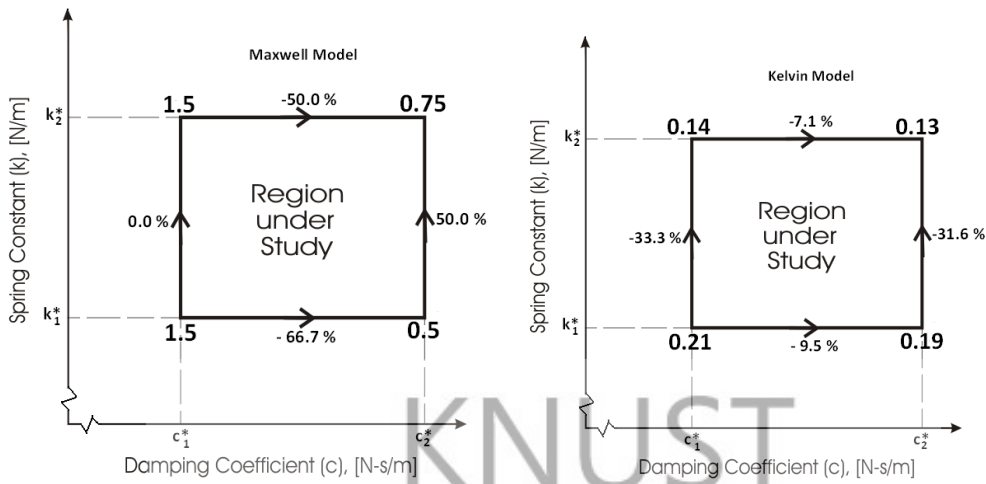
Initial Deceleration at time zero (m/s²)				
Design Point	Maxwell Model	Kelvin Model	Hybrid 1 Model	Hybrid 2 Model
1	0	-50.0	0	0
2	0	-109.0	0	0
3	0	-50.0	0	0
4	0	-109.0	0	0



(a) **(b)**
 Figure 3.29 Maximum Acceleration at design points and effects of moving from one design point to the other for the Maxwell and Kelvin Models.



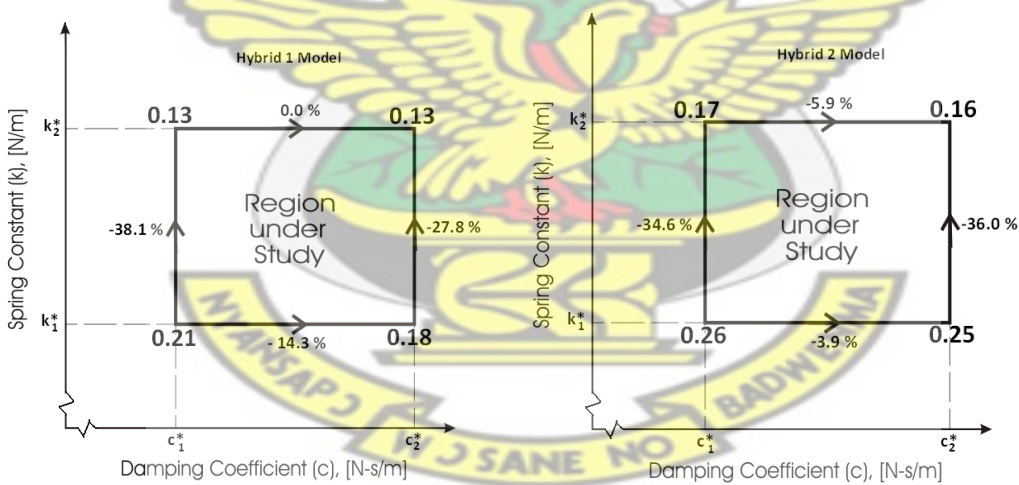
(a) **(b)**
 Figure 3.30 Maximum Acceleration at design points and effects of moving from one design point to the other for the Hybrid 1 and Hybrid 2 Models.



(a)

(b)

Figure 3.31 Duration of Pulse at design points and effects of moving from one design point to the other for the Maxwell and Kelvin Models.



(a)

(b)

Figure 3.32 Duration of Pulse at design points and effects of moving from one design point to the other for the Hybrid 1 and Hybrid 2 Models.

The following can be observed from the plots and tables:

- i. The acceleration response of the Maxwell model (Figure 3.25) starts with a zero initial value, reduces exponentially to a minimum value (the maximum deceleration) and rises again exponentially to an asymptotic maximum value.
- ii. The Maxwell model has relatively less maximum deceleration values and deviates widely from those of the other three models.
- iii. The acceleration response of the Kelvin, Hybrid 1 and Hybrid 2 models have relatively very close maximum deceleration values.
- iv. The Maxwell, Hybrid 1 and Hybrid 2 models have zero deceleration at time zero, similar to the NCAP test results in Figure 3.11.
- v. The Kelvin model has a non-zero deceleration at time zero, contrary to the NCAP test results in Figure 3.11.
- vi. From Figure 3.29 and 3.30 all models show an increase in maximum deceleration for an increase in stiffness at constant damping. They show higher responsiveness to this change at high damping, c^*_2 .
- vii. From Figure 3.29 (b) and 3.30 (b) the Kelvin and Hybrid 2 models show a decrease in maximum deceleration for an increase in damping coefficient at constant stiffness.
- viii. From Figure 3.29 (a) and 3.30 (a) the Maxwell and Hybrid 1 models show an increase in maximum deceleration for an increase in damping coefficient at constant stiffness.
- ix. Overall the Kelvin model shows higher responsiveness to changes in maximum deceleration due to changes in material properties.

3.2.4 Justification of High Speed Impact Attenuation Model

For the stiffness levels under study, the Maxwell model does not show rebound of the body except at design point 2. The Maxwell model is suitable for modelling material responses that undergo creep and relaxation but does not take into account the bending and torsion stiffness of the material (Huang, 2002). In vehicle impact modelling the Maxwell model is suitable for localized impacts where the vehicle's effective stiffness is low, and soft impacts such as localized pole and offset collisions where timing at dynamic crush is fairly long (Huang, 2002). This study aims at investigating frontal impacts at elevated speeds; that is speeds (up to about 14 m/s, 50 km/h or 31 mph) which are higher than that for which a bumper is designed (about 2.5 mph; 4.0 km/h or 1.11 m/s). The Maxwell model is therefore not suitable for the modelling in this study.

The Kelvin model gives a second order differential equation which is simpler and easier to solve than the hybrid ones that give third order differential equations or coupled first and second order differential equations. The limitation of the Kelvin model, however, is that it produces a non-zero deceleration at time zero, a deviation from a crash pulse, which is typically zero at time zero. However, in spite of the non-zero initial value in the acceleration, the Kelvin model's pulse duration, and rebound velocities do not deviate much from those of the Hybrid models. From Table 3.6 it deviates by a maximum of 0.01 s from Hybrid 1 model at design points 2 and 3, and a maximum of 0.06 s from Hybrid 2 model at design point 2.

Therefore the effect of the non-zero value of the acceleration at time zero is not very significant in the range of material properties under consideration. The Kelvin model shows an overall better responsiveness to changes in material properties in the material property range under study with respect to displacement, velocity and acceleration. It has a simpler solution as compared to those of the Hybrid models. Adding a friction damper to the Hybrid model would make the resulting system more complicated to solve.

From the discussion above, the Kelvin's model was selected for the modelling of the bumper to simulate and solve crash phenomenon in this study. By adding a friction damper to the Kelvin's model the resulting model becomes quite complicated but it can be solved by using numerical methods.

3.2.5 Modified Kelvin Model

In an effort to absorb and dissipate as much energy as possible with the bumper in crash at elevated speed, the use of coulomb friction damper is proposed. The Kelvin model was modified by adding a friction element to aid in more energy dissipation. Figure 3.33 shows a diagram of the proposed model. The aim is to greatly improve the damping performance. For this model, this is done by controlling the normal force applied on the friction damper. This notion of producing a damping force by controlling a secondary variable as used in this study is termed semi-active control (Dupont et al., 1997). Figure 3.34 shows the free body diagram of the friction damper model in Figure 3.33.

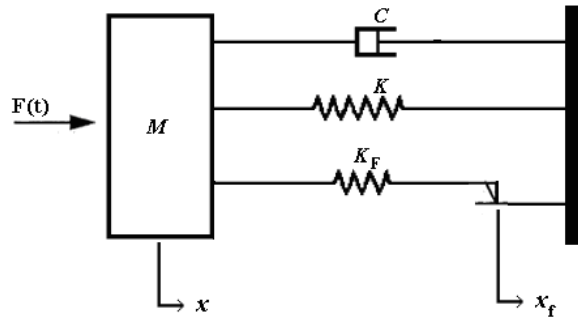


Figure 3.33 Schematic of the Bumper with Friction Damper Model

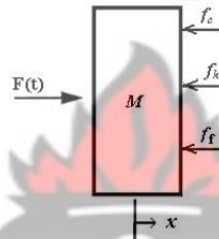


Figure 3.34 Free Body Diagram of the Friction Damper Model

Let:

force on the viscous damper = f_c

force on the spring = f_k

force on the friction damper = f_f

deflection of the mass = x

deflection of friction damper = x_f

deflection of the damper = deflection of the spring = x

spring constant = k

spring constant of friction damper = k_F

damping coefficient of the viscous damper = c

$$\sum F = Ma = M\ddot{x} \quad (3.55)$$

$$\text{Therefore } M\ddot{x} = -f_c - f_k - f_f + F(t) \quad (3.56)$$

$$f_c = c\dot{x}$$

$$f_k = kx$$

$$\text{which implies that: } M\ddot{x} = -c\dot{x} - kx - f_f + F(t) \quad (3.57)$$

which can be re-arranged as

$$M\ddot{x} + c\dot{x} + kx + f_f = F(t) \quad (3.58)$$

$$f_f = k_F(x - x_f) \quad (3.59)$$

this is the force due to the friction damper and can be written as

$$\mu_f F_N = k_F(x - x_f) \quad (3.60)$$

where F_N is the normal force on the friction damper and μ_f is the coefficient of friction of the friction surface of the friction damper.

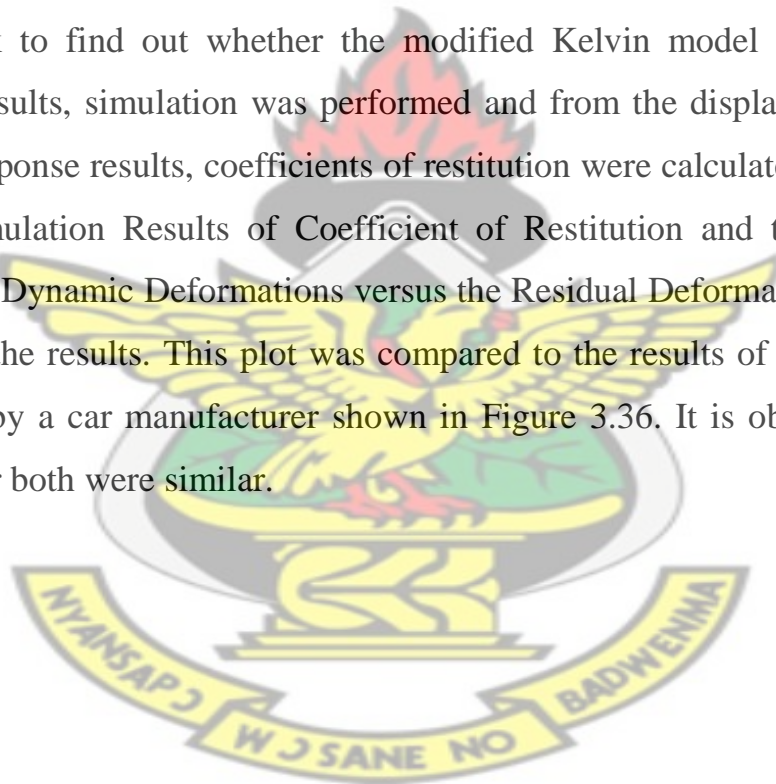
In this model the external excitation force $F(t)$, which is the impact force, is the input in the system and the vibration amplitude is the output of the system. The aim is to reduce this output response amplitude to a minimum through energy dissipation. The amount of energy dissipated can be

controlled by an appropriate choice of the normal force or coefficient of friction acting on the friction surfaces.

Damping in this model occurs when there is no relative displacement and there is sticking friction. Transition between sticking and slip is unsteady (Popp et al., 2003).

KNUST

As a check to find out whether the modified Kelvin model would give expected results, simulation was performed and from the displacement and velocity response results, coefficients of restitution were calculated and used to plot Simulation Results of Coefficient of Restitution and the ratio of Residual to Dynamic Deformations versus the Residual Deformation. Figure 3.35 show the results. This plot was compared to the results of a crash test conducted by a car manufacturer shown in Figure 3.36. It is observed that the plots for both were similar.



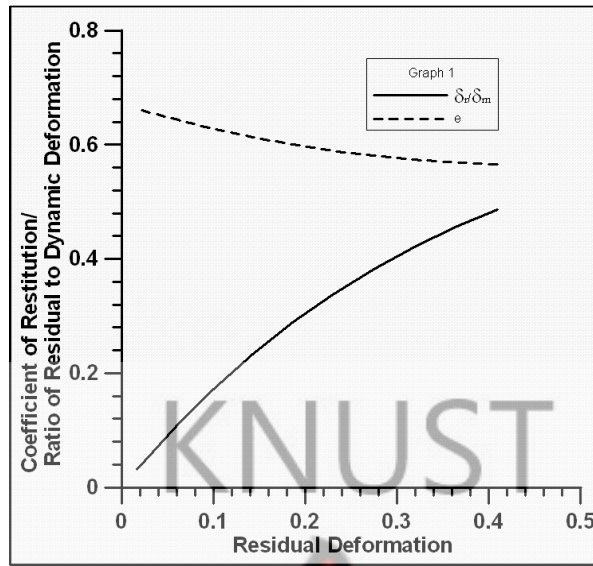


Figure 3.35 Simulation Results of Coefficient of Restitution and the ratio of Residual to Dynamic Deformations against the Residual Deformation

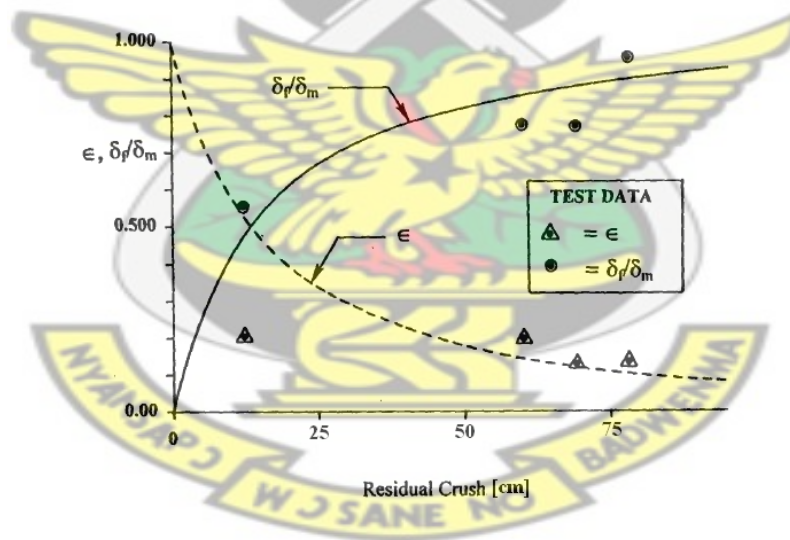


Figure 3.36 Test Results of Coefficient of Restitution and the ratio of Residual Deformation to Dynamic Deformation against the Residual Deformation from a test data (Ford, 1982)

Equation 3.58, which is equation of the modified Kelvin's model, will have to be solved to give the displacement, velocity and acceleration information for further analysis. A closed form solution for this differential equation cannot be found directly. The solution of the displacement, velocity, and acceleration responses will therefore have to be found numerically.

3.3 *Simulation and Post Processing Software*

There are several different ways of solving differential equations by numerical methods. Various software have been developed for this purpose that are available on the market. For this study, one such software, VisSim™ was selected. VisSim™ is a programming language and development tool developed by Visual Solutions Inc. that uses block diagram language for creating complex linear and nonlinear dynamic systems for the modelling and simulation of simple and complex dynamic systems. VisSim™ has an intuitive drag-and-drop block diagram interface with a powerful simulation (mathematical) engine. The use of its visual block diagram interface offers a simple method for constructing, modifying and maintaining simple to complex system models. It has an extensive tool kit, a model library, and a good interface capability with a number of programming software and was therefore found appropriate for this study.

The programming method of VisSim™ is drag-and-drop of blocks and functions followed by the “wiring” of these elements to a functioning and running program. This eliminates the traditional programming methods of

learning programming language with many rules. Each block of the diagram performs a mathematical function or an input/output function. These "blocks" may represent complex algorithms, input variables, mathematical operations or various outputs like graphs, charts, plots or data files.

MATLAB™ software was selected for the post processing of the simulation results. The main reason for the choice of MATLAB™ for post processing was its efficiency in numerical solution of complex problems.

3.4 Solving Second Order nonlinear ODE with VisSim

The car bumper can be modelled with the second order differential equation:

$$M\ddot{x} + c\dot{x} + Kx + F_{Damp} = F(t)$$

Furthermore, it is assumed that $F(t)$ is a pulse function depicting the impact of a vehicle crashing into a fixed barrier with the initial conditions at impact:

$$\ddot{x}(0) = 0; \dot{x}(0) = V_i; x(0) = 0. \text{ Where } V_i \text{ is the impact velocity of the vehicle.}$$

The expected solution should be the displacement, velocity and acceleration responses. That is $\ddot{x}(t)$, $\dot{x}(t)$ and $x(t)$.

In VisSim, such equations are best solved by numerical integration. Numerical Integration using Runge Kutta second order method was selected for this study. The first step in the programming is to isolate the highest derivative term on the left-hand side as: $\ddot{x} = \frac{1}{M}(F(t) - c\dot{x} - kx - F_{Damp})$. This

segment can be coded in VisSim using a ‘summing Junction’, ‘divide’ and ‘multiply’ blocks as shown in Figure 3.37. The model equation of the program presented in Figure 3.37 is

$$\ddot{x} = \frac{1}{M} (F(t) - c\dot{x} - kx - F_{Damp}) \quad 3.61$$

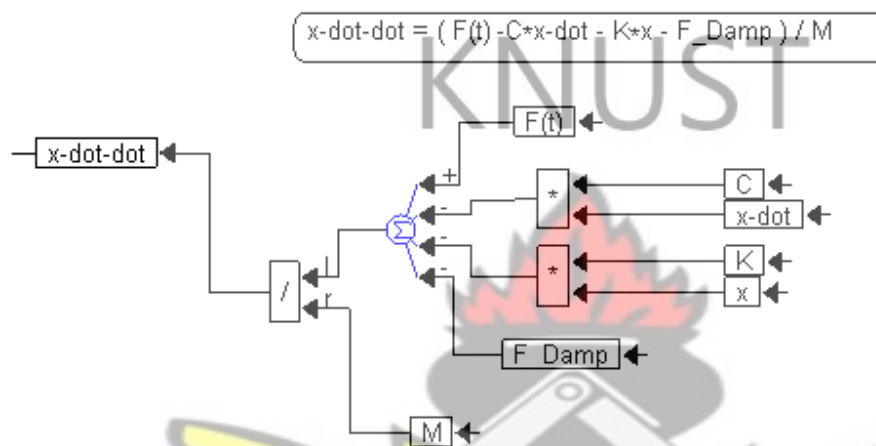


Figure 3.37 Expression of a Second Order Differential Equation in VisSim

The second step is to integrate the highest derivative term a sufficient number of times to obtain the solution. Since the highest derivative is of second order, $x\text{-dot-dot}$ must be integrated twice to obtain x . It is important to maintain consistent variable names (i.e. $x\text{-dot-dot}$, $x\text{-dot}$, x etc.) throughout. Furthermore, the initial conditions must be added. The initial conditions on any state (or variable) must be set internally on the integrator block that is generating that state. It is set by right-clicking on the integrator block and filling in the dialog box that pops up as a result with the

appropriate initial condition. By default, all integrators have zero initial condition. On the other hand, the initial condition can also be set externally with a ‘summing Junction’ block, as shown in Figure 3.38. This method is better when setting the initial condition as a variable since it facilitates making changes in the initial condition to simulate different impact scenarios easier and more transparent; as in the case of this study. The mathematical equations for the program in Figure 3.38 are:

$$\int \ddot{x} dt = \dot{x}; \quad \dot{x}(0) = V_i \quad \text{and} \quad 3.62$$

$$\int \dot{x} dt = x; \quad x(0) = 0. \quad 3.63$$

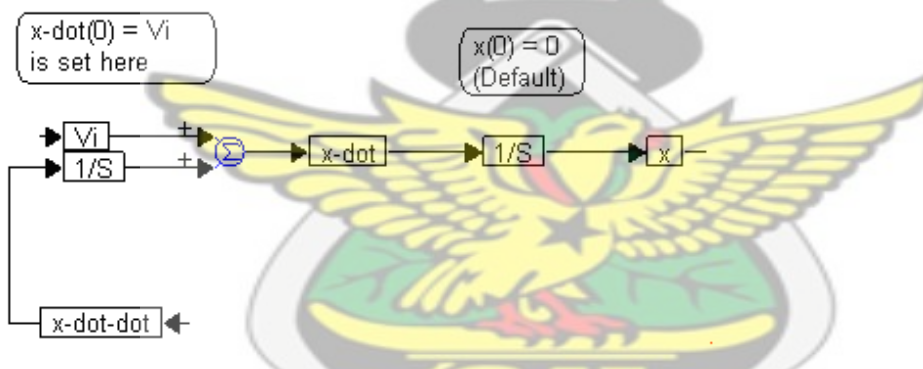


Figure 3.38 Setting the Integrator Initial Conditions Externally

To complete the code, the variables should be defined. The variables include the external force, $F(t)$, damping coefficient, c , spring constant, k , friction force from the friction damper, F_{Damp} , and mass of vehicle, M . For example, in one such scenario, the variables were set as follows: $F(t) = \text{Step input}$, $c = 11500$, $k = 542700$,

$F_{Damp} = 0$, and $M = 1900$. The program and its solution is as given in Figure 3.39. In the study, $F(t)$ is a pulse input. The solution of the equation of $x(t)$ only is shown in Figure 3.39. Solution for the velocity and acceleration responses can also be obtained by drawing an arrow from an $x\text{-dot}$ box and an $x\text{-dot-dot}$ box respectively to a graph box, as was done for x to obtain their responses. The corresponding Model Equations for Figure 3.39 are equations 3.61, 3.62 and 3.63 put together. That is,

$$\ddot{x} = \frac{1}{M}(F(t) - c\dot{x} - kx - F_{Damp}), \int \ddot{x} dt = \dot{x}; \dot{x}(0) = V_i \text{ and}$$

$$\int \dot{x} dt = x; x(0) = 0.$$

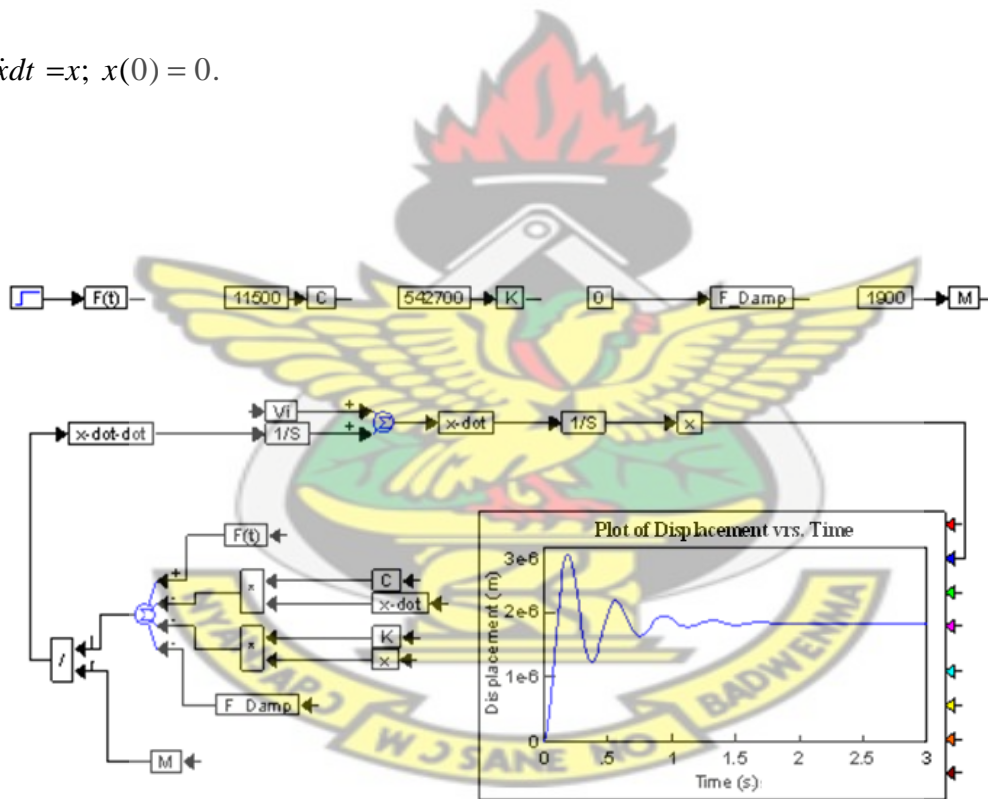


Figure 3.39 Variable Deceleration and Displacement Response of the Model

The values of variables used in the simulation are given in Table 3.8

Table 3.8 Values of Variables used

Set Variables	Value
Mass	1,900 kg
Stopping Time	0.2 s
Initial Velocity	0 to 12 m/s
Final Velocity	0 m/s
Initial Acceleration	0 m/s ²
Damping Coefficients	6.0, 6.5, 11.5, 13.5 and 14.0 kN-s/m
Stiffness	300, 400, 542.7, 750, and 850 kN/m
Number of Dampers	0 and 1
Friction Coefficient	0.5
Damping Force	0 to 228,000 N
Normal Force	0 to 456,000 N

VisSimTM allows the use of different ‘layers’ in programming. That is, some parts of the program and sub-programs can be programmed elsewhere as a different ‘layer’ and then integrated in the main program. Figure 3.39 can be

're-wired' differently and rearranged as in Figure 3.40 for better integration of additional functions. The plot has been moved to a different 'layer' to provide enough space for a better overview of the plots and data.

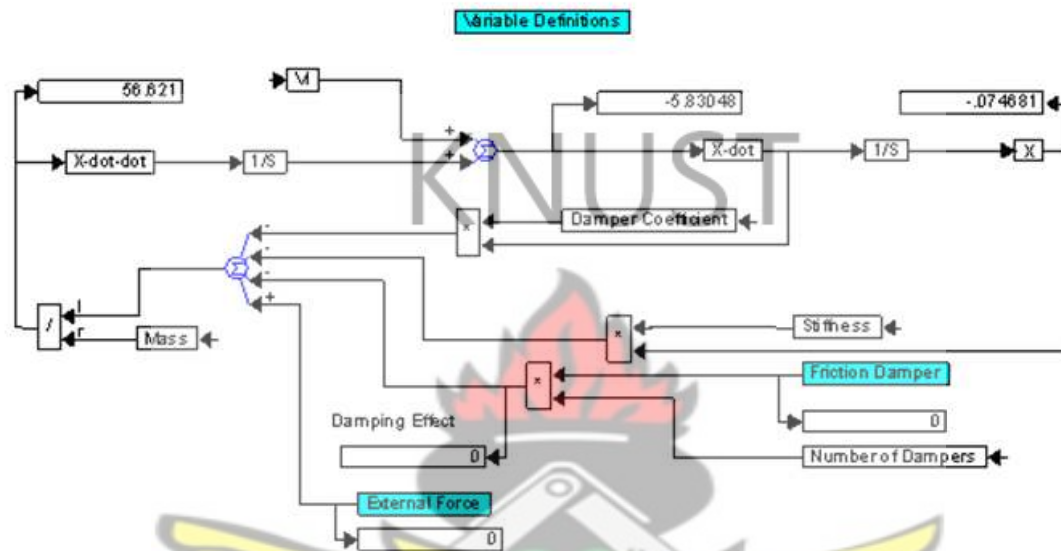


Figure 3.40 Main Program for the complete Model

The corresponding Model Equations for Figure 3.40 are: $Damping\ Effect = nF_{Damp}$, $\ddot{x} = \frac{1}{M}(F(t) - c\dot{x} - kx - F_{Damp})$, $\int \ddot{x}dt = \dot{x}$; $\dot{x}(0) = V_i$ and $\int \dot{x}dt = x$; $x(0) = 0$. where n = number of dampers.

Separate programs were written to provide the impulse force $F(t)$ and friction force. These were integrated into the block "External Force" and "Friction Damper" respectively. Figure 3.41 shows the program to effect the impulse force, $F(t)$. The impulse force was assumed to work for only a very

short time, specified with the variable ‘Stopping Time’. 0.2 seconds was selected for the initial simulation. Mathematically it is given by; $M(V_i - V_f) / \text{Stopping Time}$, where M is mass of vehicle, V_i is the impact velocity and V_f is the final velocity ($V_f=0$). The model equations of the program for the impact force as given in Figure 3.41 are therefore:

$$F_{max} = \frac{M(V_i - V_f)}{\text{Stopping Time}} \quad 3.64$$

$$F(t) = F_{max}, 0 \leq t \leq \text{Stopping Time} \quad 3.65$$

$$F(t) = 0, t > \text{Stopping Time} \quad 3.66$$

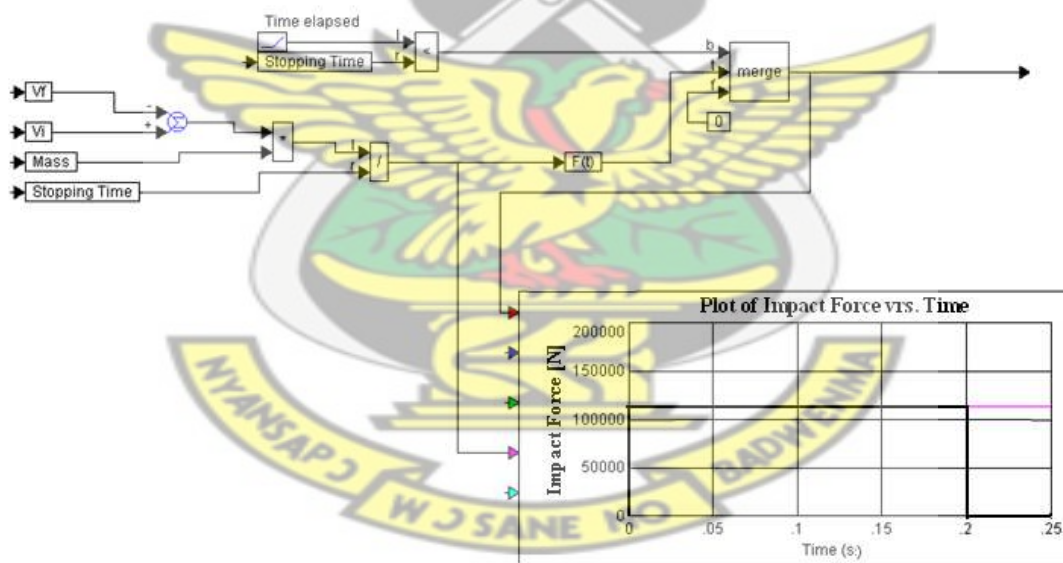


Figure 3.41 Program for Impact Force

Figure 3.42 shows a program to introduce the friction force from the friction damper. It is also programmed separately and integrated into the “Friction Damper” block. Mathematically it is $(\mu \times F_n)$, where μ is the coefficient of friction of the damper and F_n is the normal force applied to the damper. It was assumed that it works for a very short time before it slips. The variable “Stopping Friction Time”, gives the duration of the friction force.

The corresponding model equations of the program for the friction force as given in Figure 3.42 are therefore:

$$F_{Damp} = \mu F_N, \quad 0 < t < \text{Stopping Time} \quad 3.67$$

$$F_{Damp} = 0, \quad t > \text{Stopping Time} \quad 3.68$$

Where μ = coefficient of friction.

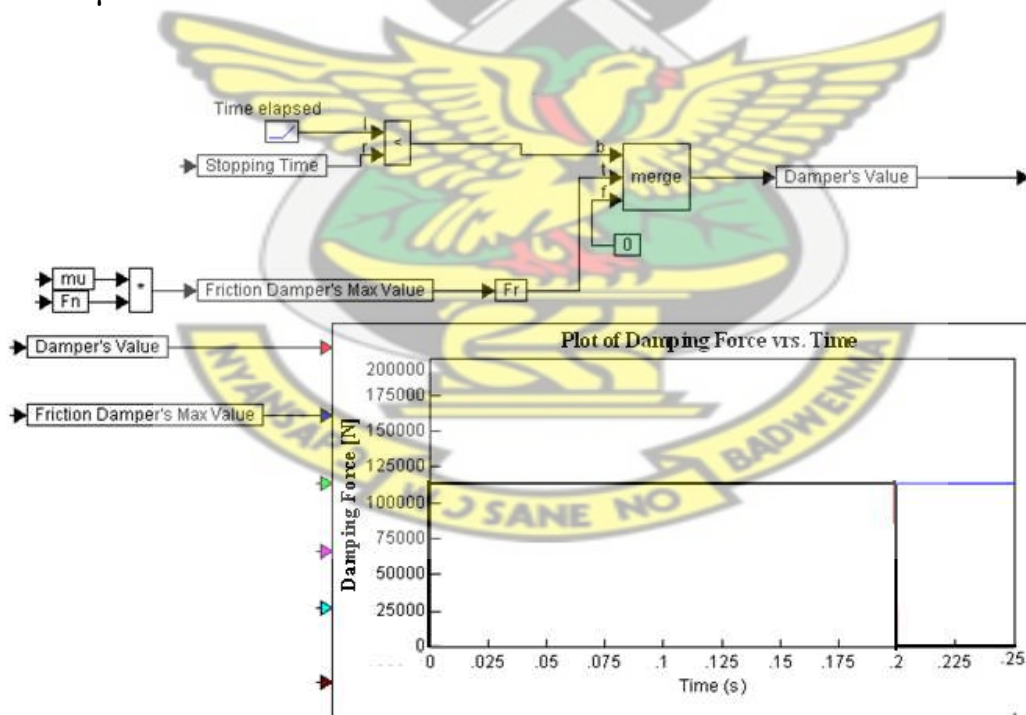


Figure 3.42 Program for the Damping Force

VisSim™ allows the direct exchange of data with other applications. However, to make use of its generated simulation data, the data was written to file before post processing it. To save data to file, the data should be plotted in a plot block. The plot block can handle up to eight different plots per plot block insert. Multiple insertions of plot blocks for one system are possible. The data is presented as a function of time or frequency; on the other hand they could be presented as the logarithmic values of the time or the frequency. The amount of data generated for each plot depends on the simulation properties selected; especially the start time, end time and the time step values used. The number of points or values generated for a plot is given by Time Interval divided by Time Step plus one. For example, for Figure 3.39 with start time = 0 s, end time = 3 s and a Time Step of 0.01 s, it gives:

$1 + (3 - 0)/0.01 = 301$ data points. That means for the displacement $x(t)$, presented in Figure 3.39, data for 301 different time steps were generated.

After plotting the results in a plot block, the data is saved as ASCII data in columns. The number of columns corresponds to a specified order. A lot of data was generated and saved to file from VisSim™ by changing the impact velocity (V_i) from 1.0 m/s to 13.8889 m/s (3.6 to 50 km/h or 2.24 mph to 31 mph) in 12 steps, data are saved for each of the twelve impact velocities. The damping force is also changed from 0 to 228,000 N (in 10 steps) to generate ten different data for each impact velocity used. This is done for all

12 impact velocities to generate in all 120 different data. Each data contains the Time (t), Acceleration ($x\text{-dot-dot}$), Velocity ($x\text{-dot}$), and Displacement (x) information at every simulation step. With an End Time = 0.25 s and a Time Step of 0.00025 s it generates: $1 + (0.25 - 0)/0.00025 = 1001$ data points. This gives data of 1001 x 4 Matrix; for each of the 120 data. Thus MATLABTM receives 120 pieces of data as 1001 x 4 matrices for post processing.

KNUST

3.5 Post Processing of Data

The data generated from VisSimTM is transferred to MATLABTM for data reduction and analysis. A MATLABTM code was developed to read the 120 data files from file after the appropriate correction in the first lines have been made. The data is re-arranged or transformed into a 1001x12 Matrices giving Acceleration only, Velocity only and Displacement only data for all 12 impact velocity simulations and for every damping force value used. That is, for example, for the re-arranged Acceleration only data for a particular damping force; each of the 12 columns contain the acceleration for the 1001 Time Steps generated for a particular impact velocity, say for $V_i = 12$ m/s. The necessary plots and analysis were made.

3.6 Summary

In this chapter the methods used in the modelling of the friction damper, the simulation of the damper responses, and data extraction from the simulation for design purposes were described. The chapter presented the Maxwell,

Kelvin and two Hybrid models for the bumper. It also presented a visual simulation software, VisSim™ and discussed how it was used to program and simulate the friction damper. It then focused on how the simulation software was used to generate the relevant information. MATLAB™ was also mentioned. MATLAB™ was used to post process the data generated from the visual simulation.

KNUST

Four models were discussed. They are the Maxwell, Kelvin, Hybrid 1, and Hybrid 2 models. The Maxwell Model consists of a spring and a damper or dashpot connected in series. The Kelvin model also consists of two elements; a spring and a dashpot, however, they are connected in parallel. The Hybrid models are a modification of the Maxwell and Kelvin models. Hybrid 1 model combines a spring in parallel with the Maxwell model while the second hybrid model, Hybrid 2 model also combines two springs with a dash pot, however it combines the Kelvin model in series with a spring.

The four models were used to simulate the bumper for the responses of the displacement, velocity and acceleration. The response results were compared with the results of a standard crash test, the NCAP test. This is a standard crash test for a vehicle in a Full width barrier test. The responses of displacement, velocity and acceleration of the four models were discussed in line with desired behaviour to evaluate them, and select the most appropriate one for further analysis. The following observations were made:

- i. The behaviour of the displacement, velocity and acceleration responses of the Maxwell model is different from the NCAP test crash plot in Figure 3.11. The deviation is quite high and therefore the Maxwell model is not good to be used for the study, especially, as far as the displacement and velocity responses are concerned.
- ii. In the Maxwell model, for a given damping coefficient, a change in stiffness has very little or no effect on the maximum displacement. With respect to acceleration however, the Maxwell model shows relatively higher responsiveness than the other three models.
- iii. The Kelvin, Hybrid 1 and Hybrid 2 models showed better responsiveness to change in response due to changes in material properties. The three models are damped sinusoidal curves for both the displacement and velocity responses. The first half cycle of the plots (which is the relevant part of the graphs) is similar to the behaviour of the NCAP test plot in Figure 3.11.
- iv. For all the three models, a change in stiffness at constant damping coefficient (i.e. from design point 1 to 3 and from design point 2 to 4), has a greater effect (about three times more) than a change in damping coefficient at a constant stiffness (i.e. from design point 1 to 2, and from design point 3 to 4).
- v. As far as the velocity responses are concerned, the Kelvin model showed higher responsiveness to changes in rebound velocity from one design point to the other in all four scenarios considered. The Kelvin model showed a minimum of 1.12 times more change in rebound velocity than Hybrid 1 (i.e. a change from design point 1 to

- design point 3); and a maximum of 2.68 times more responsiveness than Hybrid 2 for a change from design point 2 to design point 4.
- vi. With respect to change in maximum displacement, the Kelvin model was more responsive than the two hybrid models in changes from design points 3 to 4, and design point 1 to 2.
 - vii. For maximum change in displacement from design points 1 to 3 and from design point 2 to 4, the hybrid models were only slightly more responsive (a difference of 1.6 % to a maximum of 4.4 % more) than the Kelvin model.
 - viii. Concerning the change in maximum acceleration, the Kelvin model was more responsive than the two hybrid models. For all changes from one design point to the other, the Kelvin model showed more responsiveness, except for change from point 1 to 2 where the Hybrid 1 had 2.51 times more change in the maximum acceleration than that for the Kelvin model; and a change from design point 2 to 4 where the Hybrid 2 model had slightly more (1.04 times more) than the Kelvin model.
 - ix. Comparatively the Kelvin model shows the highest level of responsiveness to changes in responses due to a change in the damping coefficients and stiffness of the material.
 - x. The Maxwell, Hybrid 1 and Hybrid 2 models have zero deceleration at time zero, similar to the NCAP test results in Figure 3.11. However, the Kelvin model gave a non-zero initial acceleration.
 - xi. Overall the Kelvin model shows higher responsiveness to changes in maximum deceleration due to changes in material properties.

Justification for Selection of Kelvin Model

The Maxwell model was ruled out as being not suitable for the modelling in this study. For the three remaining models, the Kelvin model gives a second order differential equation which is simpler and easier to solve than the hybrid ones that give third order differential equations. The limitation of the Kelvin model, however, is that it produces a non-zero deceleration at time zero, a deviation from a crash pulse, which is typically zero at time zero. However, in spite of the non-zero initial value in the acceleration, the Kelvin model's pulse duration, and rebound velocities do not deviate much from those of the Hybrid models. From Table 3.6 it deviates by a maximum of 0.01 s from Hybrid 1 model at design points 2 and 3, and a maximum of 0.06 s from Hybrid 2 model at design point 2. Therefore the effect of the non-zero value of the acceleration at time zero is not very significant in the range of material properties under consideration. The Kelvin model shows an overall better responsiveness to changes in material properties in the material property range under study with respect to displacement, velocity and acceleration. It has a simpler solution as compared to those of the Hybrid models. Adding a friction damper to the Kelvin model will give a relatively simpler model equation than adding it to a Hybrid model.

Kelvin's model was therefore selected for the modelling of the bumper to simulate and solve crash phenomenon in this study. The use of a coulomb friction damper was proposed to absorb and dissipate as much energy as possible when combined with the bumper in crash at elevated speed. The Kelvin model was therefore modified by adding a friction element to aid in

more energy dissipation. This model's friction component was effected by controlling the normal force applied on the friction damper. The notion of producing a damping force by controlling a secondary variable as used in this study is termed semi-active control (Dupont et al., 1997). By adding a friction damper to the Kelvin's model the resulting model can be solved by using numerical methods.

KNUST

The resulting modified Kelvin model was mathematically formulated and the resulting differential equation solved through numerical methods. The VisSim™ software was selected for the numerical solution of the problem. VisSim™ is a programming language for solving simple and complicated problems numerically through simulation. MATLAB™ software was selected for the post processing of the simulation results.

The modified Kelvin model can be represented mathematically by the following differential equation. $M\ddot{x} + c\dot{x} + Kx + F_{Damp} = F(t)$. It was assumed that $F(t)$ is a pulse function depicting the impact of a vehicle crashing into a fixed barrier with the initial conditions at impact: $\ddot{x}(0) = 0; \dot{x}(0) = V_i; x(0) = 0$. Where V_i is the impact velocity of the vehicle. The expected solution should be the displacement, velocity and acceleration responses. That is, $\ddot{x}(t), \dot{x}(t)$ and $x(t)$.

CHAPTER FOUR

4.0 Results and Discussion

This chapter presents and discusses the results of the study. The definitions of some terminologies used are also given in this chapter. Finally, the results from experiments are also presented to validate the simulation results. The results are mainly presented as plots of graphs after post processing.

The duration of a collision in a vehicle crash starts at the time of impact (time = 0) till the time of separation (time the acceleration turns zero). The crash pulse resulting from such a crash is defined as the time history of the response of a vehicle system subjected to an impact or excitation (Huang, 2002). VisSimTM software was used to simulate such pulses and the response data was used to produce the plots presented in this chapter.

Figure 4.1 shows a simulated crash pulse from the Kelvin's model. This will be used to explain some terminologies used in the discussion. The input information for the simulation were as follows: stiffness constant, k of 542,700 N/m, damping coefficient c of 11,500 N.s/m, for a vehicle of mass, $m = 1900$ kg. This represents an underdamped response with damping factor $\zeta = 0.18$; ($\zeta = C/2\sqrt{MK}$). The pulse starts at time 0 s and ends at 0.2 s. At time t_m , the time of dynamic crush, which corresponds to 0.1 s, the velocity is zero. At t_r , the time of rebound (or time of separation), the corresponding deceleration is zero. Rebound time t_r corresponds to 0.2 s.

The response was normalized using factors of an undamped system. The aim is to make the relationship between the normalized responses independent of undamped natural frequency, ω_e and impact velocity v_0 . Factors used are v_0/ω_e for displacement, v_0 for the velocity and $v_0\omega_e$ for acceleration. The displacement at the rebound time is the static displacement or permanent deformation which corresponds to the value of 0.20. The normalized dynamic crush at time t_m is 0.75. The coefficient of restitution (e) is defined as the ratio of the relative separation velocity (0.63) to the relative approach velocity (1.0) (Huang, 2002). Here $e = 0.63/1.0 = 0.63$, which is the same as the normalized separation velocity (with respect to the relative approach velocity of one).

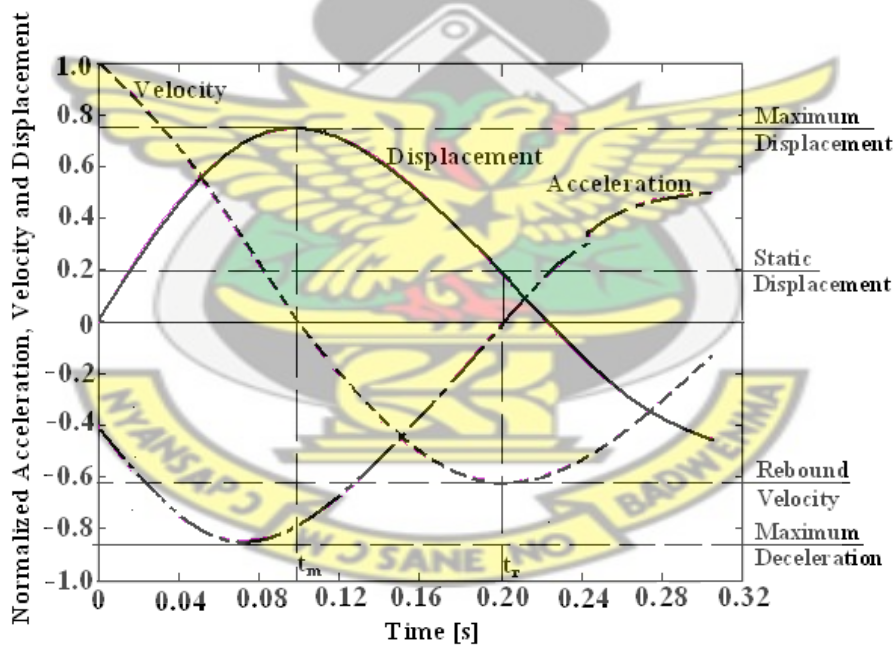


Figure 4.1 Normalized Response of a car to a Crash Pulse

The work done and coefficient of restitution of the moving mass are calculated from the output data after post-processing. From the results, information concerning threshold forces (impact and frictional forces), stiffness, and damping coefficients for the design of the friction damper can be extracted.

4.1 Acceleration Change

The acceleration can be expressed as a factor of the acceleration due to gravity ($g = 9.81 \text{ m/s}^2$) called G's. In terms of G's, an acceleration of 1 is equivalent to 9.81 m/s^2 . Simulation of the bumper-damper system with material stiffness k of 542.7 kN/m, and damping coefficient c of 11.5 kN.s/m, was performed to study the acceleration response of the 1900 kg moving mass after the introduction of a friction element. Starting with friction force of 0 kN, simulation was performed using different impact velocities and the acceleration responses. The input impact velocity was increased from 1 m/s through 13.9 m/s (in 12 steps). This simulation was repeated for different friction elements (with different friction forces). The maximum deceleration from the acceleration responses was recorded for each impact velocity used. Figure 4.2 shows the plot of maximum deceleration for different impact velocities for three friction forces; that is, 0 kN (no friction element used), 152 kN and 228 kN respectively.

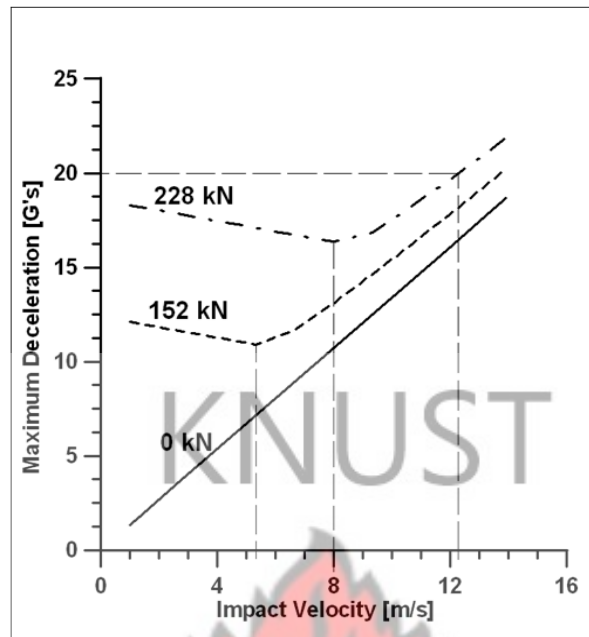


Figure 4.2 Relationship between Impact Velocity and Maximum Deceleration

The plot for the deceleration of the moving mass without any friction element as illustrated in Figure 4.2 is linear and increases with increasing impact velocity. However, with the introduction of a friction element, the trend changes. By applying a friction damper, one can change the dynamic behaviour of the impact attenuation system. Instead of the increase in maximum deceleration monotonously, the maximum deceleration decreases to a threshold value and then begins to increase. This behaviour is more desirable since the G value decreases, causing less damaging effect on the passengers. The threshold value of the impact velocity can be used as a design criterion.

Humans, otherwise in good health, can tolerate 20 G's to 27 G's of instantaneous deceleration without sustaining irreversible injuries. Higher G's may lead to internal organ damage, especially to the arteries (NASA, 2009).

4.2 Deformation

The effect of a friction element on the displacement of the 1900 kg moving mass was studied. Different friction elements were introduced, and simulations performed using a bumper-damper system with material stiffness k of 542.7 kN/m, and damping coefficient c of 11.5 kN.s/m. Starting with friction force of 0 kN, simulation was performed to record the displacement responses using different impact velocities. The results of the simulation are shown in Figure 4.3.

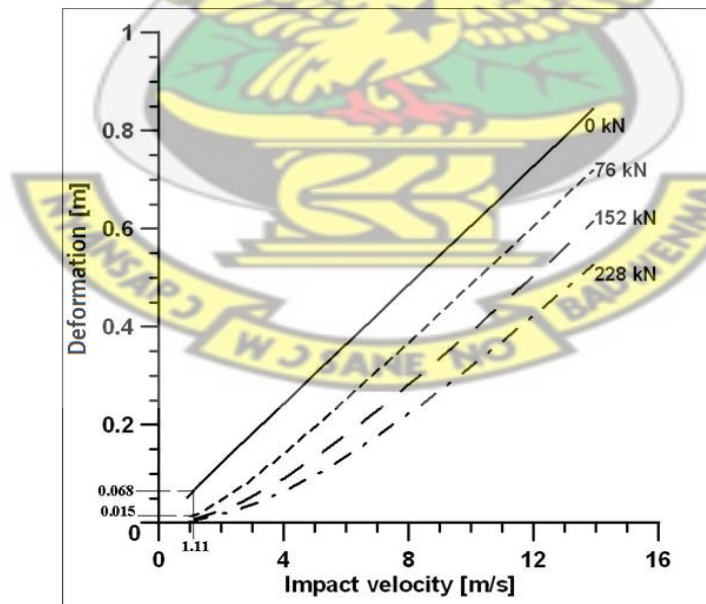
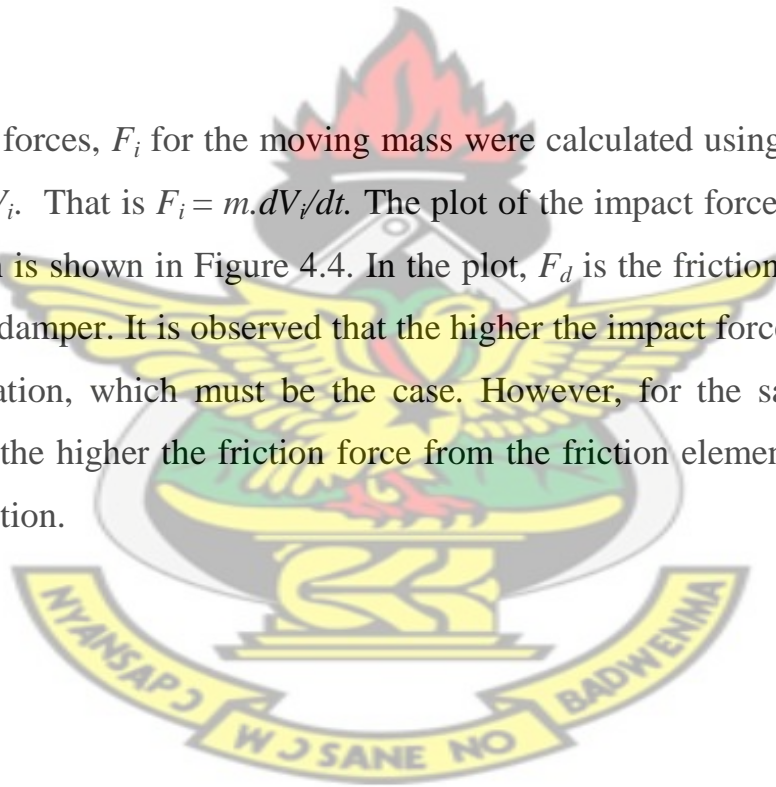


Figure 4.3 Deformation for different Friction Elements

It was observed that the deformation reduced with the introduction of the friction element. For example an impact velocity of 1.11 m/s results in a displacement of nearly 68 mm without a friction element, but 15 mm for an element supplying friction force of 76 kN, and no displacement at 228 kN or higher. For a friction damper to function properly, it is desirable for it to have no displacement. The displacement response can produce a design threshold criterion which, in this case, is 228 kN.

The impact forces, F_i for the moving mass were calculated using the impact velocities, V_i . That is $F_i = m \cdot dV_i/dt$. The plot of the impact force against the deformation is shown in Figure 4.4. In the plot, F_d is the friction force from the friction damper. It is observed that the higher the impact force the higher the deformation, which must be the case. However, for the same impact force used, the higher the friction force from the friction element the lower the deformation.



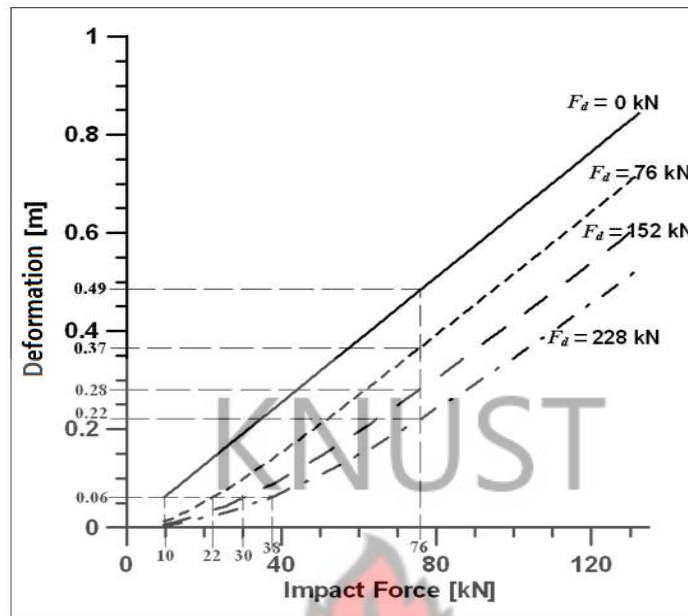


Figure 4.4 Deformation of Bumper for different Impact Forces using Different Friction Elements

The plot shows that without the friction damper the attenuation system will experience a deformation of 0.06 m (60 mm) at an impact force of 10 kN. With the introduction of a friction damper, the impact force that would cause the same deformation increases. This plot also confirms a threshold friction force of 228 kN at which no deformation results. It is desirable to obtain a relationship between the impact force and the deformation as a means to obtain the threshold impact force for a given set of system characteristics.

The threshold friction force of 228 kN was obtained using system parameter of $k = 542.7$ kN/m and $c = 11.5$ kN-s/m. It is of interest to study the effect of k and c (bumper properties) on the threshold impact velocities and how the

threshold friction force improves the threshold of the impact velocity. Figure 4.5 shows the effect of the impact velocity on the threshold friction force. The plot shows that for a given set of material characteristics, the impact velocity greater than 4.13 m/s will cause the friction damper to fail. It is also observed that the threshold friction force of 228 kN introduced could improve the performance of the design material *R* from an impact velocity of 1.11 m/s (4 km/h) to 4.13 m/s (14.9 km/h).

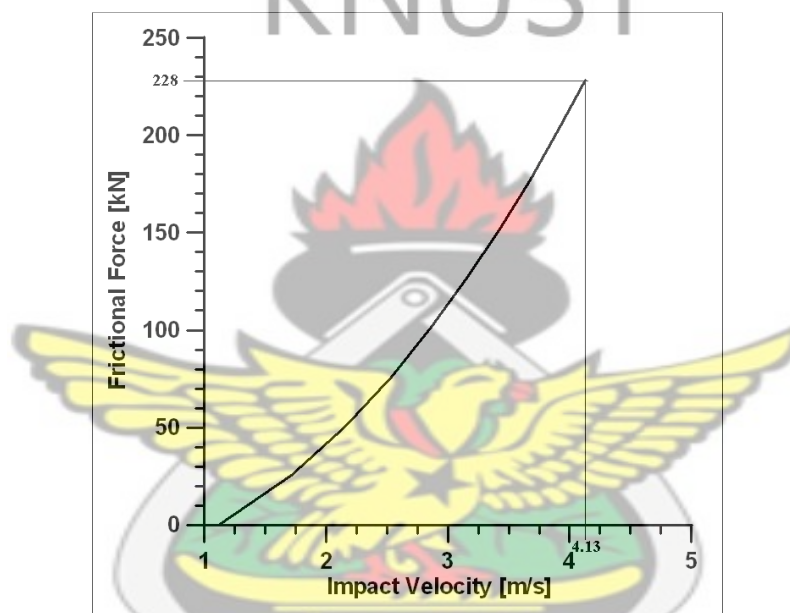


Figure 4.5 Impact velocity and corresponding Friction Force necessary to produce a deformation of 68 mm for the Material *R*

Simulations were performed for each of the remaining four design materials and the threshold impact velocities at the threshold friction force 228 kN recorded. Similar trend of results were obtained for the different design materials. Table 4.1 shows the threshold impact velocities and other information for different bumper material properties; referred to as new

design material D1 through D4. The table gives the spring constants k , damping coefficients c , damping ratios ζ used and the threshold impact velocities v_t ; ($\zeta = \frac{c}{2\sqrt{kM}}$, where M is the mass; $M = 1900$ kg). The results in Table 4.1 are plotted in the 3-D diagram in Figure 4.6.

Table 4.1 Bumper Design Material Parameters (mass = 1900 kg)

Bumper	Spring Constant, k [kN/m]	Damping Coefficient, c [kN-s/m]	Damping Factor, ζ	Threshold Impact Velocity, v_t [m/s]
Design Material R	542.7	11.5	0.1791	4.13
Design Material D1	750.0	13.5	0.1788	3.80
Design Material D2	850.0	14.0	0.1742	3.68
Design Material D3	400.0	6.5	0.1179	4.59
Design Material D4	300.0	6.0	0.125 7	4.97

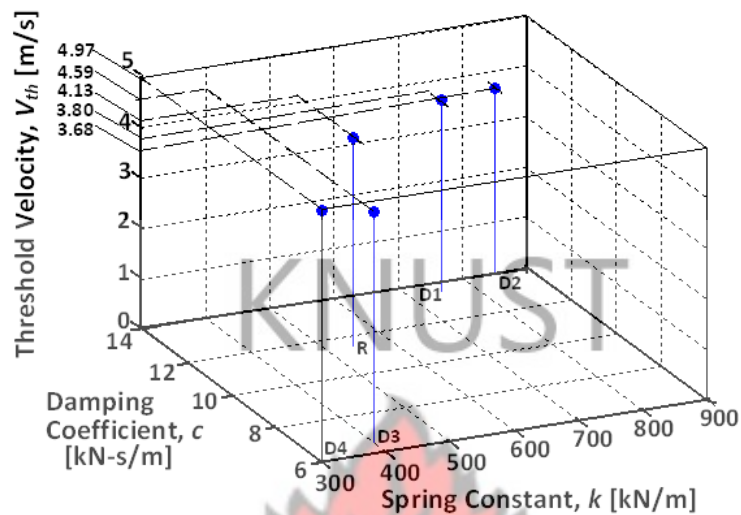


Figure 4.6 Threshold Impact Velocities for various Bumper Material Characteristics

Intuitively, one would believe that the threshold impact velocity would increase as the bumper material stiffness (k) and damping coefficient (c) increase for the same mass. The design materials D1 and D2 represent increases in k and c . The simulation results shown in Figure 4.6 and Table 4.1 indicate that the threshold impact velocity rather decreases from 4.13 m/s to 3.80 m/s and 3.68 m/s respectively. The design materials D3 and D4 were selected to study the effects of decreasing k and c . The responses show that the threshold impact velocity increases from 4.13 m/s to 4.59 and 4.97 m/s respectively, which is the desirable result. The results indicate that the

friction element is more effective for materials with lower viscoelastic properties.

4.3 Work Done

The work done by bumpers of different design materials studied were deduced from plots of impact force against the displacement for the bumpers for different friction elements. Figures 4.7 to 4.9 show plots of impact force against the displacement responses for the five design materials for different threshold friction forces. Figure 4.7 shows the displacement responses using no friction element, Figure 4.8 shows the responses using a friction element with 152 kN friction force and Figure 4.9 shows the responses using a 228 kN friction element. The work done by the bumper materials for the same amount of deformation was calculated for each case. A common deformation was used for all cases to compare the work done. A deformation of 0.3 m was used. The work done was found by calculating the relevant areas in the plot. For example, the work done by the bumper material D4 is given by the shaded area in Figure 4.7 and similarly in Figures 4.8 and 4.9.

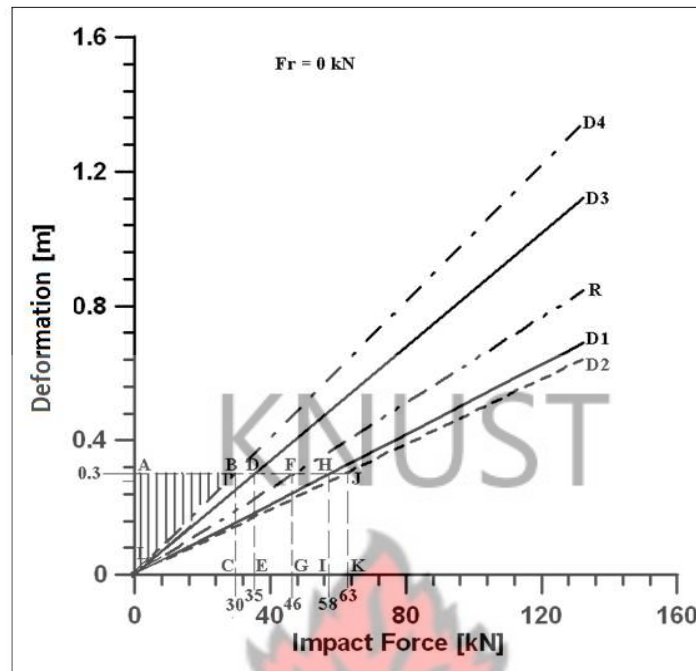


Figure 4.7 Maximum deformation of five Bumper materials at different Impact Forces without a Friction Element



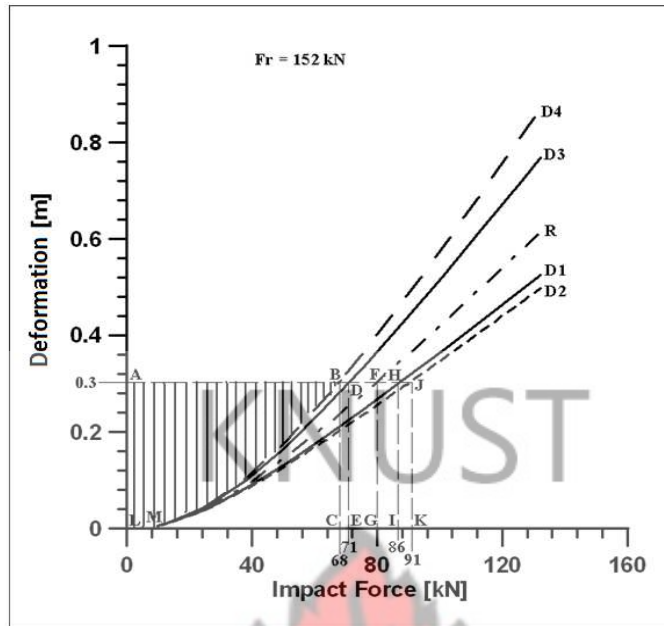
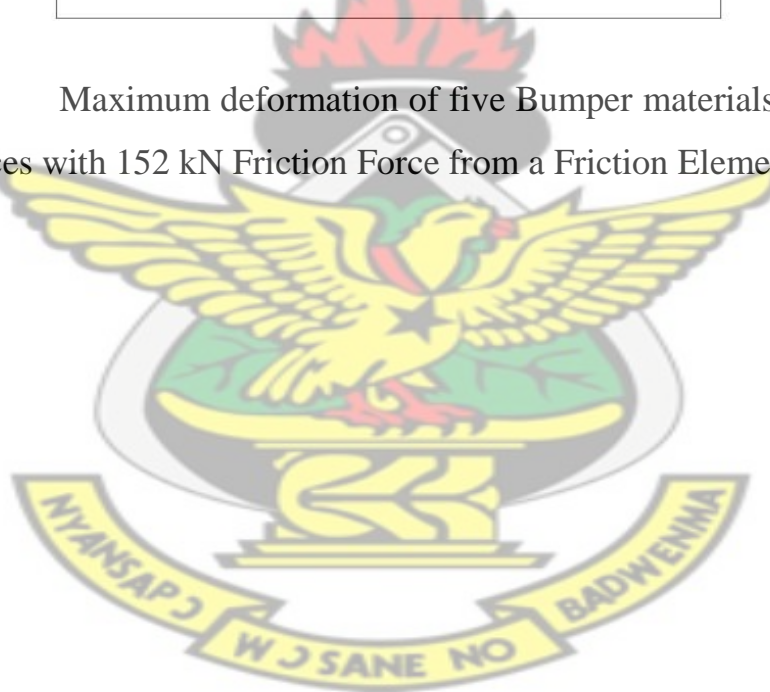


Figure 4.8 Maximum deformation of five Bumper materials at different Impact Forces with 152 kN Friction Force from a Friction Element



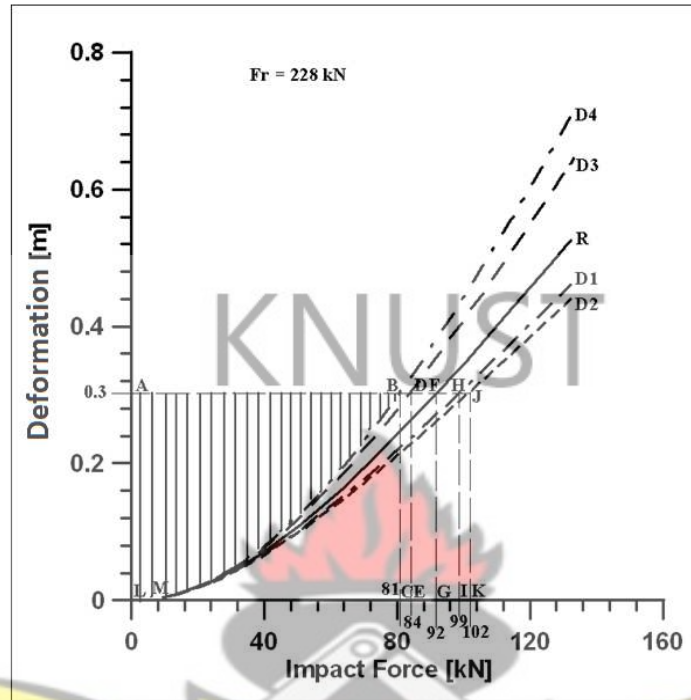


Figure 4.9 Maximum deformation of five Bumper materials at different Impact Forces with 228 kN Friction Force from a Friction Element

The results of the calculations of the work done are given in Table 4.2.

Table 4.2 Work Done by different Bumper Design Materials

Friction Force from Friction Element [kN]	Work Done by Materials [Joules]				
	R	D1	D2	D3	D4
0.0	7050	8640	9260	5310	4430
152.0	14800	15750	16140	13680	13360
228.0	17410	18270	18610	16370	16100

The work done by materials D1, D2, D3 and D4 were compared with that done by material R. The work done by material R without a friction element was subtracted from those by all the other materials to determine how much more work was done by the other materials above that done by the material R with no friction element. The results of the comparison are given in Tables 4.3 and 4.4.

Table 4.3 Extra Work done by different Bumper Design Materials compared with that done by the Design Material R without a Friction Element

Friction Force from Friction Element [kN]	Extra Work done by Bumper Design Materials [Joules]				
	R	D1	D2	D3	D4
0.0	0	1590	2210	-1740	-2620
152.0	7750	8700	9090	6630	6310
228.0	10360	11220	11560	9320	9050

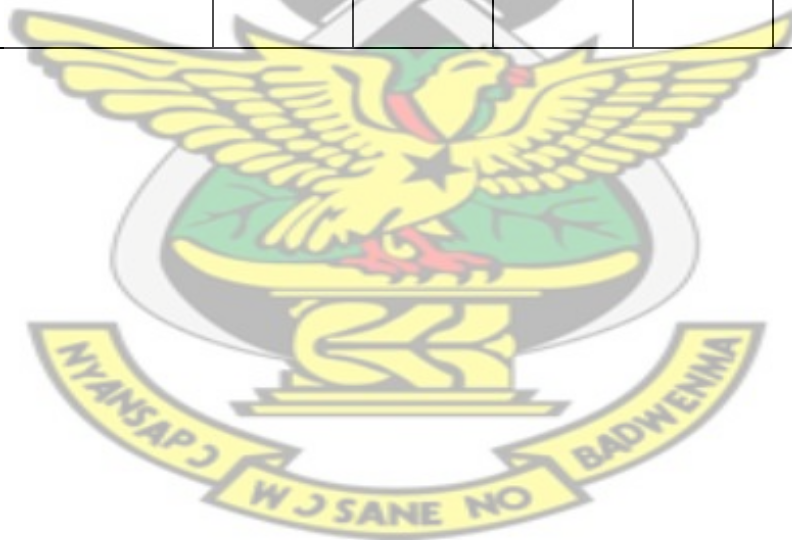


Table 4.4 Percentage Extra Work done by different Bumper Design Materials compared with that done by the Design Material R without a Friction Element

Friction Force from Friction Element [kN]	Extra Work done by Bumper Design Materials [%]				
	R	D1	D2	D3	D4
0.0	0.00	22.55	31.35	-24.68	-37.16
152.0	109.93	123.40	128.94	94.04	89.50
228.0	146.95	159.15	163.97	132.20	128.37

Another comparison with work done by the materials with and without a friction element was made. The work done by the materials without a friction element was compared with that done by the same material with a 152 kN and 228 friction elements respectively. The results are given in Tables 4.5 and 4.6. Table 4.5 gives the difference in Joules while Table 4.6 gives the difference as a percentage of the work done without a friction element.

Table 4.5 Extra Work done by different Bumper Design Materials as result of the introduction of Friction Element

Friction Force from Friction Element [kN]	Extra Work done by Bumper Design Materials [Joules]				
	R	D1	D2	D3	D4
152.0	7750.0	7110.0	6880.0	8370.0	8930.0
228.0	10360.0	9630.0	9350.0	11060.0	11670.0

Table 4.6 Extra Work done by different Bumper Design Materials as result of the introduction of Friction Element as a percentage

Friction Force from Friction Element [kN]	Extra Work done by Bumper Design Materials [%]				
	R	D1	D2	D3	D4
152.0	109.93	82.29	74.30	157.63	201.58
228.0	146.95	111.46	100.97	208.29	263.43

It is desirable for the attenuation system to do less work during its operation. From the results, the amount of work done by D4 increased the most, followed by D3, R, D1 and D2, in that order. D4's work done, the maximum, was increased by 201.58% and 263.43% with the introduction of 152 kN and 228 kN friction elements respectively; while D2's work done, the minimum, increased by 74.30% and 100.97% with the introduction of 152 kN and 228 kN friction elements respectively. It can be observed that the lower the stiffness and damping coefficient, the greater the influence of a friction element on the work done. This confirms the conclusions from the discussions from the deflection analysis in Section 4.2

It was observed that the addition of a 228 kN friction element to a bumper-damper system with the new design parameters (as in D2) can improve the work done by nearly 164 %, and the addition of a friction element to an ordinary bumper-damper system with the traditional design parameters (as in R) can improve the work done by nearly 147 %.

4.4 Design Deductions from the Simulation

Different information were extracted from the simulation results. Observation from the simulations indicates that for the selected set of system characteristics (k and c), the threshold friction damping force is 228 kN. Friction forces below this value would cause sliding to occur. From the information obtained from the deceleration, the results in Figure 4.2 suggests

that if a damping frictional force of 228 kN is used, the impact velocity should not be more than 12.2 m/s (44 km/h) in order not to exceed a 20 G limit. This gives a ceiling on the amount of impact force that can be tolerated in the scope of this study. That is for a moving mass of 1900 kg as used in this study, the ceiling impact force $\left(\frac{m(v_1 - v_2)}{t_1 - t_2}\right)$, is 115.9 kN, assuming the impact time $t_1 - t_2 = 0.2$ s and velocity change of 12.2 m/s.

From the discussions in section 4.2 under deformation, it was observed that design D2 suffered the least deformation followed by D1, R, D3 and D4 in that order. Among the five bumper materials studied, material D2 recorded the highest work done after impact for the same amount of deformation, followed by designs D1, R, D3 and D4 in that order. It is observed that the higher the stiffness constant k , and coefficient of damping c , the better the bumper would be in terms of its capacity to do work and the resistance to deformation. However, the threshold impact velocity decreases.

Overall the design material D2 can be considered best among all the five materials in terms of its ability to do more work. The design parameters selected are therefore those of D2, which are 850 kN/m for k and 14.0 kN-s/m for c . On the other hand in terms of high threshold impact velocity, D4 is better. The design parameters selected (for D4) are 300 kN/m for k and 6.0 kN-s/m for c .

4.5 Friction Damper Design Concepts

Four different friction damper concepts were put forward and one was selected for an in-depth study. Figures 4.10 – 4.18 show the concepts considered. Concept 1 is shown in Figures 4.10 and 4.11. It consists of a split stationary outer hollow cone with a mating cone carrying friction lining. The impact force is transmitted to the friction surfaces via the inner cone bar. Energy is dissipated by friction action as the inner cone moves relative to the stationary outer hollow cone.

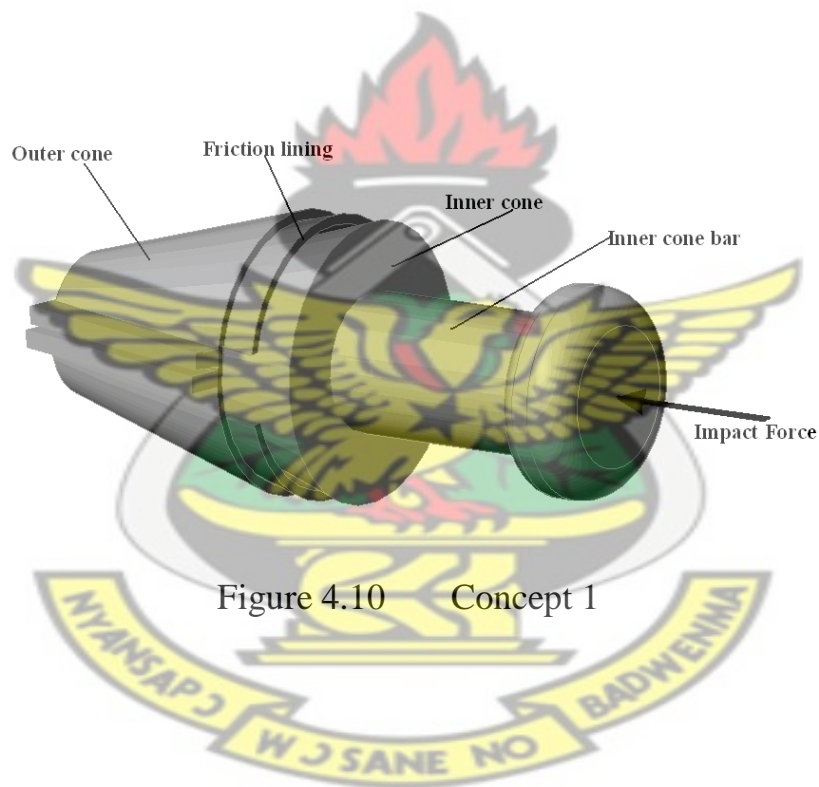


Figure 4.10 Concept 1

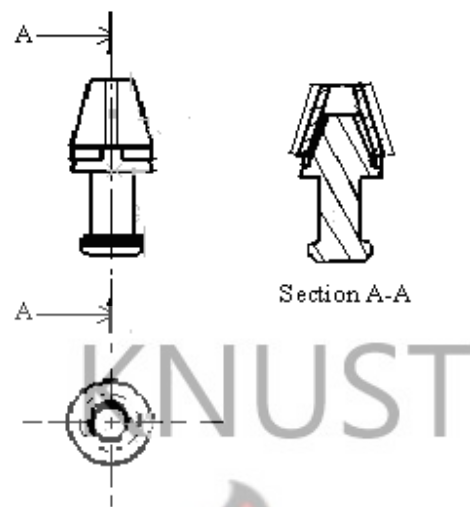


Figure 4.11 Orthographic Views of Concept 1

Concept 2 is shown in Figure 4.12. It is in the form of a box in the shape of a rectangular prism made with steel plates. It consists of four friction pads that are pressed against the inner walls of the outer case by means of two pairs of compressive springs. The compressive springs are placed at the central position of the damper and are held in place by pairs of spring guides made up of male and female parts.

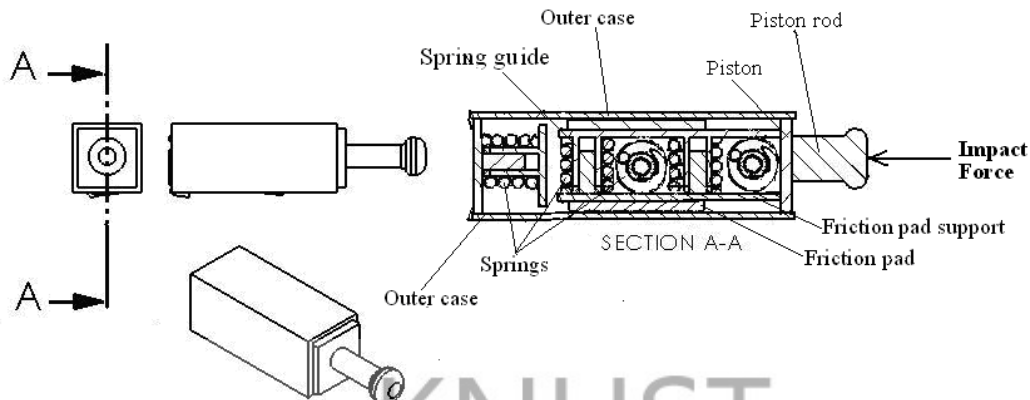


Figure 4.12 Concept 2

One pair of springs is vertically positioned to hold the top and bottom pads in place, while another pair that is horizontally positioned holds the left and right pads. A sectional view of the damper concept is also shown in the same figure. The impact force is transferred to the friction pads through the piston rod. This causes a relative motion between the friction pads and the outer case and dissipates the impact energy as a result. The return spring should return the piston after the initial impact, if necessary.

Concept 3 is similar to concept 2 and it is shown in Figures 4.13, 4.14 and 4.15. Figure 4.14 shows a sectional view and Figure 4.15 the exploded view of the damper. Unlike the concept 2, the impact force is transmitted to the frictional pads through a system of levers that diverts the direction of the impact force by 90° and pushes a rectangular piston which further pushes the friction pads to cause a relative motion between the friction pads and the

outer case to dissipate energy. A return spring at the end of the damper should return the piston after an impact, if necessary.

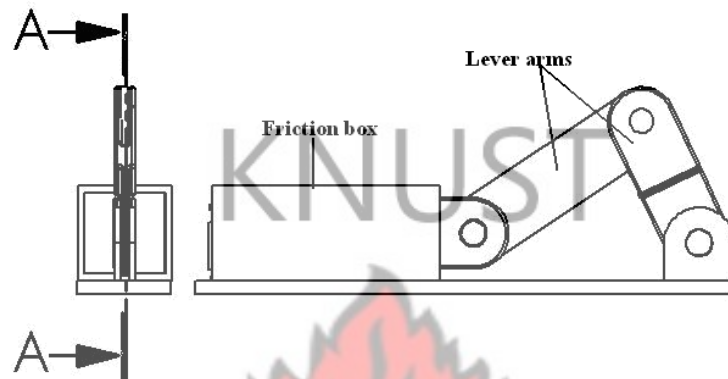


Figure 4.13 Concept 3

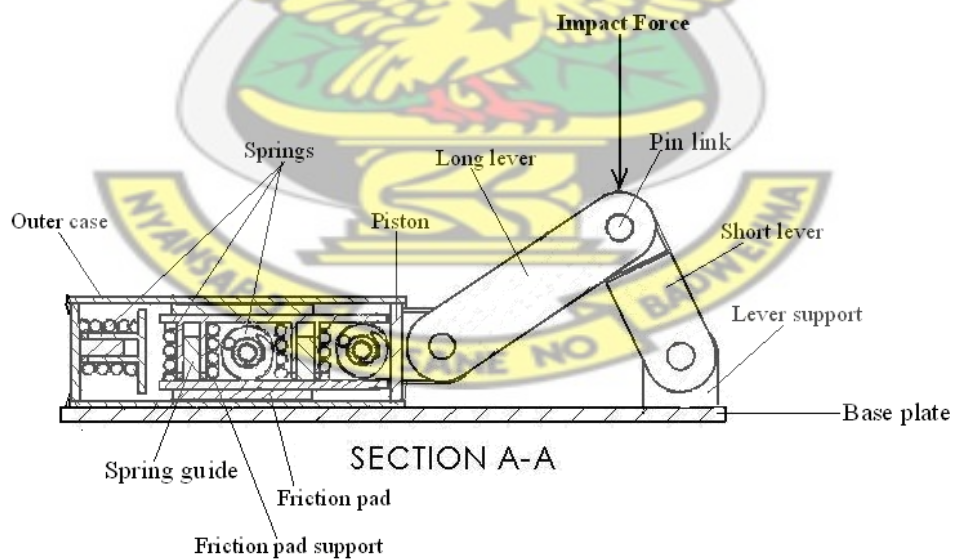


Figure 4.14 Sectional View of Concept 3

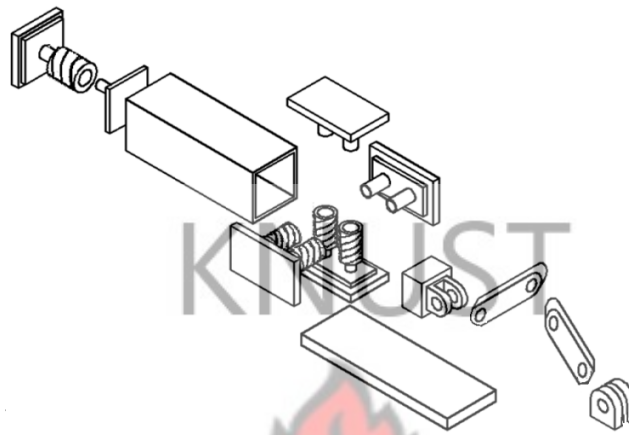


Figure 4.15 Exploded View of Concept 3

Concept 4 is cylindrical in shape. It is a slight modification of concept 3. Figure 4.16 shows an isometric view of concept 4. Figures 4.17 and 4.18 give the sectional and the exploded views of concept 4 respectively. The transmission of the impact force is through the levers as in concept 3. The difference is a cylindrical outer case, a cylindrical piston and the arc-shaped friction pads. A return spring similar to that of concepts 2 and 3 should return the piston after impact, if necessary.

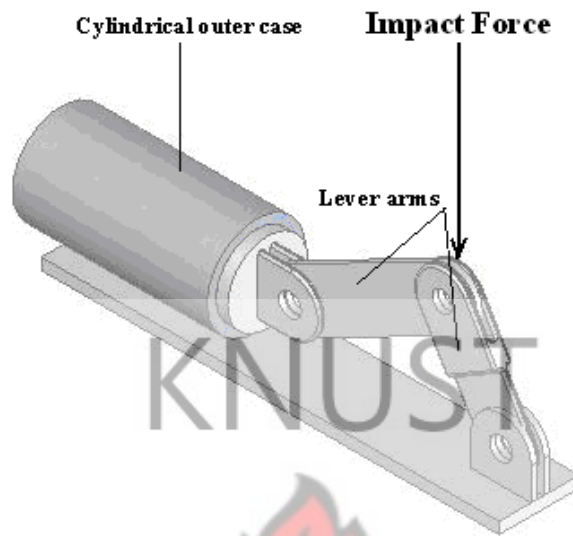


Figure 4.16 Concept 4

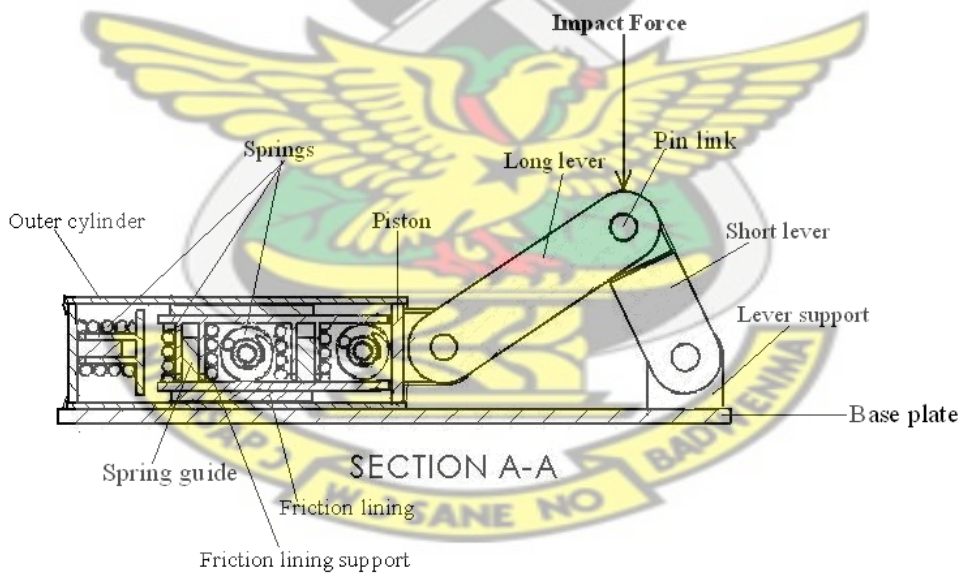


Figure 4.17 Sectional View of Concept 4

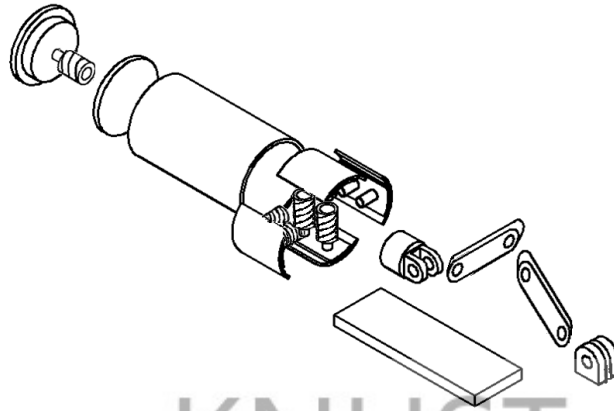


Figure 4.18 Exploded View of Concept 4

The advantages and disadvantages of the four design concepts were weighed based on the criteria given in Table 4.7. The concepts were evaluated using four objectives, namely, low cost, shock reduction, high friction contact areas, and low space occupied by damper. The objectives were given different weights, depending on their importance and influence in the selection process. High friction contact area was given 40%, the highest weight; followed by shock reduction/deflection, 30%; then low production cost, 20%; and lastly the space occupied by the damper, 10%. The scoring was done on a scale from 1 as the worst to 5 as the best. For example, in the case of cost, a very expensive design is given 1 and a very cheap one 5.

During the evaluation, the score of a particular objective was multiplied by the weight to give the value for an objective. The sum of the values gives the overall utility value for a concept. The concept with the highest overall utility value was selected as the most suitable concept.

Table 4.7 Production Cost Evaluation Scores

Low cost of Production [GHC]	1.00 to 40.00	40.01 to 80.00	80.01 to 120.00	120.01 to 160.00	Above 160
Score	5	4	3	2	1

Table 4.8 Shock Deflection Evaluation Scores

Deflection of Shock [degrees]	0 to 19	20 to 39	40 to 59	60 to 79	80 to 90
Score	1	2	3	4	5

Table 4.9 Friction Surface Area Evaluation Scores

Surface Area [cm ²]	0 to 100	101 to 200	201 to 300	301 to 400	Above 400
Score	1	2	3	4	5

Table 4.10 Space Occupied by Damper Evaluation Scores

Space Occupied [cm]	0 to 8.0	8.1 to 16.0	16.1 to 24.0	24.1 to 32.0	Above 32.0
Score	5	4	3	2	1

Table 4.11a Evaluation Table for Concept One

Objective	Weight	Parameter	Design Concept		
			Concept 1		
			Magnitude	Score	Value
Low cost of Production	0.2	Cost [GHC]	70.00	4	0.8
Deflection of shock	0.3	Angle [°]	0	1	0.3
High Friction Contact Area	0.4	Surface Area [cm ²]	198.0	2	0.8
Space Occupied	0.1	Length [cm]	20.0	3	0.3
Overall Utility Value					2.2

Table 4.11b Evaluation Table for Concept Two

Objective	Weight	Parameter	Design Concept		
			Concept 2		
			Magnitude	Score	Value
Low cost of Production	0.2	Cost [GHC]	118.50	3	0.6
Deflection of shock	0.3	Angle [°]	0	1	0.3
High Friction Contact Area	0.4	Surface Area [cm ²]	448.0	5	2.0
Space Occupied	0.1	Length [cm]	30.0	2	0.2
Overall Utility Value					3.1

Table 4.11c Evaluation Table for Concept Three

Objective	Weight	Parameter	Design Concept		
			Concept 3		
			Magnitude	Score	Value
Low cost of Production	0.2	Cost [GHC]	168.00	1	0.2
Deflection of shock	0.3	Angle [°]	90	5	1.5
High Friction Contact Area	0.4	Surface Area [cm ²]	448.0	5	2.0
Space Occupied	0.1	Length [cm]	15.0	4	0.4
Overall Utility Value					4.1

Table 4.11d Evaluation Table for Concept Four

Objective	Weight	Parameter	Design Concept		
			Concept 4		
			Magnitude	Score	Value
Low cost of Production	0.2	Cost [GHC]	181.00	1	0.2
Deflection of shock	0.3	Angle [°]	90	5	1.5
High Friction Contact Area	0.4	Surface Area [cm ²]	352.0	4	1.6
Space Occupied	0.1	Length [cm]	15.0	4	0.4
Overall Utility Value					3.7

From the information in Tables 4.11 a to 4.11 d, concept 3 had 4.1 as the overall utility value, which is the highest; therefore concept 3 was selected over the other three concepts.

Using the concept 3 as the selected model, calculations were made using impact velocity of 12 m/s (43.2 km/h) to compute for impact force and used to calculate for the dimensions of the lever of the model, using steel as the material. The calculations are given in appendix A. The results from the calculations are given in Table 4.12.

Table 4.12 Link Diameter, Width and Thickness of steel plate for the Damper

Impact Velocity [m/s]	Impact Force [kN]	Plate thickness [mm]	Plate width [mm]	Link diameter [mm]	Length of Longer Lever [mm]
12	114	39	80	42	300

Using a lever arm of 0.1 m and 0.15 m for the short and long arms respectively, an optimization code written in MATLAB™ was used to find

the appropriate plate dimensions of steel plate to produce the damper model for the experiment. The following optimization problem was solved:

Design variables used were the plate thickness, t ; the diameter of link, D ; the length of lever, L ; and height of plate, h .

The cost function for the optimization problem was:

Minimize the total volume of material: $f = tLh$

Linear Inequality constraints:

Length's constraint: $0.10 \leq L \leq 0.15$ and

Height's constraint: $0.03 \leq h \leq 0.07$

That is:

$$0.10 - L \leq 0;$$

$$L - 0.15 \leq 0;$$

$$0.03 - h \leq 0;$$

$$h - 0.07 \leq 0;$$

Non-linear inequality constraints:

Tensile strength constraint: $9123.5 - 71.4286 \times 10^6 th + 71.4286 \times 10^6 tD \leq 0$.

Johnson's Equation; Buckling constraint: $31932h - 250 \times 10^6 th^2 + 90262.0724tL^2 \leq 0$.

Link's shear constraint: $5.8082 \times 10^3 - 41.4286 \times 10^6 D^2 \leq 0$.

The optimization program is given in appendix B. The lever arms selected was to allow four dampers to be conveniently mounted on a bumper. The results of the diameter for the link, as well as width and thicknesses of plate obtained are given in Table 4.13.

Table 4.13 Link Diameter, Width and Thickness of steel plate for the Damper Model

Impact Force [kN]	Plate thickness [mm]	Plate width [mm]	Link diameter [mm]	Length of Longer Lever [mm]
9.1235	6	40	10	100

Figure 4.19 shows an isometric view of a model of the selected concept with the directions of impact force, normal force and frictional force indicated.

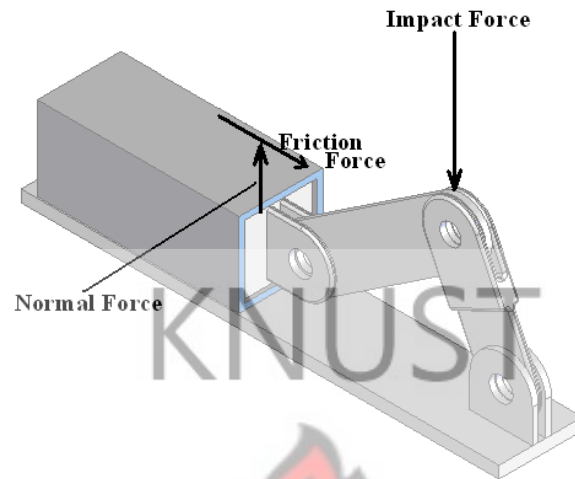


Figure 4.19 Conceptual Model of a Friction Damper showing direction of Forces

The friction pads, as shown in Figure 4.20 are pressed against the four inner walls of the box by means of compression springs. These springs provide the normal forces for the friction pads. The friction force can be changed by changing the normal force, in this case by changing the compression on the springs, since $F_n = kx$, where F_n is the normal force, k is the stiffness of the spring and x is the compression in the spring. The next section deals with the experiment.

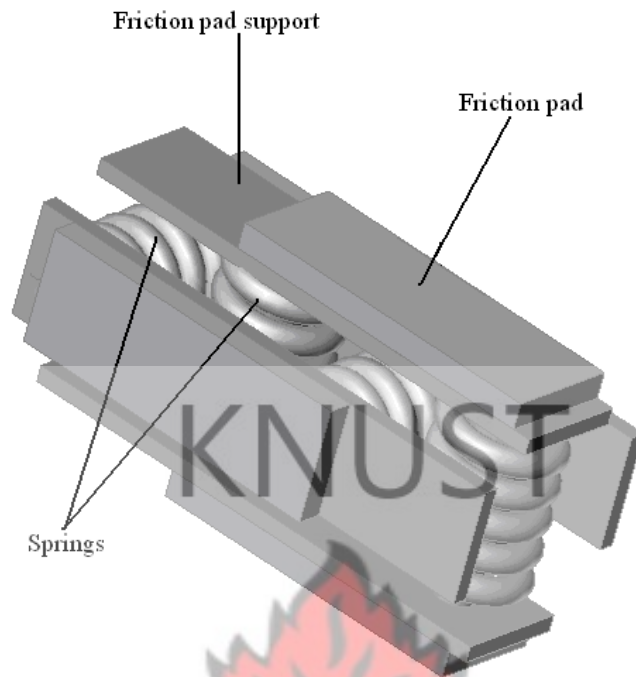


Figure 4.20 Friction Pads with Compression Springs inside Friction Box

4.6 *Experimental Validation of Model*

An experiment was performed using an impact test machine to test a model of the selected proposed friction damper to investigate the validity of the work. A schematic diagram of the impact test machine is given in Figure 4.21. The impact test machine was not designed for small specimen and not for bumper specimen, therefore two special fixtures had to be made to adapt the machine to do the test. The hammer's fixture was made with a 30 mm thick plate of size, 160 mm x 170 mm. The hammer's fixture was bolted to the hammer to give a flat surface for the impact. The impact fixture was made in the shape of an L, with webs to strengthen the welded joints. The thickness of the plate used was 30 mm and the dimensions were: 240 mm x

105 mm for the longer leg and 110 mm x 105 mm for the shorter leg. The web used had a thickness of 13 mm. It was clamped into the impact machine as shown in Figure 4.21.

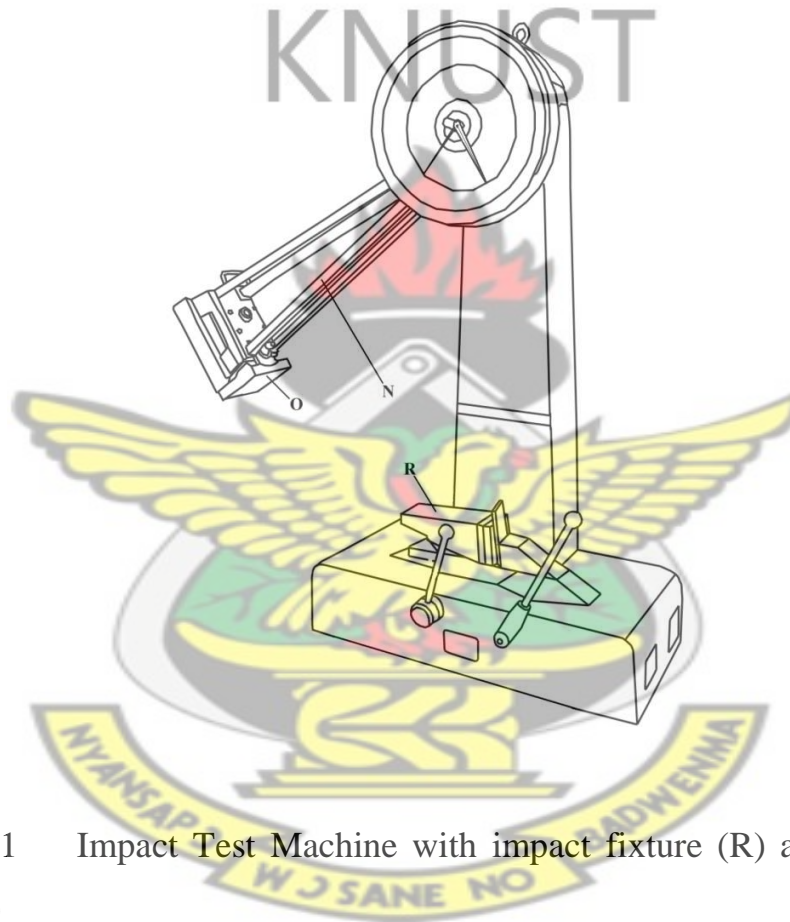


Figure 4.21 Impact Test Machine with impact fixture (R) and hammer fixture (O)

During the experiment, the bumper specimen and damper, where applicable, were arranged together and the hammer of the impact machine allowed to fall freely to impact on it. The hammer of the impact test machine is raised

to a height and allowed to fall under gravity to hit the bumper specimen in the experimental setup. During the experiments four different heights were used to give four impact forces. The deformation on the bumper specimen was then measured with a veneer caliper and noted. The impact force is calculated using the angle, θ , that the hammer swings through before impact, as indicated in Figure 4.22. A sample calculation is given in appendix C.

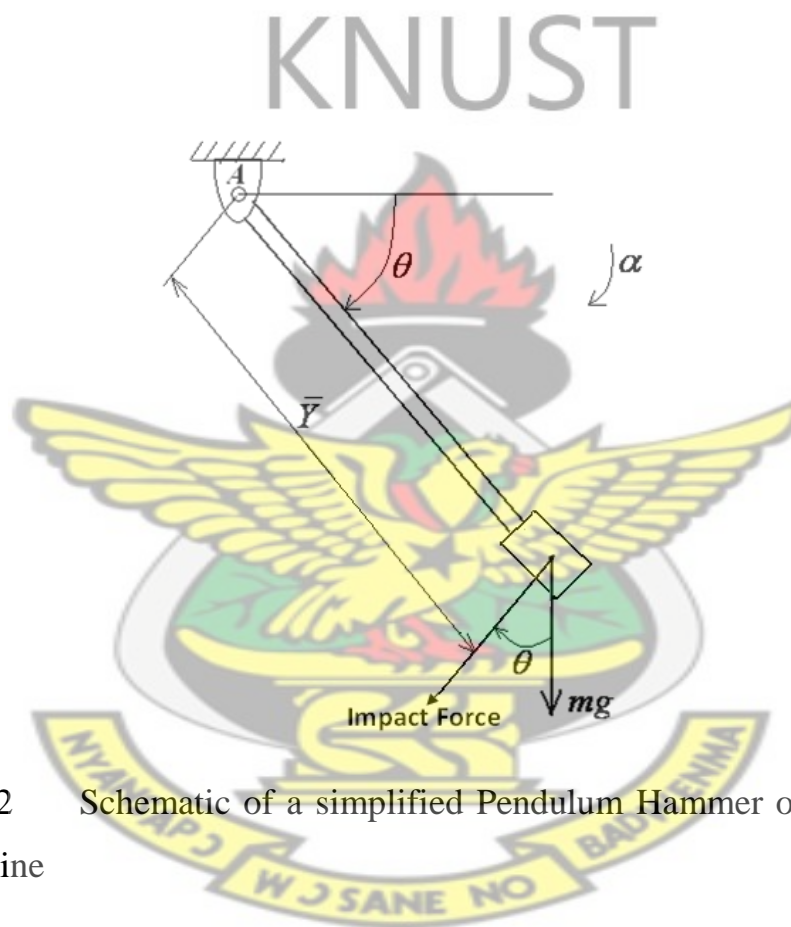


Figure 4.22 Schematic of a simplified Pendulum Hammer of an Impact Test Machine

Destructive impact tests were performed on pieces of the bumper specimen. In all, 24 different specimen were tested. The specimen were taken from four types of bumpers. The four types of bumpers from four types of cars were named A, AA, B and C. For bumper type A and AA, one bumper each

was used, however, for types B and C two bumpers each were used. Each bumper was divided into four pieces. Only the middle section of the bumper was used. That is the curved parts at the ends of the bumper were not used. The average length of the specimen was 35 cm. The specimen and damper were put together as shown in the schematic set-up in Figures 4.23 and 4.24. Figure 4.23 shows the set-up without a friction damper and Figure 4.24 shows the set-up with a friction damper.

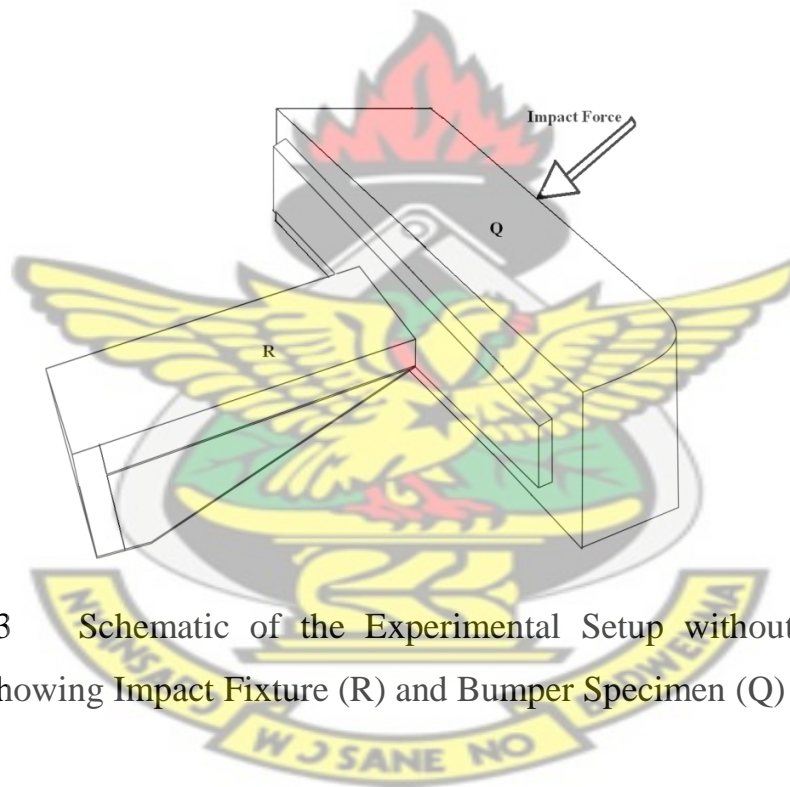


Figure 4.23 Schematic of the Experimental Setup without a Friction Damper: showing Impact Fixture (R) and Bumper Specimen (Q)

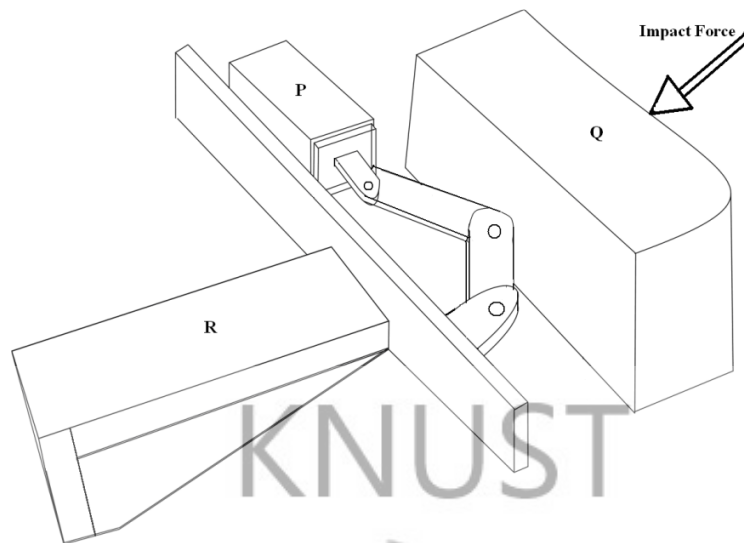


Figure 4.24 Schematic of the Experimental Setup with a Friction Damper: showing Impact Fixture (R) and Bumper Specimen (Q)

Two models of the friction damper were made for the experiment. Model 1 was made with springs of stiffness 44 kN/m and Model 2 with springs of stiffness 37 kN/m. For the four specimens of bumper AA, two were tested on the impact machine without the damper and the remaining two were tested with damper Model 1. The results are given in Table 4.14. Out of the eight specimen from bumper B, four were tested using four different impact forces without the introduction of the friction damper. The remaining four were tested using four different impact forces with damper Model 2. Similarly, for bumper C, four specimens were tested without the damper, and four tested with damper Model 1. The results of the tests are also presented in Table 4.14. Table 4.14 shows the deformations measured in the experiments for the four bumpers: namely AA, A, B and C, without friction

damper. Table 4.15 shows the deformations measured in the experiments for three bumpers: namely AA, B and C, with friction damper.

Table 4.14 Deformation of Bumper specimen in the Experiment without a Friction Damper.

Impact Load	Impact Load without a Friction Element [N]			
	3662.80	5856.50	7491.70	9122.80
AA-without a Friction Element [mm]	-	11.00	-	14.40
A- without a Friction Element [mm]	3.50	7.00	7.00	10.00
B- without a Friction Element [mm]	2.00	3.00	11.50	20.00
C- without a Friction Element [mm]	7.0	13.0	20.5	40.0

Table 4.15 Deformation of Bumper specimen in the Experiment with a Friction Damper.

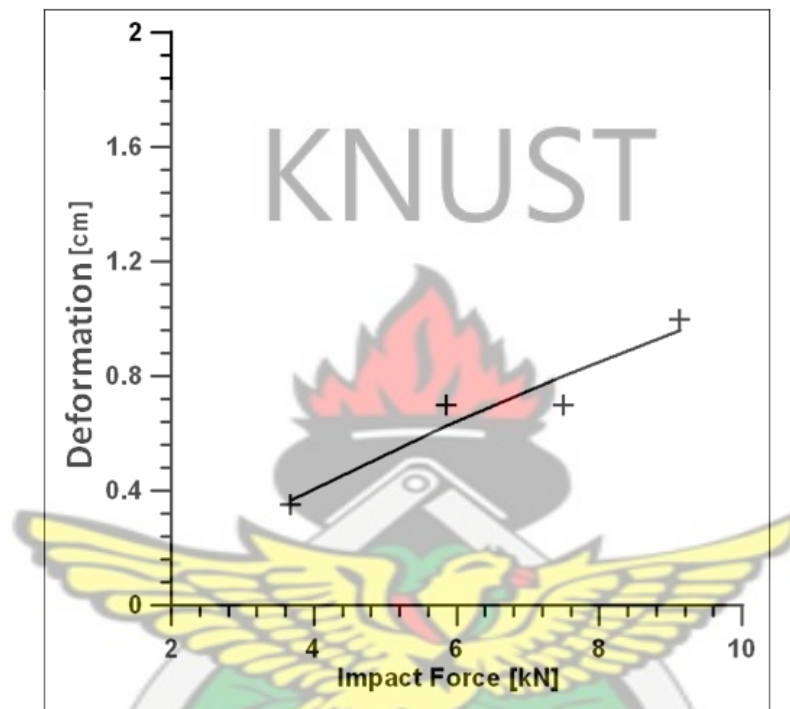
Impact Load	Impact Load with a Friction Element [N]			
	3552.26	5788.10	7438.27	9078.95
AA-with a Friction Element [mm]	-	2.30	-	8.10
B- with a Friction Element [mm]	6.00	3.30	16.50	10.00
C- with a Friction Element [mm]	4.0	8.0	9.0	27.0

Using a similar curve-fitting method used for the simulation results, the equations of the curves fitted to the experimental results were also obtained. It was similar to that for the simulation results. The general form of the equation, was: $y = Ax + B \ln x + C$; where y is the displacement and x is the impact force $\times 10^{-5}$. That is Displacement = $A(\text{Impact force} \times 10^{-5}) + B(\ln(\text{Impact force} \times 10^{-5})) + C$. the coefficients A, B, and C in the equation were found as presented in Table 4.16. Equations of the curves are also given in Table 4.16.

Table 4.16 Curve-fitted Equations of the Deformation for different Impact Forces for different Bumper Specimen

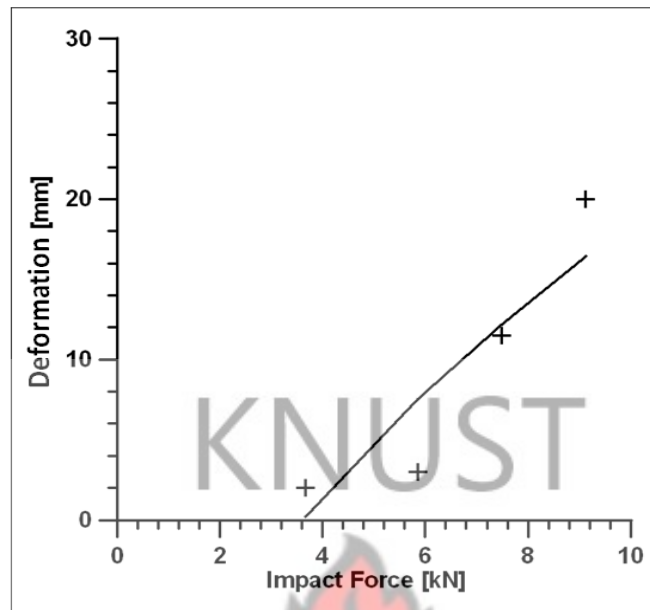
Bumper Specimen	Equation Coefficients			Curve-fitted Equation
	A	B	C	$y = Ax + B \ln x + C$
A- without a Friction Element	7.0809	0.2292	0.8625	Displacement = 7.0809 (Impact force x 10 ⁻⁵) + 0.2292 (ln (Impact force x 10 ⁻⁵)) + 0.8625
B- without a Friction Element	158.5881	8.3006	21.8150	Displacement = 158.588(Impact force x 10 ⁻⁵) + 8.3006(ln (Impact force x 10 ⁻⁵)) + 21.8150
C- without a Friction Element	93.5685	-2.1561	-10.0969	Displacement = 93.5685 (Impact force x 10 ⁻⁵) - 2.1561 (ln (Impact force x 10 ⁻⁵)) - 10.0969
C- with a Friction Element	143.3301	-6.2170	-25.4479	Displacement = 143.330(Impact force x 10 ⁻⁵) - 6.2170 (ln (Impact force x 10 ⁻⁵)) - 25.4479

Figures 4.25 – 4.30 show the experimental results with the curve-fitted plots.



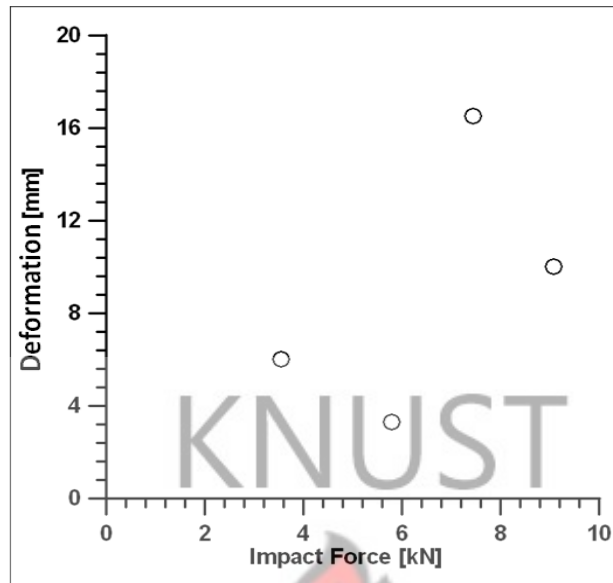
Figures 4.25 Results for Bumper A without a Friction Element

The results of Bumper A without a friction damper shows a linear relationship for the displacement response. Results from simulations gave a perfectly linear relationship for responses without a friction element, however Figure 4.25 does not give a perfect straight line.



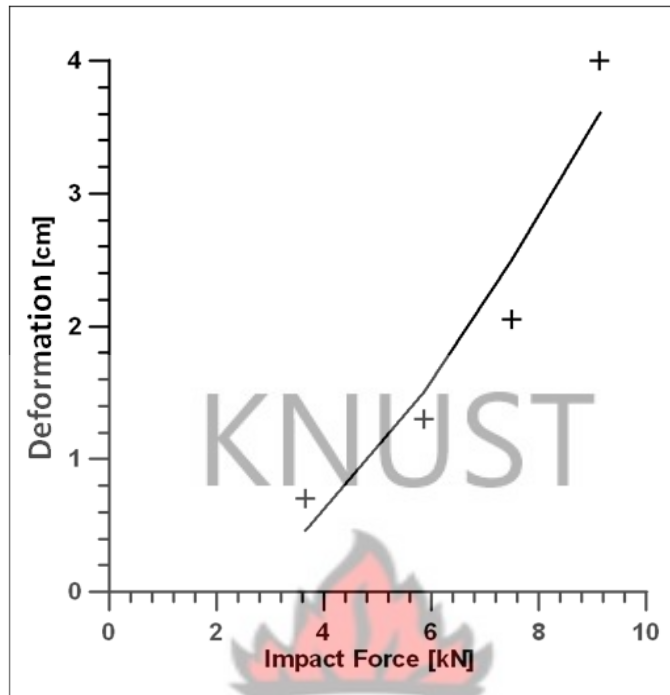
Figures 4.26 Results for Bumper B without a Friction Element

The results of Bumper B without a friction damper as shown in Figure 4.26 is also linear. As observed with the experimental results of Bumper A, the linear relationship is not a perfect one. There could have been an error in the test using the 5.857 kN force. The deformation of 3.0 mm deviates the most from the fitted curve.



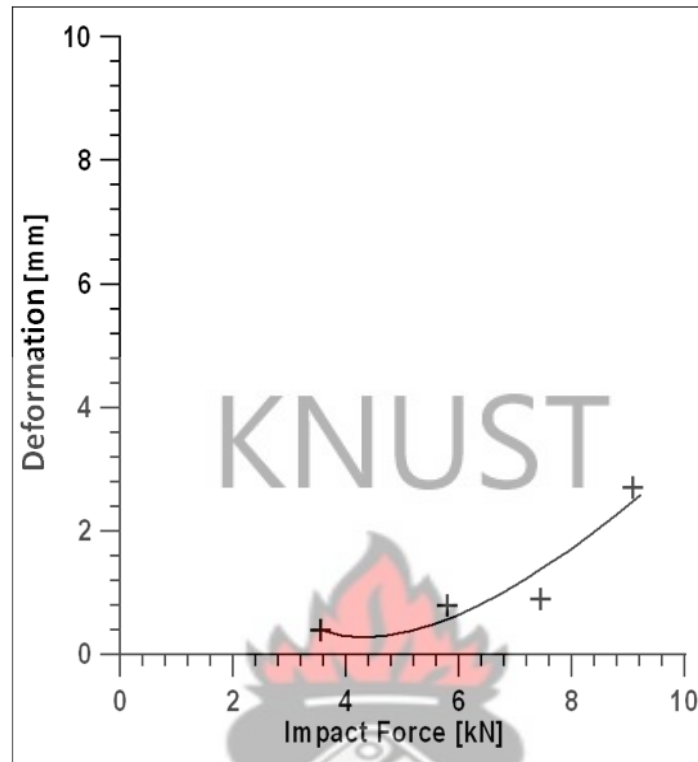
Figures 4.27 Results for Bumper B with Friction Element Model 2

It was observed that no equation could be obtained for the test results of Bumper B with damper as shown in Figure 4.27. The results showed a scatter and did not follow any trend and could not be fitted to the equation of the form: $y = Ax + B \ln x + C$; where y is the deformation and x is the impact force $\times 10^{-5}$. Damper model 2 was used for this test. There was a sliding action during the test, but tests with damper model 1 stuck during the tests. This confirms the use of sticking friction rather than sliding friction in the mathematical model. As a result of the sliding, the experiments did not give the expected results, i.e. results that could be fitted to the function: $y = Ax + B \ln x + C$ as obtained for the simulation results. The result was inconclusive as a result of the sliding of damper model 2 during the experiment.



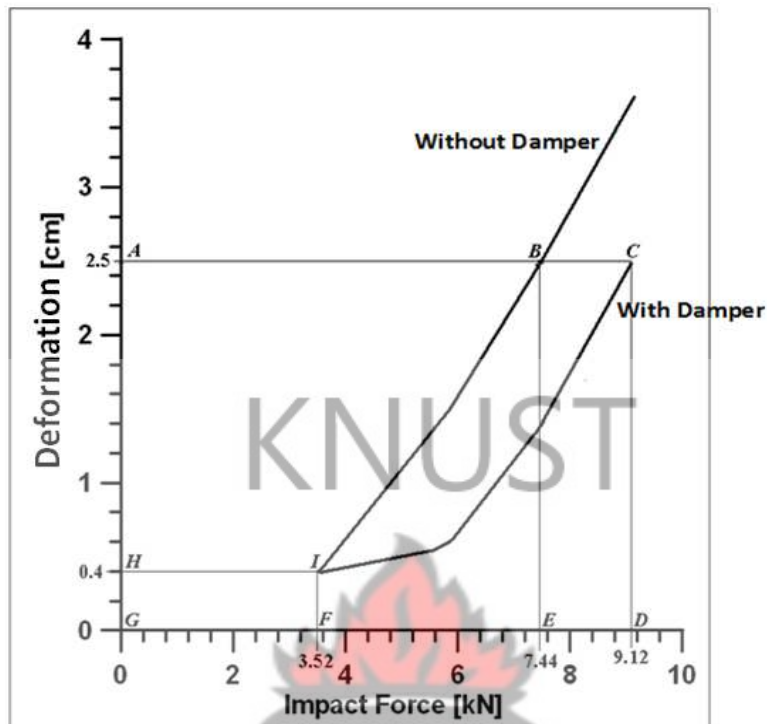
Figures 4.28 Results for Bumper C without a Damper

Figure 4.28 shows results of Bumper C with Damper Model 1. The results show a curve-fitted relationship that is very close to a linear one. There was a slight deviation from linearity. This may be due to experimental imperfections.



Figures 4.29 Results for test of Bumper C with Damper Model 1.

The Results of Bumper C with a damper gives an exponential curve as was obtained in the simulation of bumper with friction elements. During the test, the damper model 1 stuck and did not slide. This confirms that sticking friction used for the simulation was right. Both follow the same trend and the results could be curve-fitted and obeyed the relationship $y = Ax + B \ln x + C$; where y is the deformation and x is the impact force $\times 10^{-5}$.



Figures 4.30 Results for Bumper C with and without a Damper

The strain energy absorbed as a result of the deformation of the bumper is given by the areas under the respective curves. The results of the tests for bumper C with and without a friction damper were plotted together in Figure 4.30 to calculate for the strain energies absorbed by the bumper in both tests. The same amount of deformation was used. A deformation of 2.5 cm was used for the calculation. That is the amount of energy absorbed in each case for a deformation of 2.5 cm.

From Figure 4.30, for a deformation of 2.5 cm, the energy absorbed by the bumper without the friction damper is given by the area *ABIH*. The energy

absorbed as a result of the same amount of deformation when the friction damper is used is given by area $ACIH$. Calculation of the energy is given in Appendix C. From the calculations, energy absorbed by the bumper without a friction damper was 119.42 J, and that absorbed by the bumper C with friction damper was 158.22 J. This implies that the bumper absorbed 38.8 J more than that without the friction damper. This represent 32.5 % more energy for the one with the friction damper than the one without the friction damper.



CHAPTER FIVE

5.0 Conclusion and Future Work

The focus of this dissertation has been to study and propose design parameters for a damper to attenuate impact energy of colliding road vehicles. The sedan or saloon car of a gross weight of 1900 kg was used for the study. The bumper of the vehicle as a crash energy attenuation component was selected and a mathematical model developed for it. The mathematical model was used to simulate impact phenomena up to relatively medium speeds of 50 km/h (13.9 m/s).

Investigation of the dynamics of the model revealed that with the addition of a friction damper, the energy absorption capacity of the bumper was enhanced by about 26% for the experiment with friction force of 1.14 kN and 146% for the simulation of the bumper material *R* with a damper supplying a frictional force of 228 kN. The vehicle with a crash impact velocity of about 3 m/s could suffer the same amount of deformation as that experienced by a bumper without the proposed damper at 1.11 m/s. It was also observed that the deformation on the bumper without a damper caused by impact velocities up to 1.5 m/s was the same as that caused by about three times the impact velocity, about 4.5 m/s, on the bumper with a damper with friction force 228 kN.

Design parameters were derived for bumpers that could attenuate more energy. With the bumper design parameters proposed, namely stiffness, coefficient of damping and the friction necessary in the damper to be attached, the energy absorption capacity of the bumper was improved.

A friction damper was proposed and design parameters from the simulation used to build a physical model. The model was tested with a bumper to check for its effectiveness to validate the simulation results. The experimental results revealed that the addition of the friction damper to an old bumper to give a bumper-damper system could attenuate about 26 % more energy than with the bumper alone.

It was also observed that with the introduction of the damper the coefficient of restitution of the system was increased from 0.565 to 0.663 (for 228 kN frictional force) giving an increase of about 17.3% and thus could help to reduce the shock level of the impact.

It can be concluded that the operation range of automobile bumpers to withstand impact of vehicles traveling at about three times the speed bumpers have been designed for has been achieved. The initial target of attenuating impact of road vehicles traveling at speeds of up to 19.4 m/s (70 km/h), however, could not be achieved. Impacts of only up to 12 m/s (43.2 km/h) could be achieved.

5.1 Challenges and Sources of Error

The method used for the experiment was a destructive one. Therefore each specimen could be used only once. Since material manufacturing methods cannot guarantee that the material strictly had the same properties, deviation of material property in the same bumper could also have affected the experimental results. This could also have influenced the experimental results.

5.2 Future Work

For further research the following are recommended:

1. Use of friction elements with higher coefficient of friction in future damper designs.
2. Find the stiffness of bumpers experimentally, and using the values to simulate impact phenomena to compare the results for better comparison.
3. Find material properties and characteristics that can operate within a wider impact velocity range.

Appendix A Calculations of Damper's lever Dimensions

Calculations based on an Impact Velocity of 12 m/s (43.2 km/h)

KNUST

Mass of vehicle, $M = 1900$ kg

Acceleration due to gravity, $g = 9.81$ m/s²

Initial Velocity, $v_i = 12$ m/s

Final Velocity, $v_f = 0$ m/s

Time, $t_s = 0.2$ s

$$\text{Force, } F = \frac{m(v_i - v_f)}{t_s} = \frac{1900 \times 12}{0.2} = 114000 \text{ N}$$

Length, $L = 0.3$ m;

$E = 210$ GPa

$S_y = 250$ MPa

$\tau_y = 145$ MPa

Factor of safety, $N = 3.5$; (For Impact forces with uncertain stresses)(Deutschman et al., 1975)

Allowable Working normal stress

$$S_{allow} = S_y/N = 71.43 \text{ MPa}$$

Breadth = 0.08

KNUST

thickness of plate based on normal allowable stress:

$$t = \frac{114000}{71.43 \times 10^6 \times 0.08} = 0.01995m \approx 20 \text{ mm}$$

Let D be the diameter of pin, then:

$$D = \sqrt{\frac{4F}{2\pi\tau_{allow}}} = \sqrt{\frac{4 \times 114000}{2 \times \pi \times 41.4286 \times 10^6}} = 0.04185m = 41.85 \text{ mm}$$

Diameter selected: 42 mm

Calculation of thickness based on the bearing stress using diameter of 0.042 m:

$$\text{Thickness} = \frac{114000}{71.43 \times 10^6 \times 0.042} = 0.037999m \approx 38 \text{ mm}$$

Radius of gyration, $\rho = 0.289 \times h = 0.289 \times 0.08 = 0.02312$

$$\text{Slenderness ratio} = \frac{L}{\rho} = \frac{0.3}{0.02312} = 12.9758$$

Using Johnson's equation, since the slenderness ratio is low (Juvinal and Marshek, 2000):

$$A = \frac{P_{cr}}{S_y - \frac{S_y^2}{4\pi^2 E} \left(\frac{L}{\rho}\right)^2} = \frac{399000}{\left(250 \times 10^6 - \frac{(250 \times 10^6)^2}{4\pi^2 \times 210 \times 10^9} \left(\frac{0.3}{0.02312}\right)^2\right)} = 1.604144 \times 10^{-3} \text{ m}^2$$

$$t = \frac{A}{h} = \frac{1.604144 \times 10^{-3}}{0.08} = 0.02005 \text{ m} = 20.1 \text{ mm}$$

Results:

Thickness = 38 mm

Height = 80 mm

Length = 300 mm



Appendix B Optimization Program in MATLAB™

Main Program

```
clc,clear;      (clears memory and workspace/screen)

% This is the main program for optimisation; to minimize the cost

% Linearity constraint Matrix: A.x = B

% Variables x = [t; D; L; h];

% Variables : x(1) = thickness = t

% : x(2) = Diameter of Link = D

% : x(3) = Length of Lever = L

% : x(4) = Height of Plate = h

% Linear Inequality constraints:

%  $0.10 \leq L \leq 0.15$  and  $0.03 \leq h \leq 0.07$ 

% i.e:

-x(3) ≤ -0.10;

x(3) ≤ 0.15;
```

$$-x(4) \leq -0.03;$$

$$x(4) \leq 0.07;$$

$$A = [0 \ 0 \ -1 \ 0$$

$$0 \ 0 \ 1 \ 0$$

$$0 \ 0 \ 0 \ -1$$

$$0 \ 0 \ 0 \ 1];$$

$$B = [-0.10$$

$$0.15$$

$$-0.03$$

$$0.07];$$

% % Linear Equality constraints: here it sets h = 0.04 m

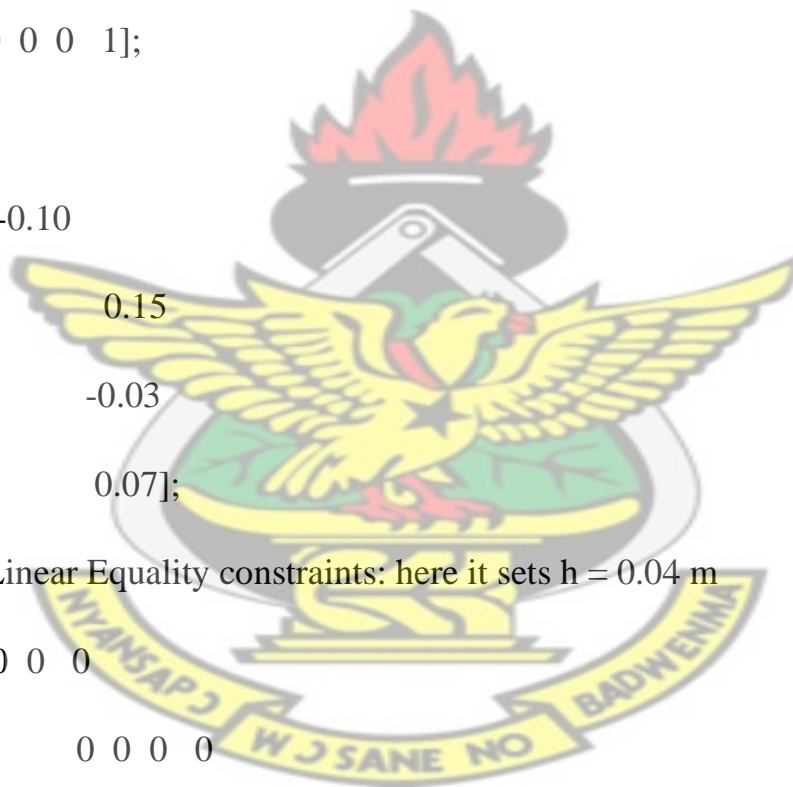
$$A_{eq} = [0 \ 0 \ 0 \ 0$$

$$0 \ 0 \ 0 \ 0$$

$$0 \ 0 \ 0 \ 0$$

$$0 \ 0 \ 0 \ 1];$$

KNUST



```

Beq = [0
      0
      0
      0.04];

x0 = [0.003, 0.010, 0.010, 0.03]; % Set a starting guess values for the
variables: t, D, L, and h respectfully

Options = optimset('LargeScale','off','Display','iter');

%
X=FMINCON(FUN,X0,A,B,Aeq,Beq,LB,UB,NONLCON,OPTIONS)
% minimizes with the
% default optimization parameters replaced by values in the structure
% OPTIONS, an argument created with the OPTIMSET function.

[x,fval] = fmincon(@costfun,x0,A,B,Aeq,Beq,0.006,0.015, ...
...ConstraintsFunction,Options)

```

Sub-Programs

Cost function Sub-program

```
function f = costfun(x)
```

```
f = x(1)*x(4)*x(3);
```

KNUST

Constraints function Sub-Program

```
function [c,ceq] = ConstraintsFunction(x)
```

```
% c is non-linear inequality constraints' vector
```

```
c = [9123.5 - 71.4286e6*x(1)*x(4) + 71.4286e6*x(1)*x(2)
```

```
31932*x(4) - (250e6*x(1)*x(4)^2) + (90262.07235*x(1)*x(3)^2)];
```

```
ceq = []; % No Nonlinear equality constraints
```

Results after running the program

$x = 0.0060 \quad 0.0100 \quad 0.1000 \quad 0.0400$

i.e.

Variables : $x(1) = \text{Thickness} = t = 6 \text{ mm}$

$x(2) = \text{Diameter of Link} = D = 10 \text{ mm}$

$x(3) = \text{Length of Lever} = L = 100 \text{ mm}$

$x(4) = \text{Height of Plate} = h = 40 \text{ mm}$



Appendix C Experimental Data – Equipment

Calculations of First Moment of Area, Q_x , the Centroid, \bar{Y}

The design calculations for the model of the proposed friction damper were based on the maximum impact force that the test machine used could exert. Calculations were as follows:

Using the First Moment of Area, Q_x , to find the Centroid, \bar{Y}

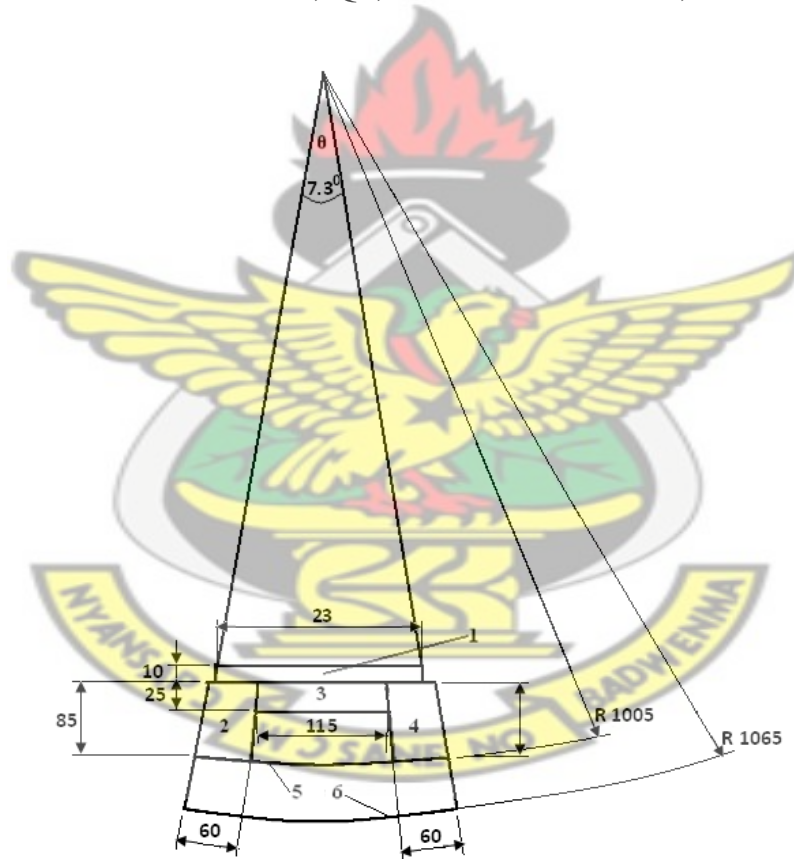


Figure A-1 Schematic Diagram of Hammer of Impact Test machine

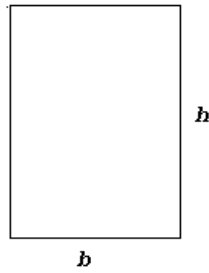


Figure A-2 Rectangular Area

KNUST

Using the rectangle with an area A , in Figure A-2 as a reference the first moment of area, Q_x –was calculated with the pivot as the reference point. Similarly the moment of Inertia I_x at the support of the hammer was calculated. With these values the centroid of the hammer was found and the impact force of the hammer computed. The impact force was further used in stress analysis of the friction damper model to find the right dimensions:

$$b_1 = 0.23 \text{ m}; h_1 = 0.01 \text{ m}; d_1 = 0.905 \text{ m}$$

$$A_1 = b_1 \times h_1 = 0.0023 \text{ m}^2$$

$$Q_1 = A_1 d_1 = 0.0021 \text{ m}^3$$

$$b_2 = 0.06 \text{ m}; h_2 = 0.085 \text{ m}; d_2 = 0.9525 \text{ m}$$

$$A_2 = b_2 \times h_2 = 0.0051 \text{ m}^2$$

$$Q_2 = A_2 d_2 = 0.0049 \text{ m}^3$$

$$b_3 = 0.115 \text{ m}; h_3 = 0.025 \text{ m}; d_3 = 0.9525 \text{ m}$$

$$A_3 = b_3 x h_3 = 0.0029 \text{ m}^2$$

$$Q_3 = A_3 d_3 = 0.0027 \text{ m}^3$$

$$Q_4 = Q_2 = 0.0049 \text{ m}^3 \text{ - (Symmetry)}$$

$$A_4 = A_2 = 0.0051 \text{ m}^2 \text{ - (Symmetry)}$$

$$\theta = 0.1271 \text{ rad}, R_5 = 1.065 \text{ m}$$

$$d_5 = \frac{2 R_5 \sin \theta}{3 \theta} = 0.7081 \text{ m}$$

$$A_5 = R_5^2 \theta = 0.1442 \text{ m}^2$$

$$Q_5 = A_5 d_5 = 0.1021 \text{ m}^3$$

$$R_6 = 1.005 \text{ m}$$

$$d_6 = \frac{2 R_6 \sin \theta}{3 \theta} = 0.6682 \text{ m}$$

$$A_6 = R_6^2 \theta = 0.1284 \text{ m}^2$$

$$Q_6 = A_6 d_6 = 0.0858 \text{ m}^3$$

$$A_{sum} = A_1 + A_2 + A_3 + A_4 + A_5 - A_6 = 0.0023 + 0.0051 + 0.0029 + 0.1442 - 0.1284 = 0.03116 \text{ m}^2$$

$$Q_x = Q_1 + Q_2 + Q_3 + Q_4 + Q_5 - Q_6 = 0.0021 + 0.0049 + 0.0027 + 0.0049 + 0.1021 - 0.0858 = 0.030748 \text{ m}^3$$

$$\bar{Y} = \frac{Q_x}{A_{sum}} = \frac{0.030748}{0.03116} = 0.9868 \text{ m}$$

where \bar{Y} is the distance of the centroid from

the axis of rotation

Calculating Second Moment of Area, I_{xi}

$$b_1 = 0.23 \text{ m}; h_1 = 0.01 \text{ m}; d_1 = 0.905 \text{ m}; A_1 = b_1 h_1 = 0.0023 \text{ m}^2$$

$$I_{x_1} = \frac{b_1 h_1^3}{12} + A_1 d_1^2 = \frac{0.23 \times 0.01^3}{12} + 0.0023 \times 0.905^2 = 0.0019 \text{ m}^4$$

$$b_2 = 0.06 \text{ m}; h_2 = 0.085 \text{ m}; d_2 = 0.9525 \text{ m}; A_2 = b_2 h_2 = 0.0051 \text{ m}^2$$

$$I_{x_2} = \frac{b_2 h_2^3}{12} + A_2 d_2^2 = \frac{0.06 \times 0.085^3}{12} + 0.0051 \times 0.9525^2 = 0.0046 \text{ m}^4$$

$$b_3 = 0.115 \text{ m}; h_3 = 0.025 \text{ m}; d_3 = 0.9225 \text{ m}; A_3 = b_3 h_3 = 0.0029 \text{ m}^2$$

$$I_{x_3} = \frac{b_3 h_3^3}{12} + A_3 d_3^2 = \frac{0.115 \times 0.025^3}{12} + 0.0029 \times 0.9225^2 = 0.0024 \text{ m}^4$$

$$I_{x_4} = \frac{b_4 h_4^3}{12} + A_4 d_4^2 = I_{x_2} = 0.0046; (\text{Symmetry})$$

$$= 0.0046 \text{ m}^4$$

But $\theta = 0.1271 \text{ rad}$,

$$r_5 = 1.065 \text{ m}; d_5 = \frac{2}{3} r_5 \frac{\sin \theta}{\theta} = 0.7081 \text{ m}; A_5 = \theta r_5^2 = 0.1442 \text{ m}^2$$

$$r_6 = 1.005 \text{ m}; d_6 = \frac{2}{3} r_6 \frac{\sin \theta}{\theta} = 0.6682 \text{ m}; A_6 = \theta r_6^2 = 0.1284 \text{ m}^2$$

$$I_{x_5} = \frac{1}{4} r_5^4 \left(\theta + \frac{1}{2} \sin 2\theta \right) + A_5 d_5^2 = \frac{1}{4} \times 1.065^4 \times \left(0.1271 + \frac{1}{2} \sin(2 \times 0.1271) \right) + 0.1442 \times 0.7081^2 = 0.1536 \text{ m}^4$$

$$I_{x_6} = \frac{1}{4} r_6^4 \left(\theta + \frac{1}{2} \sin 2\theta \right) + A_6 d_6^2 = \frac{1}{4} \times 1.005^4 \times \left(0.1271 + \frac{1}{2} \sin(2 \times 0.1271) \right) + 0.1284 \times 0.6682^2 = 0.1218 \text{ m}^4$$

$$\begin{aligned}
 I_x &= I_{x_1} + I_{x_2} + I_{x_3} + I_{x_4} + I_{x_5} - I_{x_6} \\
 &= 0.0019 + 0.0046 + 0.0024 + 0.0046 + 0.1536 - 0.1218 \\
 &= 0.0453 \\
 &= 0.0453 \text{ m}^4
 \end{aligned}$$

Calculating the impact force of hammer, F

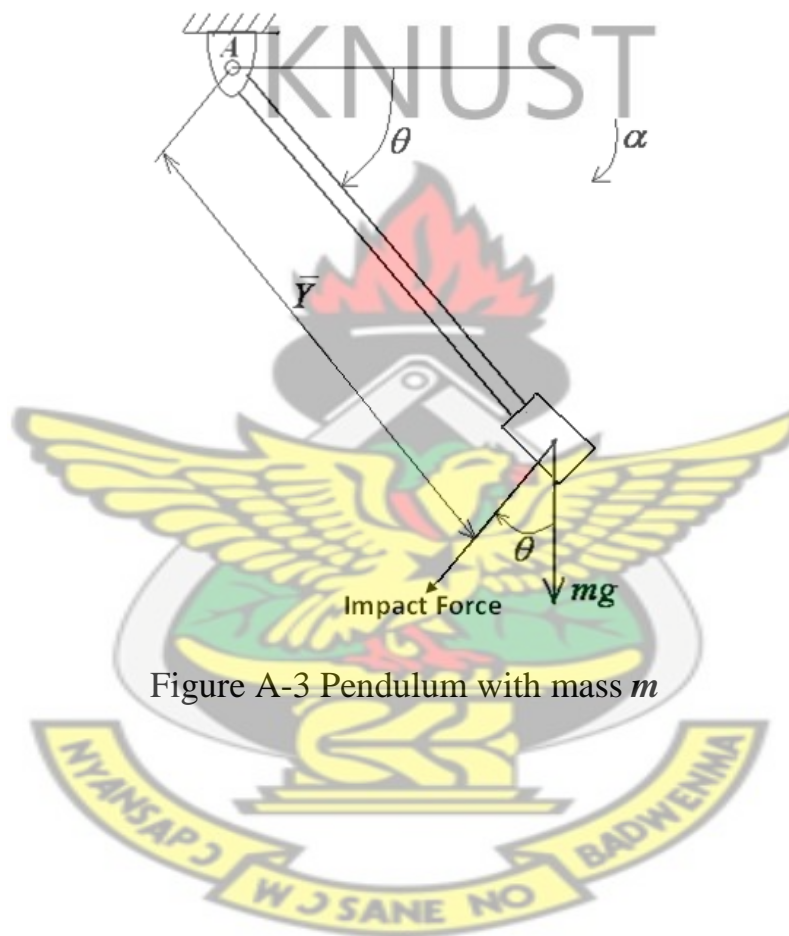


Figure A-3 Pendulum with mass m

$$\sum M_A = I_A \alpha$$

$$mg\bar{Y} \cos \theta = I_A \alpha$$

$$\alpha = \frac{mg\bar{Y} \cos \theta}{I_A}$$

$$\omega = \frac{d\theta}{dt}; \alpha = \frac{d\omega}{dt}; \Rightarrow \frac{d\theta}{\omega} = \frac{d\omega}{\alpha}; \Rightarrow \alpha d\theta = \omega d\omega$$

$$\int_0^\omega \omega d\omega = \int_0^{\frac{\pi}{2}} \frac{mg\bar{Y} \cos \theta}{I_A} d\theta$$

$$\omega^2 = \frac{2mg\bar{Y}}{I_A}; \Rightarrow \omega = \sqrt{\frac{2mg\bar{Y}}{I_A}}$$

KNUST

$$-m\bar{Y}\omega + \int F dt = 0$$

$$-m\bar{Y}\omega + \int_0^t F dt = 0$$

$$\therefore F = \frac{m\bar{Y}\omega}{t} = \frac{m\bar{Y}}{t} \sqrt{\frac{2mg\bar{Y}}{I_A}} = \frac{m\bar{Y}}{t} \sqrt{\frac{2mg\bar{Y}}{I_x}}$$

But:

$$m = 20 \text{ kg}; \bar{Y} = 0.9868 \text{ m}; t = 0.2 \text{ s}; g = 9.81 \text{ m/s}^2; I_x = 0.0453 \text{ m}^4$$

$$\therefore F = \frac{20 \times 0.9868}{0.2} \sqrt{\frac{2 \times 20 \times 9.81 \times 0.9868}{0.0453}} = 9.123450279006314 \text{e} + 003 \approx 9123.5 \text{ N}$$

$$F = 9123.5 \text{ N}$$

The maximum impact force from the pendulum is $F = 9123.5 \text{ N}$

Checking for buckling using steel as design material:

Let L be the length of the lever arm:

Using $L = 0.15 \text{ m}$ for the longer arm and 0.1 m for the shorter one.

Let $E = 210 \text{ GPa}$

Yield Strength, $S_y = 250 \text{ MPa}$

Factor of Safety, $N = 3.5$ (Deutschman et al., 1975)

Height of cross-section, $h = 0.04 \text{ m}$

Let the thickness of cross-section = t

Radius of gyration, $\rho = 0.289 \times h = 0.289 \times 0.04 = 0.01156$

Slenderness ratio = $\frac{L}{\rho} = \frac{0.15}{0.01156} = 12.9758$

Using Johnson's equation, since the slenderness ratio is low (Juvinal and Marshek, 2000):

$$A = \frac{P_{cr}}{S_y - \frac{S_y^2}{4\pi^2 E} \left(\frac{L}{\rho}\right)^2} = \frac{31932}{\left(250 \times 10^6 - \frac{(250 \times 10^6)^2}{4\pi^2 \times 210 \times 10^9} \left(\frac{0.15}{0.01156}\right)^2\right)} = 1.2838 \times 10^{-4} \text{ m}^2$$

$$t = \frac{A}{h} = \frac{1.2928 \times 10^{-4}}{0.04} = 0.00321 \text{ m} = 3.2 \text{ mm}$$

$F = 9123.5 \text{ N}$

$m = 20 \text{ kg}$

$g = 9.81 \text{ m/s}^2$

time = $t_s = 0.2 \text{ s}$

Moment of Inertia, $I_x = 0.0453 \text{ m}^4$

Yield Strength, Tension $S_y = 250 \text{ MPa}$ (Beer et al., 2006)

Yield Strength, Shear, $\tau_y = 145$ MPa (Beer et al., 2006)

Calculation of the thickness of plate based on compression of plate:

$$S_{\text{allow}} = \frac{S_y}{N} = \frac{250}{3.5} = 71.4286 \text{ MPa (Beer et al., 2006)}$$

But breadth of cross-section, $h = 0.04$ m

$$\text{Cross sectional Area, } A = \frac{F}{S_{\text{allow}}} = \frac{9123.5}{71.4286 \times 10^6} = 1.2773 \times 10^{-4} \text{ m}^2$$

$$t = \frac{A}{h} = \frac{1.2773 \times 10^{-4}}{0.04} = 0.00319 \text{ m}$$

$$t = 3.2 \text{ mm}$$

Calculation of the diameter of pin based on double shear:

$$\tau_{\text{allow}} = \frac{\tau_y}{N} = \frac{145}{3.5} = 41.4286 \text{ MPa}$$

Let D be the diameter of pin, then:

$$D = \sqrt{\frac{4F}{2\pi\tau_{\text{allow}}}} = \sqrt{\frac{4 \times 9123.5}{2 \times \pi \times 41.4286 \times 10^6}} = 0.01184 \text{ m} = 11.84 \text{ mm}$$

Diameter selected: 12 mm

Calculation of the thickness of plate based on diameter of pin in double shear:

Using $D = 12$ mm

Thickness t , of plate:

$$t = \frac{F}{2S_{allow}D} = \frac{9123.5}{2 \times 71.4286 \times 10^6 \times 0.01184} = 0.005322 \text{ m}$$

Thickness selected: 6 mm

KNUST

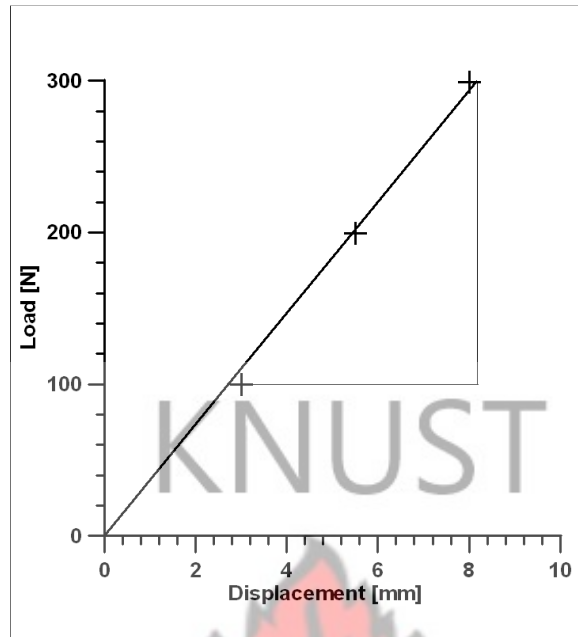


Appendix D Experimental Data – Components

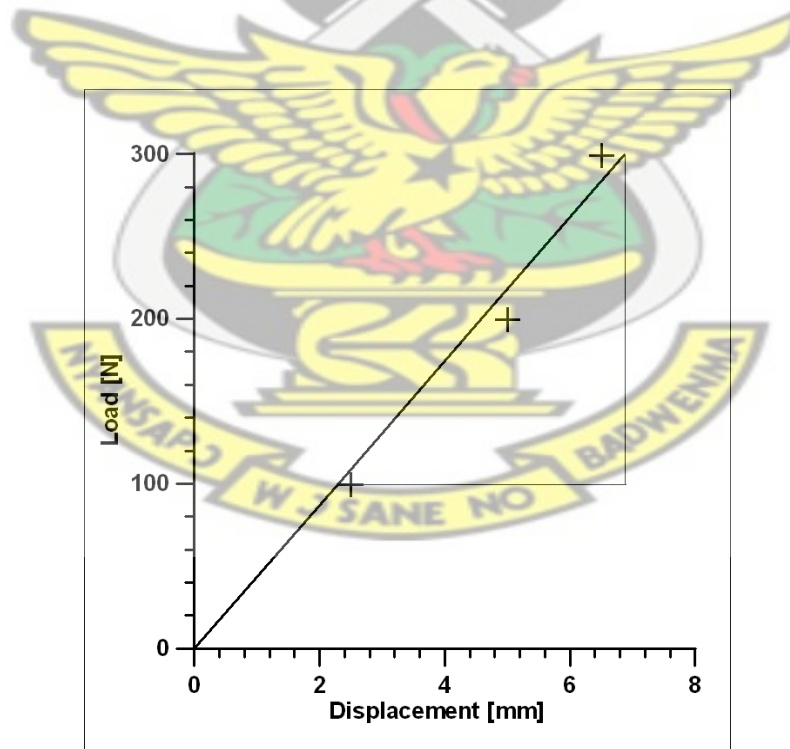
The calculations for the spring stiffness constants, k , were calculated from Figures D-1 and D-2. To determine the spring stiffness k , of the springs used in the experimental model of the friction damper, static loads were applied to the springs and the corresponding compressed displacements measured. Table D-1 shows the loads and the corresponding displacements.

Table D-1 Loads and corresponding Displacement of Spring

Load [kN]	0.9967	1.9935	2.9902
Displacement for Spring A [mm]	3.0	5.5	8.0
Displacement for Spring B [mm]	2.5	5.0	6.5



Figures D-1 Displacement of Spring A for Applied Loads



Figures D-2 Displacement of Spring B for Applied Loads

$$\text{Spring Constant for Spring A} = \frac{299.0226 - 99.6742}{8.1429 - 2.7143} = 36.72188 \text{ N/mm}$$

$$= 36721.88 \text{ N/m}$$

$$\text{Spring Constant for Spring B} = \frac{299.0226 - 99.6742}{6.8571 - 2.2857} = 43.60774 \text{ N/mm}$$

$$= 43607.74 \text{ N/m}$$

Frictional Force Supplied by the Damper with Springs A and B were calculated using the coefficient of static friction and normal forces on the pads.

An experiment was carried out to measure the coefficient of static friction of the friction pad on steel plate. Two pads of the same material were used. For each pad seven measurements of angle of inclination at which sliding of pads just begin were taken and tangents of the angles computed to find the coefficients of friction. The average of the seven values was found for each pad, and subsequently the average of the coefficients of the two pads was found and used as the coefficient of static friction for the pads. Table D-2 shows the angle of inclination of plate at which sliding just started. Table D-3 shows the tangents of the angles for the two pads.

Table D-2 Inclined angle of plate

Friction Pad	Angle of Inclination of Plate, θ [°]						
Pad 1	21	28	26	22	21	23	19
Pad 2	34	26	28	26	31	26	17

Table D-3 Tangent of Angle of Inclination

Friction Pad	Coefficient of Static Friction; Tangent of Angle of Inclination, $[\tan \theta]$			
Pad 1	0.3839	0.5317	0.4877	0.4040
Pad 1	0.3839	0.4245	0.3443	
Pad 2	0.6745	0.4877	0.5317	0.4877
Pad 2	0.6009	0.4877	0.3057	

Average Coefficient of Static Friction for Pad 1

$$= \frac{0.3839 + 0.5317 + 0.4877 + 0.4040 + 0.3839 + 0.4245 + 0.3443}{7}$$

$$= 0.422857$$

Average Coefficient of Static Friction for Pad 2

$$= \frac{0.6745+0.4877+0.5317+0.4877+0.6009+0.4877+0.3057}{7}$$

$$= 0.510843$$

$$\text{Average Coefficient of Static Friction for the Pads} = \frac{0.422857+0.510843}{2}$$

$$= 0.466850 \approx 0.467$$

KNUST

Let:

Coefficient of static friction of pad on steel plate = $\mu = 0.467$

Spring Constant for Spring A = $k_A = 36721.88 \text{ N/m}$

Uncompressed height of Spring A = $H_{uA} = 44.5 \text{ mm}$

Compressed height of Spring A = $H_{cA} = 39 \text{ mm}$

Displacement of Spring A = $x_A = H_{uA} - H_{cA} = 44.5 - 39 = 5.5 \text{ mm} = 0.0055 \text{ m}$

Normal force from two pieces of Spring A = $N_A = k_A x_A = 36721.88 \times 0.0055$
 $\times 2$

$$= 403.94 \text{ N}$$

Frictional Force Supplied by one pad in the damper with Spring A = μN_A

$$= 0.467 \times 403.94 \text{ N} = 118.64 \text{ N}$$

Frictional Force Supplied by the 4 pads in the damper with Spring A =

$$118.64 \times 4 = 754.56 \text{ N}$$

There friction force on Damper model 2 = 754.56 N

Spring Constant for Spring B = $K_B = 43607.74 \text{ N/m}$

Uncompressed height of Spring B = $H_{uB} = 52 \text{ mm}$

Compressed height of Spring B = $H_{cB} = 45 \text{ mm}$

Displacement of Spring B = $x_B = H_{uB} - H_{cB} = 52 - 39 = 7 \text{ mm} = 0.007 \text{ m}$

Normal force from two pieces of Spring B = $N_B = K_B x_B = 43607.74 \times 0.007$
 $\times 2$

$$= 610.51 \text{ N}$$

Frictional Force Supplied by one pad in the Damper with Spring B = μN_B

$$= 0.467 \times 610.51 = 285.11 \text{ N}$$

Frictional Force Supplied by the 4 pads in the damper with Spring B =

$$285.11 \times 4 = 1140.43 \text{ N}$$

The friction force on Damper model 1 = 1140.43 N

Appendix E Experimental Data – Work Done

To find the work done by Bumper C with and without a friction element, the areas under the curves in Figure C-1 were calculated.

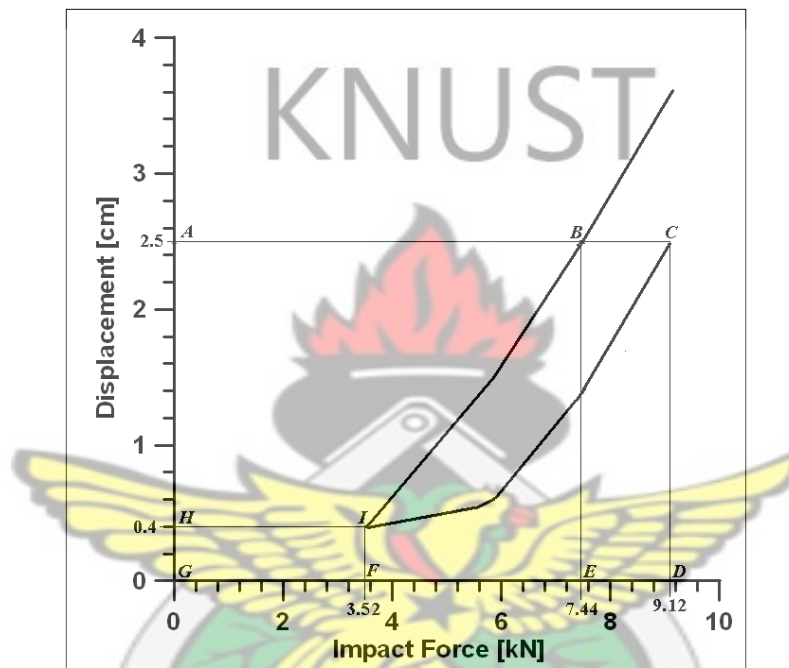


Figure E-1 Experimental results of Bumper C

The strain work done as a result of the deformation of the bumper is given by the areas under the respective curves. From Figure E-1, for a deformation of 2.5 cm, the work done by the bumper without the friction element is given by the area $ABIH$. The work done as a result of the same amount of deformation when the friction element is used is given by area $ACIH$.

$$\text{area } ABIH = \text{area } ABEG - \text{area } HIFG - \text{area } IBEF$$

$$\text{area } ACIH = \text{area } ACDG - \text{area } HIFG - \text{area } ICDF$$

$$\text{area } IBEF = \int_{0.0352}^{0.0744} (93.5685x - 2.1561 \ln x - 10.0969) dx$$

$$= \left[\frac{93.5685}{2} x^2 - 2.1561 (x \ln x - x) - 10.0969 x \right]_{0.0352}^{0.0744}$$

$$= 0.0525$$

$$\text{area } ICDF = \int_{0.0352}^{0.0912} (143.3301x - 6.217 \ln x - 25.4479) dx$$

$$= \left[\frac{143.3301}{2} x^2 - 6.217 (x \ln x - x) - 25.4479 x \right]_{0.0352}^{0.0912}$$

$$= 0.0557$$

$$\text{area } ABIH = \text{area } ABEG - \text{area } HIFG - \text{area } IBEF$$

$$= ((2.5 \times 0.0744) - (0.4 \times 0.0352) - 0.0525) \times 100 \text{ Joules}$$

$$= (0.186 - 0.01408 - 0.0525) \times 1000 \text{ J}$$

$$= 0.11942 \times 1000 \text{ J}$$

$$= 119.42 \text{ J}$$

$$\text{area } ACIH = \text{area } ACDG - \text{area } HIFG - \text{area } ICDF$$

$$= (2.5 \times 0.0912) - (0.4 \times 0.0352) - 0.0557$$

$$= (0.228 - 0.01408 - 0.0557) \times 1000 \text{ J}$$

$$= 0.15822 \times 1000 \text{ J}$$

$$= 158.22 \text{ J}$$

Extra Work Done = $158.22 - 119.42 = 38.8 \text{ J}$.

Percentage Extra Work Done = $100 \times 38.8/119.42 = 32.49 \%$.

That implies the extra work done as a result of the introduction of the friction element for Bumper C was about 32.5 %.

KNUST



References

AASHTO (2001). A Policy on Geometric Design of Highways and Streets: American Association of State Highway and Transportation Officials, Washington D.C.

Abe, G. and Richardson, J. (2006). Alarm timing, trust and driver expectation for forward collision warning systems: Applied Ergonomics; 37: 577-586.

Afukaar, F. K., ANTWI, P. and Ofosu-Amaah, S. (2003). "Pattern of Road Traffic Injuries in Ghana: Implications for Control." Injury Control and Safety Promotion 10 (1-2): p. 69-76.

Aiken, I. D., Nims, D. K. Whittaker, A. S. and Kelly, J. M. (1993), Testing of Passive Energy Dissipation Systems: Earthquake Spectra, v. 3

Appiah, N. J. (2009) *"Implementing a Decade of Action in Africa: Examples of Road Safety Interventions."* National Road Safety Commission, Ghana, Make Roads Safe Conference, Dar es Salaam, Tanzania. (8-10 July, 2009).

Avery, M. and Weekes, A. M. (2006), The development of a new low speed impact test to improve bumper performance and compatibility, ICrash, Athens, Greece.

Aylor, D., Ramirez, D. L., Brumbelow, M. and Nolan, J. M. (2005). "Limitations of current bumper designs and potential improvements." SAE Technical Paper Series 1 (2005-01-1337).

Baker, B. C., Nolan, J. M. O'Neill, B. and Genetos, A. P. (2007), Crash compatibility between cars and light trucks: Benefits of lowering front-end energy-absorbing structure in SUVs and pickups, Arlington, VA, United States, Insurance Institute for Highway Safety.

Beer, F. P., Russel, E., Johnston, Jr. and DeWolf, J. T. (2006.). Mechanics of Materials. New York, McGraw-Hill.

Brideson, A. R., B. Aitken, Douglas, A. and Grogan, L. (2001). Report of the Road Safety Committee on the Inquiry into Victoria's Vehicle Roadworthiness System, in R. S. Committee, ed., Australia, Victoria Parliament

BRRRI (2006), Estimation of cost of road traffic accidents in Ghana

CarPros (2009). Air Bags in Steering Column, 2 Car Pros.

Cebon, D. (1993). Interaction Between Heavy Vehicles and Roads. L. R. B. Lecture. Cambridge, Cambridge University Engineering Department.

KNUST

Cho, Y.-B., Bae, C.-H. Suh, M.-W. and Sin, H.-C. (2006). "A vehicle front frame crash design optimization using hole-type and dent-type crush initiator." *Thin-Walled Structures* 44: 415-428.

Ciğeroğlu, E. and Özgüven, H. N. (2006). "Nonlinear vibration analysis of bladed disks with dry friction dampers." *Journal of Sound and Vibration* 295: 1028-1043.

Davey, J., Wishart, D. , Freeman, J. and Watson, B. (2007). "An application of the driver behaviour questionnaire in an Australian organisational fleet setting." *Transportation Research Centre for Accident Research and Road Safety* (10): p. 11–21.

Deutschman, A. D., Michels, W. J. and Wilson, C. E. (1975). *Machine Design, Theory and Practice*. New York, Macmillan Publishing Co., Inc.

DMV (2006). Driver's Handbook, North Carolina Department of Transportation.

Dupont, P., Kasturi, P. and Stokes, A. (1997). "Semi-Active Control of Friction Dampers." *Journal of Sound and Vibration* 202(2): 203-218.

Filiatrault, A., Tremblay, R. and Kar, R. (2000). "Performance evaluation of friction spring seismic damper." *Journal of Structural Engineering* 126(4): 491-499.

Griškevičius, P. and Žiliukas, A. (2003). "The energy absorption of the vehicles front structures." *Transport* 18(2): 97-101.

Guglielmino, E., and Edge, K. A. (2004). A Controlled Friction Damper for Vehicle Applications: *Control Engineering Practice*; 12: 431-443.

Hofstra-University (2007). "Automobile Production " from <http://people.hofstra.edu/geotrans/eng/ch1en/conc1en/carprod1950-1999.html>. (Accessed 2007 April 12)

How-Stuff-Works. (2007). <http://www.howstuffworks.com/airbag1.htm>.
(Accessed 2007 April 12)

Huang, M. (2002), Vehicle Crash Mechanics, CRC Press, Boca Raton, London & New York, p. 100 -320.

Inman, D. J. (1996). Engineering Vibration. Upper Side River, NJ, Prentice Hall. p. 38 - 60

Juvinall, R. C. and Marshek, K. M. (2000). Fundamentals of Machine Component Design. Hoboken, N.J., USA, John Wiley & Sons, Inc., .

Lametrie, C. W. (2001). A Literary Review of Structural Control: Earthquake Forces. Warren, Michigan, USA, Parksons Brinckerhoff Automotive Division.

Leneman, F., Kellendonk, G. and Coop, P. d. (2004) "Assessment of Energy Absorbing Underrun Protection devices" TNO Automotive, Delft, VC-COMPAT truck leg consortium, Netherlands

Lord, D., Schalkwyk, I. v., Chrysler, S. and Staplin, L. (2006). "A strategy to reduce older driver injuries at intersections using more accommodating roundabout design practices."

Malhotra, A., Carson, D., Gopal, P., Braimah, A., Giovanni, G. D. and Pall, R. (2004). Friction Dampers For Seismic Upgrade of St. Vincent Hospital, Ottawa, 13th World Conference on Earthquake Engineering, Vancouver, B.C., Canada.

Mualla, I. H., and Belev, B. (2002). Performance of steel frames with a new friction damper device under earthquake excitation: *Engineering Structures*; 24: 365-371.

Nantulya, V. and Reich, M. R. (2003). "Equity Dimensions of traffic in low- and middle-income Countries." *Injury and Safety Promotion* 10(1 -2): 13 – 20.

NASA (2009). "History of Research in Space Biology and Biodynamics".

<http://www.hq.nasa.gov/office/pao/History/afspbio/part5-7.htm>,

(Accessed 2009 October 20)

NHTSA (1977). Bumper Standard. Title 49 Code of Federal Regulations Part 581. Washington, DC, USA. 49.

NHTSA (2007). "The New Car Assessment Program Suggested Approaches for Future Program Enhancements", United States Department of Transportation, DOT HS 810 698, 2007.

<http://www.safercar.gov/NewCarAssessmentEnhancements-2007.pdf>;
(Accessed 2007 April 19)

Nripen, S. K. (1993). "Numerical simulation of vehicle crashworthiness and occupant protection." Computational Methods for Crashworthiness: p. 125-139.

NRTC (1995). Roadworthiness Guidelines. NRTC. Australia.

NRSC (2010) Statistics. NRTC. Ghana.

<http://www.nrsc.gov.gh/statistics/docs/number%20of%20registered%20vehicles.pdf>

(Accessed 2010 July 28)

O'Neill, B. and Kyrychenko, S. Y. (2003). Potential Benefits from Enhancing Crash Compatibility between Cars and Light Trucks in Front-to-Front Crashes. Insurance Institute for Highway Safety. Arlington, VA,

Odero, W. (2006). Africa's Epidemic Of Road Traffic Injuries: Trends, Risk Factors And Strategies For Improvement. The Harvard Center For Population And Development Studies on the Occasion of the World Health Day 2004. Harvard.

Oxley, J., B. Fildes, Corben, B. and Langford, J. (2006). Intersection design for older drivers: Transportation Research Part F; 9: 335-346.

Paine, M., Crashlab, D. M. and Haley, J. (1998). Offset Crash Tests Observations about Vehicle Design and Structural Performance, Sixteenth International Technical Conference of the Enhanced Safety of Vehicles (ESV) Windsor, Canada, NHTSA, Washington, USA.

Panning, L., Sextro, W. and Popp, K. (2003). Design of Friction Dampers for Mistuned Bladed Disks, Proc. Appl. Math. Mech. 3, p. 118-119.

Peden, M., Scurfield, R., Sleet, D., Mohan, D., Hyder, A. A., Jarawan, E. and Mathers, C. (2004). World report on road traffic injury prevention. World Health Organization, Geneva, Switzerland

Petrov, E. P. and Ewins, D. J. (2007). "Advanced Modeling of Underplatform Friction Dampers for Analysis of Bladed Disk Vibration." ASME Journal of Turbomachinery; 129: 143.

Popp, K., Panning, L. and Sextro, W. (2003) "Vibration Damping by Friction Forces: Theory and Applications. Journal of Vibration and Control, 9; Sage Publication, p. 419-448

Rechnitzer, G., Haworth, N. and Kowadlo, N. (2000). The Effect of Vehicle Roadworthiness on Crash Incidence and Severity. Australia, Monash University Accident Research Centre; 164.

Ruiz, V., Walsh, K. and Abdullah, M. M. (2005). Investigating The Energy Dissipating Properties of Passive Friction Devices, Florida State University, Tallahassee, Florida; Tokyo Institute of Technology, Tokyo, Japan. <http://cive.seas.wustl.edu/wusceel/reujat/2005/Vince.pdf> ; (Accessed 2007 April 20)

Sanliturk, K. Y., Ewins, D. J., Elliott R., and Green J. S. (2001). The American Society of Mechanical Engineers (ASME): Journal of Engineering for Gas Turbines and Power; 123: 930-939.

Schuster, P. (2004). Current Trends in Bumper Design for Pedestrian Impact: A Review of Design Concepts from Literature and Patents, Bumper Project, The American Iron and Steel Institute.

SDI (2007). Silicon Designs Inc. SDI. <http://www.silicondesigns.com/digchip.html>. (Accessed 2007 June 4)

Tremblay, R. and Stiemer S. F. (1993). Energy dissipation through friction bolted connections in concentrically braced steel frames. ATC 17-1 Seminar on Seismic Isolation, passive energy dissipation and active control, ATC. 2: 557-568.

Unsal, M., Niezrecki, C. and Crane, C. D. III (2002), A New Semi-Active Piezoelectric Based Friction Damper, Fiction Damper, Department of Mechanical Engineering, University of Florida, Gainesville, Florida. http://cimar.mae.ufl.edu/CIMAR/pages/pubs/unsal_ICSV_07_11_02.pdf; (Accessed 2007 April 22)

Witteman, W. J. and Kriens R. F. C. (1998). Modeling of an Innovative Frontal Car Structure: Similar Deceleration Curves at Full Overlap, 40 Per Cent Offset and 30 Degrees Collisions. Eindhoven University of Technology, Eindhoven, Netherlands. Paper Number 98-S 1-0-04.

Witteman, W. (2005). Adaptive Frontal Structure Design To Achieve Optimal Deceleration Pulses. Eindhoven, Technische Universiteit Eindhoven. Paper Number 05-0243.

Zheng, Y. (2006). "A preliminary evaluation of the impact of local accident information on the public perception of road safety." Reliability Engineering and System Safety.

